TAMPEREEN TEKNILLINEN YLIOPISTO
TAMPERE UNIVERSITY OF TECHNOLOGY

JENNA TAINIO

IMPACT OF MAGNESIUM AND STRONTIUM ON DISSOLUTION AND SINTERING OF BIOACTIVE BOROSILICATE GLASSES

Master of Science Thesis

Examiner: Adj. Prof, Academy Research Fellow Jonathan Massera
Examiner and topic approved in the Faculty Council of Natural Sciences 5th of October 2016

ABSTRACT

JENNA TAINIO: Impact of magnesium and strontium on dissolution and sintering of bioactive borosilicate glasses
Tampere University of Technology
Master of Science Thesis, 67 pages, 8 Appendix pages
November 2016
Master's Degree Programme in Bioengineering
Major: Tissue Engineering
Examiner: Adj. Prof, Academy Research Fellow Jonathan Massera

Keywords: bioactive glass, borosilicate, bone tissue engineering, sintering, dissolution

Bioactive glasses are a promising, relatively new material group to be utilized in regenerative medicine. The main target area of these materials is in bone tissue engineering, where commercial products are already used; in the form of as granules and pastes. In future, there is an ever increasing demand for artificial bone grafts having 3-D structure and high mechanical strength.

Traditional bioactive glasses are silica-based. Despite their known biological properties, they tend to crystallize easily upon heat processing. In clinical studies it has been found that they do not completely convert to hydroxyapatite (HA); the substance which is replaceable by bones' remodeling mechanism. Boron containing glasses may overcome these problems as they convert faster to HA and have enhanced thermal properties. The objective of the study was to assess if magnesium and strontium could further improve the properties of a borosilicate glass composition. In the study, part of the calcium was substituted with magnesium and/or strontium and the impact on (i) sintering and (ii) dissolution of the produced glasses studied.

Six different glass compositions were prepared. A borosilicate glass with composition 47.1 SiO_2 - 6.7 B_2O_3 - 22.7 Na_2O - 21.8 CaO - 1.7 P_2O_5 in mol-% (labelled B12.5) was prepared and used as reference. This glass composition corresponds to the current commercial silicate bioactive glass, S53P4, where 12.5% of the SiO_2 is replaced with B_2O_3. From this composition, glasses with different amounts of Mg and/or Sr were produced. The change in physical, structural and thermal properties, induced by the substitution, were studied. Sintering and crystallization was studied at various temperatures and analyzed with scanning electron microscopy (SEM) and X-ray diffraction (XRD). The bioactivity of the glasses was assessed by dissolution in simulated body fluid (SBF), for immersion time from 6 hours to 2 weeks. Upon dissolution the pH of the solution and the amount of ions leached out from the glass to the SBF was measured. Fourier transform infrared (FTIR) spectroscopy was utilized to evaluate HA formation on the glass surface.

Results showed that Mg and Sr assume similar structural role, in the glass network, as calcium. Mg and Sr seemed to improve the overall sintering behavior by decreasing the glass viscosity. Ions released from the glasses upon immersion decreased with increasing Ca substitution. The formation of HA layer appeared quite rapidly on all of the glasses. Mg and Sr are suspected to be introduced in the HA layer formed at the surface of the glass. The mixed glass (containing both Mg and Sr) seem to be the best candidate for future work on glass scaffold sintering for tissue engineering.

TIIVISTELMÄ

JENNA TAINIO: Magnesiumin ja strontiumin vaikutus bioaktiivisen borosilikaattilasin liukenemiseen ja sintrautumiseen
Tampereen teknillinen yliopisto
Diplomityö, 67 sivua, 8 liitesivua
Marraskuu 2016
Biotekniikan diplomi-insinöörin tutkinto-ohjelma
Pääaine: Kudosteknologia
Tarkastaja: Apulaisprofessori, akatemiatutkija Jonathan Massera

Avainsanat: bioaktiivinen lasi, borosilikaatti, luukudosteknologia, sintraus, liukeneminen

Bioaktiiviset lasit ovat lupaava, suhteellisen uusi materiaaliryhmä, joista valmistettuja tuotteita hyödynnetään kudosteknologian sovelluksissa. Kyseisten materiaalien eräs tärkeimmistä käyttökohteista on rekonstruktiivinen kirurgia, jossa kaupallisia tuotteita hyödynnetään luunsiirteiden korvikkeina, esimerkiksi lasirakeiden ja kittien muodossa. Keinotekoisten, luuta korvaavien sovellusten kysyntä onkin jatkuvassa kasvussa.

Perinteiset bioaktiiviset lasit ovat tyypillisesti piidioksidipohjaisia. Vaikkakin näillä materiaaleilla on useita erinomaisia ominaisuuksia, kuumennusta vaativat käsittelyt saavat niissä aikaan epätoivottua kiteytymistä. Kliinisissä tutkimuksissa on myös havaittu että implantoidut materiaalit eivät ole muuntuneet täysin hydroksiapatiitiksi (HA); yhdisteeksi, jonka luun solut pystyvät korvaamaan regeneroituvalla kudoksella. Booripitoiset lasit ovat monilta ominaisuuksiltaan nykyisiä kaupallisia koostumuksia lupaavampia. Työn tavoitteena oli tutkia, parantuvatko borosilikaattilasin ominaisuudet kun lasin koostumukseen lisätään magnesiumia tai strontiumia. Tutkimuksen perustana käytetty borosilikaattilasi B12,5 (47,1 SiO_2 - 6,7 B_2O_3 - 22,7 Na_2O - 21,8 CaO - 1,7 P_2O_5, mol-%) valmistettiin kaupallisen piidioksidilasin S53P4 koostumusta muuntaen. Osa borosilikaattilasin sisältämästä kalsiumista korvattiin vaihtelevilla magnesium ja/tai strontium pitoisuuksilla. Tämän vaikutusta valmistettujen lasien sintrautuvuuteen ja liukenemiseen arvioitiin tarkastelemalla muutoksia lasien fyysisissä, rakenne- sekä lämpöominaisuuksissa. Työssä tutkittiin yhteensä kuutta eri lasikoostumusta.

Valmistettuen lasien sintrautumista tarkasteltiin useassa lämpötilassa, ja näytteitä analysoitiin pyyhkäisyelektronimikroskopialla (SEM) sekä röntgendiffraktiolla (XRD). Lasien bioaktiivisuutta tutkittiin liottamalla laseja fysiologisia nesteitä simuloivassa SBF-liuoksessa. Näytteiden immersioaika vaihteli kuudesta tunnista kahteen viikkoon. Jokaisen aikapisteen jälkeen immersioliuosten pH mitattiin, sekä liuoksen ionipitoisuus määritettiin induktiivisesti kytketyllä plasma-atomiemissiospektrometrialla (ICP-AES). FTIR-spektroskopiaa käytettiin arvioimaan HA:n muodostumista lasien pinnalle.

Työssä havaittiin magnesiumin ja strontiumin ottaneen lasien rakenteessa kalsiumia vastaava rooli. Yleisesti ottaen, magnesium ja strontium vaikuttivat parantavan lasien yleistä sintrautuvuutta laskemalla lasien viskositeettiä. Tämän lisäksi, kaikkien tutkittujen lasien pinnalle muodostui bioaktiivisuutta indikoiva HA kerros. Lasien liukenevuus laski kun kalsiumpitoisuutta korvattiin kasvavissa määrin. Lasikoostumuksessa, jossa esiintyi sekä magnesiumia että strontiumia, yhdistyi kummankin elementin suotuisat vaikutukset. Tämä koostumus vaikutti lupaavimmalta luukudosteknologian sovelluksiin.

PREFACE

This study was performed in Biomaterials and Tissue Engineering Group of the Institute of Biosciences and Medical Technology (BioMediTech) at the Tampere University of Technology. Part of the experiments were conducted during researcher exchange in Structure-Property Relationship in Glasses Group of the Otto-Schott Institute of Materials Research, Friedrich Schiller University Jena, Germany.

First of all, I would like to express my deepest gratitude to Adj. Prof, Academy Research Fellow Jonathan Massera for offering me the opportunity to work in such an interesting project. I am extremely thankful for his guidance and important insights throughout the process. I am also grateful to Prof. Dr. Delia Brauer for welcoming me to visit her research group. Her excellent advices helped immensely in the successful completion of this thesis.

This thesis would not have been possible without the help and support of a number of wonderful coworkers. In no specific order, I therefore thank Amy (my favourite post-doc), Auysh, Inari, Juliane, Thilo, Nutty, Roland and Hawshan. I am extremely grateful to the whole Biomaterials and Tissue Engineering research group for creating a pleasant and supportive working environment. In addition, I would like to acknowledge Dr. Christian Bocker, Dr. Sindy Furmann, MSc. Christian Teichmann and laboratory technician Nadja Buchert for their help with the analysis of the samples.

I am forever thankful to my parents for their love, support and encouragement. My thanks are also extend to my dear friends, both old and new, for being an important part of this journey by giving me the necessary distractions from my thesis and studies. Most of all, I express my sincere gratitude to my beloved husband Henri. Thank you for always being there for me.

Tampere, 25.10.2016

Jenna Tainio

TABLE OF CONTENTS

ABBREVIATIONS

ATR	Attenuated total reflectance
B	Boron
Ca	Calcium
CaP	Calcium phosphate
DTA	Differential thermal analysis
ECM	Extracellular matrix
EDX	Energy-dispersive X-ray spectroscopy
ESC	Embryonic stem cell
FTIR	Fourier transform infrared spectroscopy
HA	Hydroxyapatite
HCA	Hydroxycarbonated apatite
ICP-OES	Inductively coupled plasma optical emission spectrometry
iPSC	Induced pluripotent stem cell
Mg	Magnesium
mol-%	Molecular percentage
MPa	Megapascal; unit of pressure and stress (N/mm^2)
MSC	Mesenchymal stem cell
Na	Sodium
P	Phosphate
ppm	Parts per million
SBF	Simulated body fluid
SEM	Scanning electron microscopy
Si	Silicon
Sr	Strontium
T_g	Glass transition temperature
T_p	Temperature maximum of the crystallization peak
T_x	Temperature at the onset of the crystallization peak
RT	Room temperature
RPM	Rounds per minute
XRD	X-ray diffraction

m	mass
M_w	molecular weight (g/mol)
ρ	Density (g/cm^3)
V_m	Molar volume (mol/cm^3)

1. INTRODUCTION

Currently, regenerative medicine still utilizes tissue grafts as the golden standard in reconstruction of bone defects. Tissue grafts have many limitations, where the availability is one of the most substantial. Although major progresses in field of bone tissue engineering have been achieved during the years, no adequate bone substitute have yet been developed. (Amini *et al.* 2012; Salgado *et al.* 2004).

Tissue engineering is an interdisciplinary field utilized in regenerative medicine. The main target of tissue engineering is to restore or improve functionality to damaged or diseased tissues. This usually approached by use of implantable temporary structures, referred as scaffolds. Scaffolds are structural matrixes used to support the regenerative tissue. Therefore, it is understandable that the scaffolds need to fulfill many requirements considering both biological and mechanical aspects. For example in field of bone tissue engineering, these include biocompatibility, structural properties such as porosity and surface properties, osteostimulative properties, adequate mechanical properties and biodegradability. Most of the essential properties are attributed to the material from which the device is manufactured. (Langer & Vacanti 1993; Salgado *et al.* 2004).

Bioactive glasses are a relatively young material group, which are categorized under bioceramic materials. In general, a material is considered bioactive when it can evoke a specific biological response at the materials interface, resulting in the formation of a bond between the surrounding tissues and the material. Bioactivity of a glass is a result of the materials composition and its amorphous open network that enables reactions with physiological fluids. The leaching of ions from the glass leads to reaction whereas a hydroxyapatite (HA) layer forms at the glasses surface. The formed HA is similar to the mineral phase of bone, providing an optimum substrate for cells to attach, proliferate and differentiate. Bioactive glasses have, in fact, been among the first synthetic materials shown to form a rapid bonding to bone tissue. (Brauer 2015; Hench & Jones 2015).

Although bioactive glasses have been in clinical use for over thirty years, the commercial applications are still restricted to products such as glass granules and pastes (Jones 2013). Even though the current bioactive glasses on the market hold many desirable properties, they however have been found, for example, to have a strong tendency to undergo crystallization when exposed to heat processing. This limits the possible products obtainable via hot forming. Since the bioactivity of the bioactive glasses is linked to their amorphous structure, crystallization is problematic as it makes the glass network more stable, thus less reactive. (Arstila *et al.* 2008; Bellucci *et al.* 2010; Groh *et al.* 2014; Massera *et al.* 2012a) In addition, in clinical studies remnants of implanted bioactive glass granules can

be found even after 14 years post operation. This indicates that degradation of the material has be restricted, and hence the granules could not been entirely replaced by the regenerating tissue. (Lindfors *et al.* 2010).

Many of the challenges can be linked to the silica-based composition of the commercial glasses. The low silica content along with high alkali and alkaline earth ions in the glass structure leads to a highly disordered and open network that is prone to crystallization. (Arstila *et al.* 2008; Massera *et al.* 2012a). Fortunately, glass properties can be improved by making slight alteration to their compositions. For example, introduction of alkali earth such as magnesium can enhance e.g. the thermal properties of a bioactive glass. (Brink 1997). Borate glasses possess wider hot forming domain and slower crystallization kinetics than bioactive silicate glasses. Therefore, borosilicate glasses containing ions such as Mg can have favourable properties for the processing of scaffolds. In addition, unlike silica-based glasses, borate glasses have higher degradation rate and they have been found to completely convert into HA-like material. Their degradation rate is also adjustable, and can be matched with the regeneration of the tissue. (Huang *et al.* 2006; Rahaman *et al.* 2011).

During this study, the composition of a borosilicate glass was modified by substituting some of the calcium content with magnesium and/or strontium. The addition of Mg was expected to affect to the thermal properties, giving the material a wider temperature range for thermal processing (Massera *et al*. 2012b) and Sr was utilized as it has been, for instance, found to enhance the proliferation of osteoblast; therefore being beneficial for e.g. treatment of osteoporosis (Gentleman *et al.* 2010; Goel, *et al.* 2011). Objective of this thesis was to characterize some of the most essential properties of the produced borosilicate glasses, and assess whether the partial substitution of calcium with magnesium and/or strontium had an impact on *(i)* thermal and sintering properties of the glasses; e.g. to thermal processing window as well as to crystallization tendency, and *(ii)* assess bioactivity of the produced glasses based on *in vitro* dissolution in SBF. Initial aim was to assess if the investigated glass compositions would be suitable for bone tissue engineering applications, e.g. production of scaffolds.

THEORETICAL BACKGROUND

2. TISSUE ENGINEERING OF BONE

Bone is a very forgiving tissue. However, besides major traumas, there exist multiple medical situations which cause loss, failure or need for removal of bone tissue in extent that the tissues natural repair mechanism is impaired. Such causes include for example tumors and cancers, and diseases such as osteoporosis and degenerative disc disease. (Schoeder & Mosheiff 2011). It is worth noting that the need for regenerative medicine increases, as the aging population increases. As a solution to this, a field of tissue engineering has emerged. The main target of tissue engineering is to restore, maintain or improve functionality to damaged or diseased tissues by the means of combining cell biology, material sciences and engineering. (Langer & Vacanti 1993; van Blitterswijk, *et al.* 2008, p. 14-21).

The use of scaffolds, devices that function as template structures and a carrier for biologically active factors, to support the normal regeneration of the tissue. Scaffolds can be utilized either as acellular, or as cellular systems where the matrix is embedded with cells. The biologically active factors can include, besides cells, molecules that stimulate the host tissue cells, such as growth factors. (Rahaman *et al.* 2011; Nguyen *et al.* 2012). Scaffolds used in tissue engineering are usually porous three dimensional (3-D) structures of biocompatible material that provides mechanical support and enables the regeneration of the compensated tissue. (van Blitterswijk *et al.* 2008, p. 404-405). Nowadays, it is preferred that the scaffold, as a foreign material itself inside living body, is removed from the body by the means of degradation and absorption. Therefore, there is need to produce materials which can provide the desired mechanical properties and still degrade during acceptable timeframe. (Hutmacher 2000).

2.1 Biology of the bone

Bone is a complex living tissue comprising cells and the extracellular matrix (ECM). The tissue develops by osteogenesis, the process of ossification, and grows by deposition of additional matrix on free surfaces, i.e. apposition. Bone is continually remodeled by the cells within it. The formation and reformation of the bone tissue is maintained mainly by two different cell types; the osteoblasts (‘bone-forming’) and the osteoclasts (‘bone resorbing’), illustrated in Figure 1. (Alberts *et al.* 2008, p. 1469-1474; Ross & Pawlina 2011, p.219, 223-232).

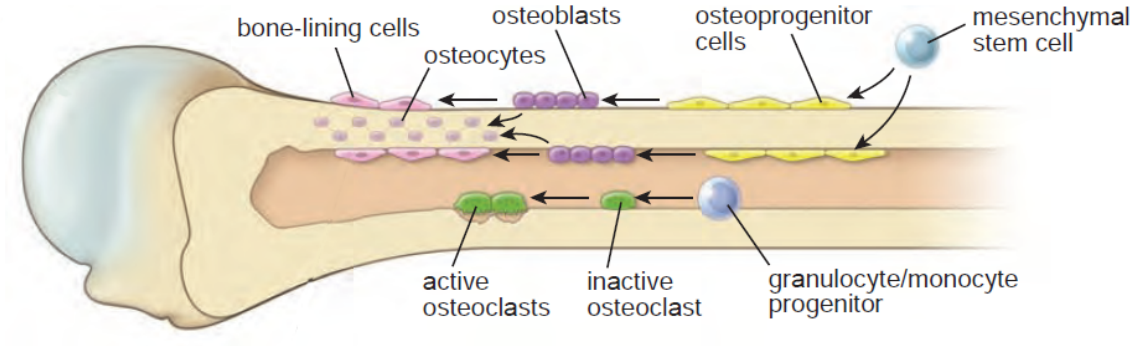

Figure 1. *Schematic drawing of cells associated with bone. Modified from Ross & Pawlina 2011, p. 224.*

Osteoblasts are the cells that secrete the organic ECM of bone, which comprises mainly of type I collagen, in addition with noncollagenous proteins such as osteocalcin, bone sialoprotein and osteopontin. The secreted ECM is initially amorphous and noncrystalline, but gradually mineralizes due to calcium salt deposition. (van Blitterswijk *et al.* 2008, p. 560). When the bone deposition ceases, the osteoblasts give rise to either osteocytes or bone-lining cells. As the name suggests, the cells that remain on the surface of the bone in their resting state are referred as bone-lining cells. Osteocytes are type of osteoblasts, which have eventually been trapped and surrounded by their secreted matrix into spaces called lacunae. Active osteoblasts arise from the bone-lining cells, or are derived from osteoprogenitor cells. Osteoprogenitor cells are, by definition, mesenchymal precursor cells committed to the bone lineage by differentiating into osteoblasts. The mesenchymal precursor or stem cells are located usually in bone marrow or other connective tissue. (Ross & Pawlina 2011, p. 219, 225-227).

As new bone is constantly reformed, similarly the old needs to be removed. The resorption of the bone is conducted by osteoclasts, multi-nuclei phagocytic cells. They differ from their lineage compared to other bone cells, as the osteoclasts are derived from hematopoietic progenitor cells. Osteoclast formation occurs from fusion of macrophage progenitor cells under influence of multiple cytokines, in close association with stromal cells in bone marrow. (Alberts *et al.* 2008 p. 1457; Ross & Pawlina 2011 p. 227-232).

Imbalance or malfunction in the normal process of remodelling can lead to several complications. One of these is osteoporosis, a disease common among post-menopausal women. In osteoporotic bone, osteoclasts resorb too much bone while osteoblasts fail to create enough, resulting in disruption of the bone microarchitecture, leaving the structure porous and prone to fracture. (Gentleman *et al.* 2010).

2.2 Structural properties of bone tissue

Healthy bone is a dynamic and well-organized tissue with high tensile and loading strength. Bone is categorized as a specialized form of connective tissue, composed with the mineralized ECM. The mineralization makes the tissue highly durable, and thus bones are capable to provide supporting system and protection to the human body (van Blitterswijk *et al.* 2008, p. 560). As mentioned, the organic component of the ECM is mainly formed from type I collagen. The elastic collagen fibers located within the matrix provide the framework for tissue structure and additionally, lead to a degree of elasticity within the structure. The inorganic part of the bone is comprised of calcium phosphate (CaP) in form of hydroxyapatite, being the component that provides the structure rigidity. Hence, from materials science perspective, bone can be considered as composite material. Bone as a tissue also serves as a storage site of, for example, calcium and therefore it has a secondary role in homeostatic regulation of blood calcium levels. (Ross & Pawlina 2011, p. 218-219, 241-243; Salgado *et al.* 2004).

Bones can be classified into cortical (also known as dense or compact) bone and trabecular (additionally; spongy or cancellous) bone (illustrated in Figure 2). These types of bone differ in their structure and mechanical properties. Cortical bone has compact structure and it is located on the outside of the bones. Trabecular bone, in the other hand, can be found on the interior of the bone structure; it is highly porous matrix that contains for example hematopoietic tissue, fat tissue and blood vessels. (Nguyen *et al.* 2012).

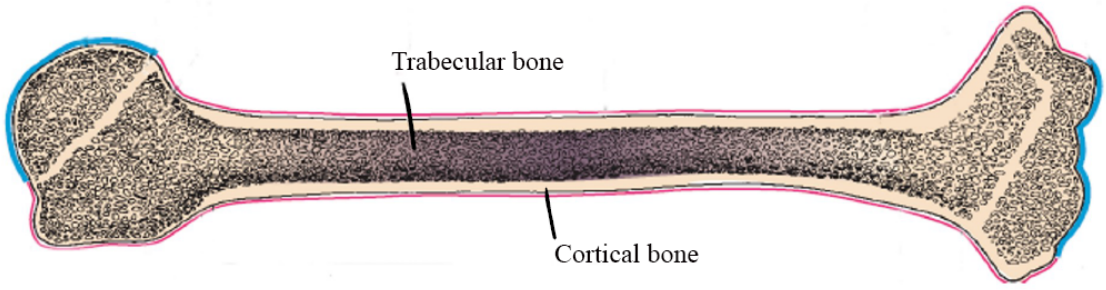

Figure 2. *Bone comprises structurally from dense layer present on the outside of the bone (cortical bone), and a spongelike meshwork on the interior (trabecular bone). Bones are covered by layer of connective tissue, periosteum (indicated in pink), expect for the articular surfaces, which are covered by hyaline cartilage (indicated in blue). Modified from Ross & Pawlina 2011, p. 220.*

Depending on the anatomical sites, bones exist in many different sizes and shapes. The structure of the bone also depends on the maturity of the tissue; mature bone is composed mainly of cylindrical units, which are called osteons or Haversian systems, presented in Figure 3a. Osteons consist of concentric lamellae that surround a central canal system (i.e. osteonal or Haversian canal) which enables the vascularization and nerve supply of the osteon. Immature bone can be found in newborn, fracture calluses or metaphyseal region of growing bone. The structure of immature bone is nonlamellar and the cells are arranged randomly within the tissue, as illustrated in Figure 3b. Immature bone is also referred as woven bone. (van Blitterswijk *et al.* 2008, p. 560-562; Ross & Pawlina 2011, p. 219-223).

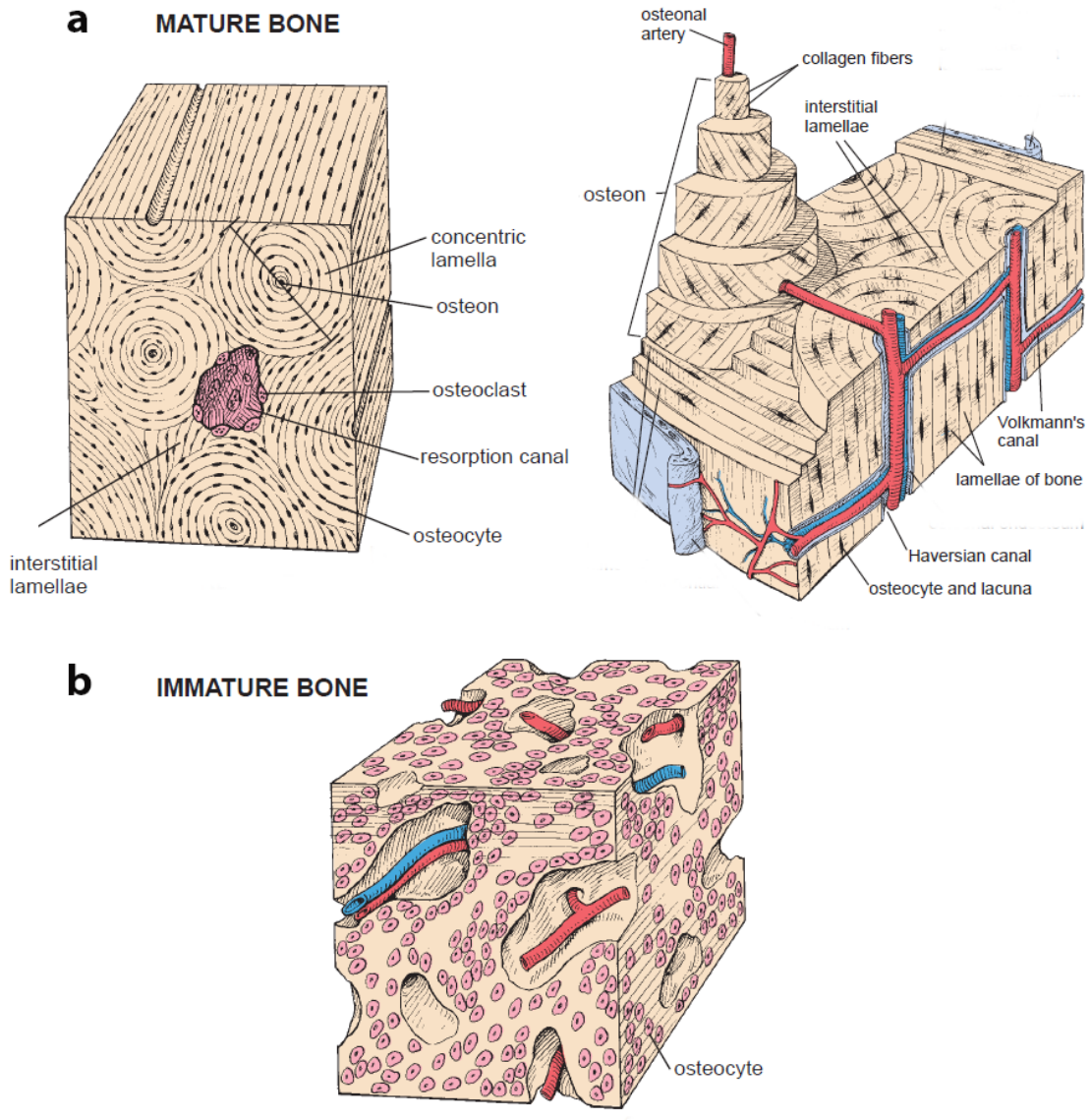

Figure 3. *Structures of mature and immature bone. Modified from Ross & Pawlina 2011, p. 222-223.*

As a result of the oriented structure, mature bone possesses anisotropic mechanical characteristics. This implies that the response and tolerance of the tissue for load applications will be different, depending of the direction of the load in relation to bone structure orientation. Bones are also viscoelastic; the behavior of the tissue differs depending on the speed to which the load is applied. In general, bones tolerate higher forces in the longitudinal direction, as it is also the direction of the natural strain of the tissue in normal conditions. This feature is due to high adaptivity of the bone tissue. The inherent architecture of bone is influenced by applied mechanical stresses via mechanotransduction, and hence e.g. rising mechanical demand from the environment may result in notable changes within the structure. This structure-function relationship of the bone tissue was determined and described as Wolff's law already in 1892. (Bankoff 2012; Sikavitsas *et al.* 2001).

2.3 Current methods of treatment

To certain extant, bones are able to reform by themselves through the bone repair mechanism, and via constant remodeling. However, due to the magnitude of fracture, infection or other causes, in some cases reconstructive surgery is needed. Large bone defects, beyond the normal potential of self-healing, are usually treated with implants or transplants. (Amini *et al.* 2012; Meyer *et al.* 2009, p. 211-212; Salgado *et al.* 2004; Schoeder & Mosheiff 2011).

For decades, the use of grafts has been the golden standard in tissue engineering. In grafting, bone from somewhere else is applied to stimulate the formation of new bone. In fact, bone is one of the most transplanted tissue after blood. (Dimitriou *et al.* 2011). The use of grafts as a treatment method has however some noteworthy disadvantages. For example, autologous grafts that are harvested from patients own locations of relative excess, e.g. from pelvis, prolong patients operation and healing time. Availability of the tissue is limited, and there is also increase of the risk of surgical complications, such as excess pain or infections. With allogenic and xenogenic grafts, tissue harvested from individuals of same or different species, respectively, lies a risk of immunogenicity problems and transmission of diseases. Additionally the sterilization steps and preservation of the harvested tissue can affect and change the material's properties substantially. (Salgado *et al.* 2004; Schoeder & Mosheiff 2011; van Blitterswijk *et al.* 2008, p. 563-567)

Bone fractures and other defects will in the future increase due to ageing population. As the availability of graft tissue is already limited, there is therefore an ever increasing demand for alternative, adequate solutions. (Langer & Vacanti 1993).

2.4 Stem cells in tissue engineering

Stem cells are defined as unspecialized cells with ability to renew themselves, but also to differentiate in various specialized cell types. Stem cells are usually divided by their differentiation capacity to totipotent, pluripotent, multipotent, oligopotent and unipotent stem cells. The most potent ones are the totipotent stem cells, which have the ability to form an entire organism. (van Blitterswijk *et al.* 2008, p. 2-3; Kolios & Moodley 2012).

Pluripotent stem cells, such as embryonic stem cells (ESC) and induced pluripotent stem cells (iPSC), are under high interest in current research. While ESCs and iPS cells have shown nearly unlimited differential potential, the applications are still limited by ethical and legal concerns, as well as by issues of efficacy and safety. Because of this, as an alternative approach of tissue-specific multipotent stem cells circumvent many of the mentioned concerns. These cells can therefore be utilized in tissue engineering applications. (Gimble *et al.* 2007; Lindroos *et al.* 2011; Takahashi *et al.* 2007).

Multipotency indicates the ability to form multiple cell lines. Despite multipotent stem cells such as the mesenchymal stem cells (MSCs) cannot differentiate in every type of tissue, they can be easily harvested and isolated, and additionally the cell culture is easily expanded. MSCs are a population of self-renewing, undifferentiated cells, which reside in differentiated tissues. As MSCs can be derived from adult human beings, they are ethically the least controversial stem cell type. (Gimble *et al.* 2007; Kokai *et al.* 2014; Kolios & Moodley 2012). MSCs have ability to differentiate many different pathways towards multiple cell lines, including osteoblasts, adipocytes and chondroblasts, and also large variety of other specialized mesenchymal cell types, as for example myocytes, tendocytes and ligament cells. (Lindroos *et al.* 2011). MSCs can be harvested from easily-accessible tissues, such as bone marrow, fat or muscle tissue, but ultimately have been found from nearly every type of tissue (Romagnoli & Brandi 2014; Tsuji *et al.* 2014).

As mentioned, mesenchymal stem cells have excellent osteogenic differentiation capacity, as one of these cell lineages are the osteoprogenitor-derived bone cells (Ross & Pawlina 2011, p. 225). The differentiation may be induced via several mechanisms. One of the major methods is chemical stimulation e.g. with growth factors, but also the biophysical effects and stimulation are considered to be important regulators in bone formation. It has been studied, that even the degradation byproducts from implant material can induce the differentiation. (Gimble *et al.* 2007; Hench & Jones 2015; Lindroos *et al.* 2011).

2.5 Scaffolds for bone applications

Scaffolds are the temporary template structures used to support and promote regeneration of the damaged tissue. To great extent, the selected material will determine the most essential properties of the scaffold. (Salgado *et al.* 2004).

2.5.1 Properties

Several essential aspects need to be regarded when designing scaffold properties, both from the biological and the mechanical point of view. First, it is most important that the scaffold is tolerated by the host tissue. Therefore, the desired properties for scaffold material include biocompatibility; ability to induce appropriate host response depending on the application, and promotion of cell adhesion and proliferation. (Hench & Wilson 2013, p. 1-26; Hutmacher 2000; Baino *et al.* 2011). Permanent implant materials are associated with undesirable reactions, such as infections, corrosion, fatigue and failure, which eventually result in implant replacement. In addition, there are concerns about stress shielding; a phenomena when natural load is transmitted only through the implant, and not to the surrounding bone. When bones are not loaded, osteoclast activity overcomes formation of new bone, and loss in bone volume occurs. (Hench & Jones 2015; Salgado *et al.* 2004). Nowadays, many new generation implant materials are preferred as biodegradable, i.e. the implanted material is gradually, and eventually wholly replaced by the regenerating tissue. Therefore, the degradation products that the material releases should be easily resorbed or excreted by body, and additionally released by metabolically accepted rates, as the cells of the host tissue need to, in most cases, handle large quantities of the material. (Brauer *et al.* 2006; van Blitterswijk *et al.* 2008, p. 569-570 ; Hench & Wilson 2013, p.5-9; Hupa *et al.* 2016). It is also beneficial that the scaffold promotes bioactivity. Bioactivity can be determined as materials ability to induct specific biological activity, which is usually indicated by materials ability to undergo specific surface reactions when implanted into the body, i.e. *in vivo*. The ability of a material to form a hydroxyapatite-like surface is often taken as an indication of bioactivity, as it has been found to promote the formation of new bone. (Brauer 2015; Rahaman *et al.* 2010).

The structure of the implanted device needs to be porous, with interconnected porous network to enable the penetration of cells, tissue ingrowth, vascularization and diffusion of nutrients (Salgado *et al.* 2004; van Blitterswijk *et al.* 2008, p. 569). Certain pore size is needed to produce desirable effects; for instance, too small pores (diameter smaller than 100 µm) can contribute the formation of fibrous tissue instead of bone. The pore size over 300 µm has been found to be beneficial for enhancing new bone formation and formation of capillaries. (Karageorgiou & Kaplan 2005). However, the microporosity can be crucial as it results in large surface area of the material, which contributes to protein and cell adhesion (Vitale-Brovarone *et al.* 2008).

As the bone tissue is a rigid structure under continuous stress, also the scaffolds should possess sufficient mechanical properties. Ideally, mechanical properties of the scaffold should match those of the native bone tissue, which are different for e.g. maxillofacial and load bearing sites. Furthermore the type, size and location of the bone cause variation to the requirements. For example, compressive strength, which indicates materials capacity to withstand loads, for cancellous bone can range from 2 to 12 MPa, and for cortical bone 100-230 MPa. (Hench & Wilson 2013, p. 13; Salgado *et al.* 2004). Bone tissues

have also other characteristic properties such as tensile strength; capacity to withstand elongation, and elastic modules i.e. stiffness. As porosity of the material affects greatly to mechanical properties of a device, a compromise between mechanical properties of the device and density of the pores has usually to be made. (Chen *et al.* 2006). The mechanical properties of the implantable devices shouldn't either exceed the mechanical properties of the host bone, as the stress shielding effect may cause further loss of the contacted bone (i.e. osteolysis). (van Blitterswijk *et al.* 2008, p. 565).

Additionally, treatment of large segmental bone defects can be a significant challenge due to need of incorporation of vascular networks within engineered bone constructs. The processability of the scaffold material is important, as the devices are needed in anatomically relevant shapes, sizes and dimensions, depending on the nature of the surrounding intact bone and soft tissue. (Amini *et al.* 2012; Hutmacher 2000; Nguyen *et al.* 2012).

2.5.2 Materials

Many different materials are utilized in bone related applications, ranging from the permanent metallic implants to biodegradable materials, such as bioceramics, and biodegradable polymers of both natural and synthetic origin. One of the new interests are composite materials, which can combine the good properties of the components to overcome the limitations of the raw materials. (Baino *et al.* 2015; Liu *et al.* 2013; Rahaman *et al.* 2000; Salgado *et al.* 2004). One example are the mentioned bioceramics, which despite being otherwise promising group of materials, are brittle and do not tolerate cyclic loads. The brittleness of the ceramics can be avoided by combining them with viscoelastic polymers, which by themselves suffer from poor strength. Therefore, hybrid devices prepared from these type of materials have the potential to be durable with adjustable properties, such as tailored degradation rate. (Hench 1991; Jones 2013).

Bioactive ceramics are artificial materials with ability to form a chemical bond with bone. According to previous studies, bioactive glasses are more efficient in formation of bond between the tissue and the material, and additionally more potent to stimulate the regeneration of the tissue than other bioactive ceramics. However, bioactive glasses still lag behind other bioceramics in terms of commercial success. (Hench 2006; Jones 2013).

3. BIOACTIVE GLASSES

Glass is considered bioactive, when it can evoke a specific biological response at the materials interface, resulting in the formation of a bond between the surrounding tissues and the material. Bioactive glasses are a relatively young material group, which can be categorized under ceramics. Mainly, their interesting properties are generated by materials composition and structure. Bioactive glasses have been among the first synthetic material to be shown to form a rapid bonding to bone tissue. (Brauer 2015; Hench & Jones 2015).

3.1 Glass structure

The composition of the glass determines several properties of the material. Some to mention are for example the thermal properties, bioactivity and overall degradation rate. For the glass to be bioactive, in general, it has been noted that composition requirements are following; the silica content must be less than 60% (which, in comparison, is in normal window glass over 70%), and the composition needs to have high Na_2O and CaO content with high CaO/P_2O_5 ratio. Composition of this kind makes the glasses surface reactive in physiological fluids. The glass' tendency to react in aqueous solution depends on the relative proportion of bridging and non-bridging bonds in the glass network. (Hench & Jones 2015; Rahaman *et al.* 2011).

Glass is amorphous with a continuous and random network. This network is formed, in general, of three different components; network forming ions, network modifiers and intermediate oxides. This is illustrated in Figure 4.

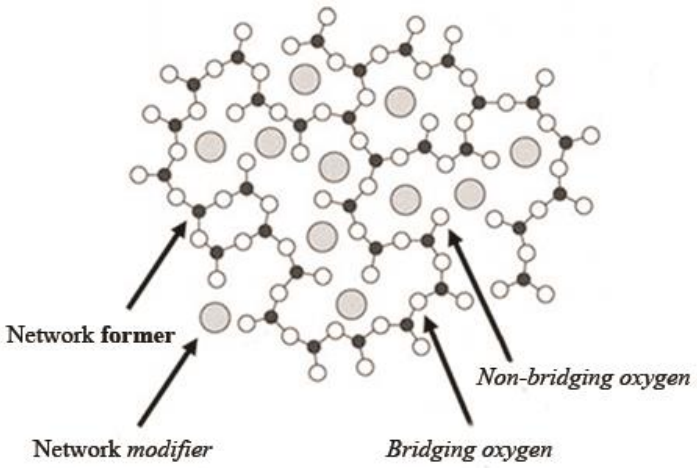

Figure 4. *Illustration of bioactive glass network. The network consists of network forming ions, network modifiers, and intermediate oxygens. Modified from Hench & Wilson 2013, p. 18.*

Network formers include components such as silica (SiO_2), phosphorus pentoxide (P_2O_5) and boron trioxide (B_2O_3). Glass network thus in these cases forms from Si, P and B that are connected with bridging oxygens. Network modifiers affect the structure by forming ionic bonds with the bridging oxygens, turning them into non-bridging and making the structure more disrupted, open and, in the case of silicate glasses, more reactive. Modifiers typically include alkali or alkaline-earth metals as oxides. Intermediate oxygens can function in both roles; as network modifiers, or possibly enter the network forming the backbone structure. This is the case for example of Al_2O_3 or ZnO. (Brauer 2015; Hench & Wilson 2013, p.18-19).

3.2 Bioactivity

Reactivity of the bioactive glasses comes from their more open network compared to the conventional glasses. When bioactive glasses come in contact with aqueous solutions, they start to dissolve and release ions to their surroundings, making them surface-active biomaterials. As a result of the ion release and network dissolution, the surrounding of the glass is saturated with Ca^{2+} ions. Supersaturation of the surrounding medium leads to the formation of an apatite surface layer. This phenomenon is often referred to as bioactivity, although somewhat incorrectly as the apatite formation by itself does not prove the biocompatibility or functionality in *in vivo* conditions. (Brauer 2015; Rahaman *et al.* 2011.) The hydroxycarbonated apatite (HCA) layer on the surface of the glass does however enable the ability of bioactive glasses to form a strong bond with living, primarily bone, tissue. HCA is similar to bone mineral and is thought to interact with collagen fibrils to integrate with the host bone. It has been extensively proved that with this bonding, bioactive glasses are able to create a stable interface that trigger a range of biological responses, such as tissue regeneration and angiogenesis, while the glass degrades over time. (Hench 2006; Jones 2013; Rahaman *et al.* 2011).

It has been found that *in vivo*, bioactive glass stimulates more rapid bone repair than other bioactive ceramics. In addition, bioactive glasses possess antibacterial properties. The osteoinductive properties of the glass are thought to be due to the dissolution products of the glass, i.e. soluble silica and calcium ions that stimulate osteogenic cells to produce bone matrix. In *in vitro* studies this has been shown to cause stimulation of genes in primary human osteoblasts. (Oonishi *et al.* 2000; Xynos *et al.* 2001). Bioactive glasses can be further incorporated with trace quantities of other elements which are known to be beneficial for healthy bone growth (Hench & Jones 2015).

Currently, there exist a standard used in *in vitro* evaluation for apatite-forming ability of implant materials. The standard specifies a method for detecting apatite formed on a surface of a material in simulated body fluid (SBF). It is applicable to implant surfaces intended to come into direct bone contact. (ISO 23317:2014). The standard is intended to provide research laboratories around the world a protocol to allow comparison of dissolution rates and apatite nucleation. The standard in its current form does take into account

the surface area of the analyzed bioactive glass. The surface area that is in contact with the surrounding aqueous medium is a critical factor in reaction rate. Therefore, Macon *et al.* 2015 proposed a new unified method, where fixed mass per solution volume ratio and agitated solution is used. This method has proved to be efficient in studying and comparing samples with similar density. It should however be noted, that *in vitro* testing does not truly match conditions *in vivo*, as SBF does not exactly match those of the human body. Therefore, also *in vitro* cell tests need to be conducted to gain more appropriate estimation about the possible *in vivo* reactivity. (Bohner & Lemaitre 2009; Macon *et al.* 2015).

3.3 Processing by heat treatment

As previously mentioned, there is an increasing demand and interest to prepare porous scaffolds from bioactive glass. This could be achieved using several methods, including for example chemically-based sol-gel-method, polymer foam replication, freeze-casting and 3D-printing (Fu *et al.* 2011a,b; Jones *et al.* 2006). In this thesis the focus of interest is thermal bonding, i.e. sintering. With this processing method, a scaffolds with various geometry can be prepared without the need of complex machinery. (Baino & Vitale-Brovarone 2011).

Glasses are conventionally produced by melting precursor compounds in high temperatures and fast quenching. The obtained structure is liquid-like. Sintering refers to thermal bonding of glass particles, where material is heat treated from room temperature to an elevated temperatures, resulting in spontaneous adhesion and a solid structure. If a desired geometry or a shape is made from the glass particles, it is referred as forming. Sintering occurs by thermal activation, i.e. heating, of molecules; the reduction of surface energy gradients drives the grain interfaces to contact and eventually fuse together. In the late stages of sintering, pores between the particles are closed and grains become tightly bonded. Grain boundary diffusion and other related phenomena depend of for example processing temperature, atmosphere and of composition of the material. Sintering is a processing method that can be used to produce materials with controlled microstructure and porosity. (Bellucci *et al.* 2010; Hench & Wilson 2013, p. 15-22; De Jonghe & Rahaman 2003). The sintering process is illustrated in Figure 5.

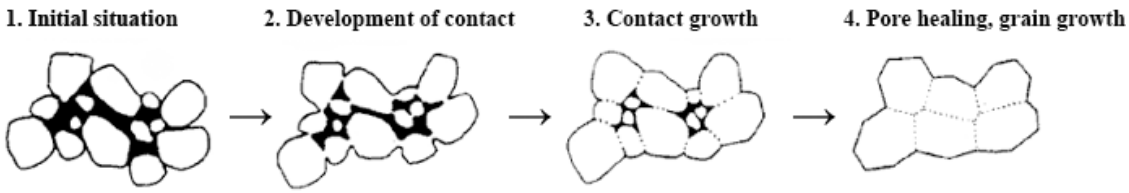

Figure 5. *Stages of sintering. Early stages, development of contact (**1,2**), followed by contact growth (**3**) and eventually, sintered product (**4**). Modified from figure available at keramvarband.de, 2016.*

All glasses pertaining to their amorphous structure exhibits a glass transition temperature or domain (T_g) which is the interval where a system transforms from a supercooled liquid to a solid glass (Brauer 2015). Viscous flow sintering happens above this temperature. At certain temperature, the network starts to form in more orderly structure. This temperature is referred as onset of crystallization (T_x). These temperatures are characteristic for each glass composition, and depend also from several conditions, such as the volume or size of the analyzed glass specimen. Glasses, by definition, are distinguished from other ceramics by having random network. Crystallization in the structure can happen during the preparation of glass, or in further processing steps. Therefore, processing window for heat treatment or hot forming for glass is referred as the temperature range between T_g and T_x (Arstila *et al.* 2007; Rahaman *et al.* 2011). Crystallized glasses or a glass-ceramics have more arranged or ordered network, and are, typically, less reactive to surrounding conditions. Due to their low silica content, bioactive glasses such as 45S5 and S53P4 are susceptible to crystallization during heat treatments and forming operations. The tendency depends on the glass composition, but also from glasses surface condition. For example, surface defects are prone to function as a nucleation site. (Arstila *et al.* 2008; Fagerlund *et al.* 2012; Massera *et al.* 2012a, 2015a).

3.4 Current commercial products

The first bioactive glass – BioGlass® 45S5 – developed by Larry Hench in 1969, was approved to clinical use already in 1985 and is currently sold under trade names such as NovaBone and PerioGlas (Hench & Jones 2015; Jones 2013). The composition of 45S5, presented in molecular percentage (mol-%) is SiO_2 46.3%, Na_2O 24.3%, CaO 26.9% and P_2O_5 2.5%. Since then, few other glass composition have been approved to clinical use; for some to mention, bioactive glass 13–93 and S53P4 (BonAlive®). 13-93 (composition of SiO_2 54.6%, CaO 22.1%, K_2O 7.9 %, MgO 7.7%, Na_2O 6%P_2O_5 1.7% in mol-%) is a silicate glass based on 45S5, with higher SiO_2 and additional network modifiers, is approved for *in vivo* use in Europe. (Brown *et al.* 2008; Rahaman *et al.* 2011). S53P4, the first non-45S5 composition to reach markets, is osteostimulative bioactive glass with composition of SiO_2 53.9%, Na_2O 22.7%, CaO 21.8%, P_2O_5 1.7% in mol-%. (BonAlive Biomaterials 2016; Hench & Jones 2015).

Already, bioactive glasses have been utilized in many dental and tissue engineering applications, such as in repair of a variety of craniofacial, maxillofacial, and periodontal defects. (Baino *et al.* 2015; Brauer 2015) However, despite being available for over 30 years, clinical applications for these materials are still restricted mostly to glass granules and pastes, where glass is present in form of fine powder. (BonAlive Biomaterials 2016; Hench & Jones 2015).

Feature in common with commercial bioactive glasses is that they are usually silica-based. They, otherwise excellent materials, have been found to possess some restrictive properties, such as tendency to crystallize. Crystallization of bioactive glasses is problematic, as the more stable structure is in chemical respect less reactive. Commercial glasses, such as 45S5, crystallize because of their low thermal stability and therefore are not suitable to be used in applications or products which require heat-treatments. (Arstila *et al.* 2008; Fagerlund *et al.* 2012; Massera *et al.*, 2012a; Vedel *et al.* 2007). Additionally, in clinical trials utilizing S53P4 as bone graft substitute in benign bone tumor surgery, it was found that even after being 14 years *in vivo*, remnants of the used glass granules were still observed in some patient cases. (Lindfors *et al.* 2010). This indicates that the used glass did not completely degrade, as bones' remodeling system was not able to completely overturn it. This is partly attributable to non-congruent dissolution mechanism of silicate bioactive glasses and the formation of the HA layer as well as the SiO_2-rich layer, which will act as a barrier to the glass dissolution. The degradation rate is a property that can be controlled by making changes in the glass composition. This way, it should be possible to match the degradation rate of bioactive glass with the bone regeneration rate. (Rahaman *et al.* 2011).

3.5 Modification of the glass composition

Besides degradation rate, the bioactivity of the glass can be changed by tailoring the composition in a way that the material also can serve as a source of many of the minor elements known to favor bone growth. As the glass degrades *in vivo*, these elements are to be released at a biologically acceptable rate. (Rahaman *et al.* 2011).

3.5.1 Borate-based bioactive glasses

Borate-based glasses have been shown to have especially desirable bioactive properties. They can be produced by replacing the SiO_2 in silicate glass with B_2O_3 partially or fully, yielding respectively a borosilicate or borate bioactive glass. Like other bioactive glasses, borate glasses have been shown to support cell proliferation and differentiation *in vitro*, and tissue infiltration *in vivo*. (Marion *et al*. 2005; Fu *et al.* 2009, 2010). There has been some concern about boron's toxicity as released boron ions in the solution. This has sometimes been the case in conventional, static *in vitro* cell cultures, however in dynamic cultures and *in vivo* conditions, the toxicity has been diminished. (Huang *et al.* 2006). In fact,

borate bioactive glasses have been found to possess enhanced bone formation properties when compared to silicate bioactive glasses; controlled release of boron ions have displayed osteogenic and angiogenic properties. (Durand *et al.* 2015; George 2015; Rahaman *et al.* 2011; Zhang *et al.* 2010). The borate-based glasses have lower chemical durability than in silicate 45S5, or 13-93 glass. This contributes in a way that the borate glasses degrade faster than the commercial silica glasses, and in addition can convert more completely to HA-like material. Hence, borate glasses are eventually more likely to be replaced by the bone remodeling mechanism. (Liang *et al.* 2008; Rahaman *et al.* 2011).

3.5.2 Addition of alkali earth metals

Calcium, one typical elements in bioactive glasses, can be found in group 2A of the periodic table; belonging thus to alkaline earth metals. In modification of glass composition, e.g. the calcium can be replaced or substituted with other elements from the same group, which share chemically similar properties. (Brauer 2015; Brink 1997; Rahaman *et al.* 2011).

Partial substitution of the CaO with MgO has not been found to greatly affect the ion release kinetics, but can slightly increase the overall durability of the material. Mg seems to contribute towards stronger glass network, which makes materials reactivity in SBF decrease to some extent, however providing also better resistance to crystallization. In addition, the glass transition temperature decreases, as the crystallization peak emerges in higher temperature; giving the material wider thermal processing range. (Hupa *et al.* 2016; Massera *et al.* 2012b.). Mg is an interesting elements for bone tissue engineering applications as it additionally has an important role in bone development, by stimulating osteoblast proliferation and angiogenesis. (Ma *et al.* 2010; Massera *et al.* 2012b)

In the other hand, strontium shares some biological effects that are related to the chemical similarities to calcium. In bioactive glass, the strontium exists in form of SrO. Replacing CaO with SrO has been found to increase the initial dissolution rate of the glass in SBF, indicating faster reaction with the physiological fluids, and thus faster degradation in physiological conditions. Therefore, doping the glass with Sr can enable the modification of the glass resorption rate to match with the new bone formation, while simultaneously releasing Sr ions which can be beneficial to the ossification. Sr has also been found to substitute some of the Ca in HA layer. (Fredholm *et al.* 2010, 2012; Hupa *et al.* 2016; Isaac *et al.* 2011; Massera & Hupa 2014). Strontium has so called bone-seeking properties, and therefore it has been found interesting for the purpose of treating osteoporosis already in the 1950s (Goel, *et al.* 2011). It has been shown that ions released from bioactive glass, where some of the Ca has been substituted with Sr, enhance the metabolic activity in osteoblasts while inhibiting the activity in osteoclasts, promoting thus new bone formation and strengthening of the original tissue; property useful e.g. in treatment of osteoporosis (Bonnelye *et al.* 2008*;* Gentleman *et al.* 2010; Massera *et al.* 2015b).

EXPERIMENTAL PART

4. MATERIALS AND METHODS

The objective of the study was to assess the impact of Mg and Sr on the thermal and dissolution properties of a borosilicate bioactive glass. The aim was to define a glass with thermal properties enabling thermal sintering without inducing crystallization while converting more completely to hydroxyapatite without too large release of boron.

A base borosilicate glass with potential for tissue engineering was used as starting glass composition. The Ca was replaced with up to 10 mol% of Mg and or Sr. The thermal properties as well as the dissolution in simulated body fluid (SBF) of the glasses were studied for two particle sizes.

4.1 Preparation of the samples

Borosilicate glass with composition of 47.12 SiO_2 – 6.73 B_2O_2 – 21.77CaO – 22.65 Na_2O – 1.72 P_2O_5 in mole percentage (mol%) was used as a base glass for this study. The glass was referred as B12.5. This composition is a modification of the commercial silicate bioactive glass S53P4 (BonAlive Biomaterials Ltd, Turku, Finland), where 12.5 mol% of the SiO_2 was substituted with B_2O_3. Tests with glasses containing larger substitution of B_2O_3 for SiO_2 have been conducted in the Master's thesis of Ojha, 2016.

Six different glass compositions based on B12.5 were prepared for the study. The glasses of investigation follow the general equation: 47.12 SiO_2 – 6.73 B_2O_2 – 21.77 (-x-y) CaO – 22.65 Na_2O – 1.72 P_2O_5 – x MgO – y SrO (mol%), where x,y = 0, 5 or 10 mol%. The glass composition are presented in Table 1.

Batches were prepared from mixtures of sand (99,4 % of pure SiO_2) and analytical grades of reagents acquired from Sigma Aldrich (H_3BO_2, MgO, $SrCO_3$, $(NH_4)H_2PO_4$, Na_2CO_3) and ThermoFisher ($CaCO_3$). The glasses were melted in a platinum crucible, in a Nabertherm P310 (Nabertherm GmbH, Lilienhal, Germany) electric furnace. Melting was conducted in air, from room temperature (RT) at rate of ~10 °C/min to 800 °C, where melt was let to stabilize for 15 min. The aim of this isothermal step was to let the reagent decompose and control the batch foaming. The batch was then heat up to 1300 °C at a heating rate of ~26 °C/min and held for 30 min. The melt was then casted into a graphite mold and annealed at 500 °C for 5 hours in Nabertherm P330 electric oven, and let to cool to RT overnight. The heat treatment is also presented in Table 2.

Table 1. *Compositions (in mol%) of the novel borosilicate glass batches.*

Glass / composition	**B12.5**	B12.5 - **Mg5**	B12.5- **Mg10**	B12.5- **Sr5**	B12.5- **Sr10**	B12.5-**Mg5-Sr10 ('mix')**
SiO_2	47.12	47.12	47.12	47.12	47.12	47.12
B_2O_3	6.73	6.73	6.73	6.73	6.73	6.73
CaO	21.77	16.77	11.77	16.77	11.77	6.77
Na_2O	22.66	22.66	22.66	22.66	22.66	22.66
P_2O_5	1.72	1.72	1.72	1.72	1.72	1.72
MgO	-	5	10	-	-	5
SrO	-	-	-	5	10	10

Table 2. *Thermal cycle for the processing of the glasses.*

Protocol	**Time**	**End temperature**
Heating ~ 10 °C /min	80 min	800 °C
Stabilization	15 min	
Heating ~ 26 °C /min	50 min	1300 °C
Stabilization	30 min	
Casting to a graphite mold, and then annealed in preheated electrical oven		
Annealing	~ 5 h	500 °C
Cooling	overnight	RT

After melting, the glasses were grinded to two different particle sizes. The block obtained from melting was crushed first in a mortar and pestle to obtain coarse particles, sieved with test sieves (Retsch Gmbh, Germany). Particles in the range 250-500 µm were collected. The rest of the glass was milled further with ball mill (KM 1, Janetzki, Poland) and mortar and pestle to obtain finer particles of diameters smaller than 38 µm. These particle sizes were used to study the thermal properties, sintering and dissolution of the glass compositions. The accurate particle size distribution of the grinded glasses was analyzed with Mastersizer 2000 with Hydro 2000S module (Malvern Instruments, Worcestershire, United Kingdom).

4.2 Physical properties

The final density of the prepared compositions was measured using two different methods; Archimedes' principle in water for the bulk material, melt-derived glass blocks with three to four parallel measurements, and helium pycnometry for untreated coarse glass particles. The gas displacement helium pycnometer AccuPyc 1330 (Micromeritics, Georgia, USA) was used with an accuracy of ± 0.01 g/cm^3.

Archimedes' principle is based on the assumption that an object of density (ρ) in a fluid has a buoyant force equal to the weight of displaced fluid, while

m_{fluid} = Apparent weight in fluid of density ρ_o

m_{air} = Weight of object determined in air

$$\rho = \rho_o * \frac{m_{air}}{m_{air} - m_{fluid}} \quad (1)$$

Based on the results, molar volume (V_m) was calculated using the following equation:

$$V_m = \frac{\sum x_i M_i}{\rho} \quad (2)$$

where ρ is the measured density, x_i is molar fraction of i glass component and M_i is the molecular weight for component i. (Sharmin *et al.* 2013).

4.3 Structural properties

Molecular vibrations in the glasses of investigation were assessed via Raman spectroscopy (InVia confocal Raman microscope, Renishaw, UK). The measurements were performed on block materials. The wavelength of the laser was 514 nm, the laser power was 100 W, the exposure time was 10 s and 20 accumulations were recorded for within the range 200-1500 cm^{-1}. All spectrum were baseline corrected and normalized to the band with maximum intensity.

To complement the structural analysis, Fourier transform infra-red (FTIR) Spectrum One FTIR (PerkinElmer, Inc., USA) in attenuated total reflectance (ATR) mode was used. Measurements were performed on powdered glasses for untreated fine particle size < 38 µm. All FTIR spectra were recorded within the range 600-4000 cm^{-1}, corrected for Fresnel losses and normalized to the absorption band showing the maximum intensity.

4.4 Thermal properties and sintering

For determination of sintering temperatures, differential thermal analysis (DTA) was needed. Sintering was then conducted for both coarse and fine glass particles of all studied compositions.

4.4.1 Differential thermal analysis

SDTA was conducted for both coarse and fine particle sizes with STA 449 F1 Jupiter Simultaneous Thermal Analyzer (Netzsch Group, Selb, Germany) in Pt-Rd crucibles. The heating was conducted at a rate of 10 °C/min from 40 °C to 1200 °C in N_2 atmosphere. Temperatures for the glass transition (T_g), onset of crystallization (T_x) and the crystallization peak (T_p) were determined from the acquired data. Example of a thermograph and position of the temperatures of interest is presented Figure 6.

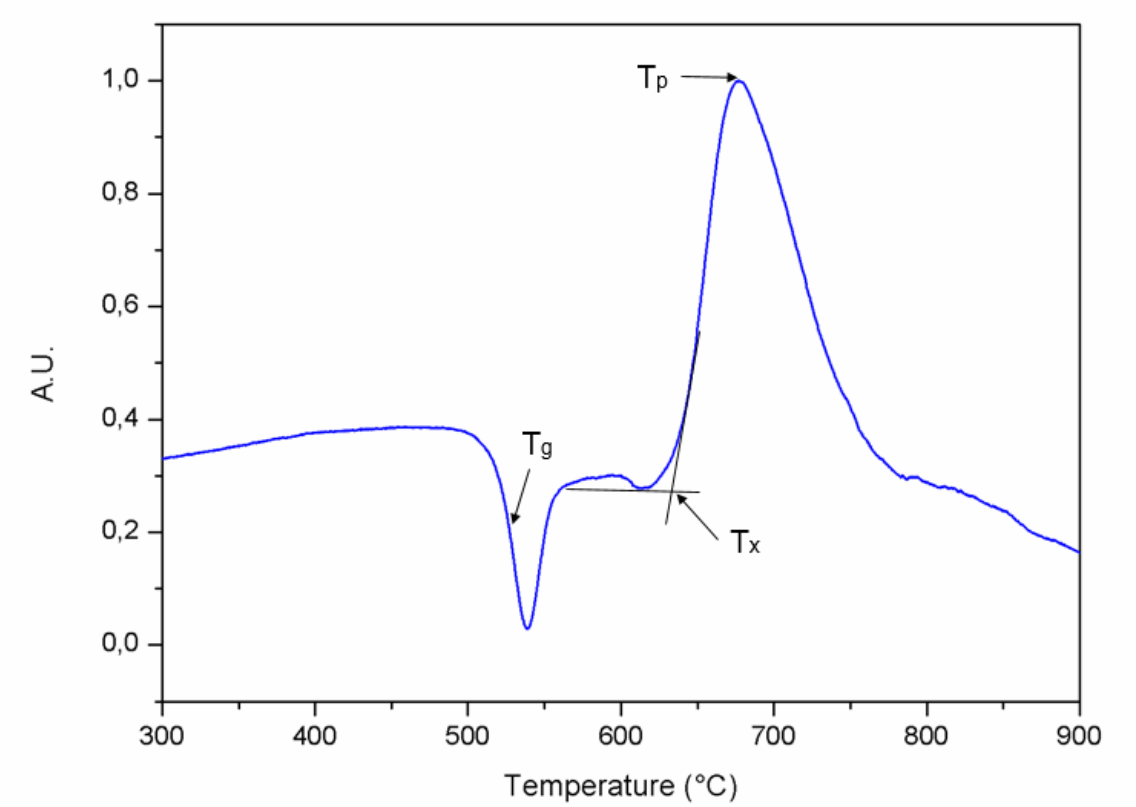

Figure 6. *Example of a SDTA thermogram recorded for glasses with composition B12.5, indicating the position of the temperature of interest; glass transition temperature (T_g), onset of crystallization (T_x) and maximum of the crystallization peak (T_p).*

The glass transition temperature was taken at the inflection point of the first endothermic event. The onset of crystallization was taken at the beginning of the crystallization peak (tangent method) and the crystallization temperature at the maximum of exothermic peak. Working range (ΔT) is an indication of the glass stability to crystallization and corresponds to $\Delta T = T_x - T_g$.

4.4.2 Sintering

The glass particles were sintered in an electrical furnace (Nabertherm B410), in a stainless steel mold. The mold contained cylindrical holes of 10 mm depth and 5mm diameter, where internal sides were covered with boron nitride to reduce the attachment of glass to the mold surface.

Several sintering conditions were tested for glass samples of size [250,500] µm, 'coarse particles' and < 38 µm, 'fine particles' before the proper test series. Fine particle size specimens were heated at the rate of 20 °C /min from RT to temperatures of T_x - 20 °C, T_x - 40 °C and T_x - 60 °C ±2 °C, temperatures characteristic for each glass composition, presented in Table 3. Here T_x corresponds to the onset of crystallization recorded using

the SDTA thermogram for the various glass composition using the fine particle size. The sintering temperature was held constant for 1h, then the samples were let to cool down to RT overnight. Similar heat-treatment was tested for the coarse glass of B12.5 at various temperatures ranging from 561 °C – 638 °C, i.e. from T_x-130 °C to temperature of T_x, where T_x corresponds to the onset of crystallization recorded using the SDTA thermogram using the coarse particle size.

Table 3. *Sintering temperatures studied for all glasses with fine particles size < 38 µm.*

glass / T	**T_x - 60 (°C)**	**T_x - 40 (°C)**	**T_x - 20 (°C)**
B12.5	578	598	618
B12.5-Mg5	590	612	632
B12.5-Mg10	600	620	640
B12.5-Sr5	562	580	604
B12.5-Sr10	570	590	610
B12.5-Mg5-Sr10	551	570	590

Scanning electron microscopy (SEM) combined with energy-dispersive X-ray spectroscopy (EDX), and X-ray diffraction (XRD) were performed to evidence crystallization and/or phase separation. For the EDX, sintered specimen were cut in half and the fracture surface of the samples were carbon coated. Samples were imaged with low vacuum JSM-6510LV Scanning Electron Microscope (Jeol, Tokyo, Japan.). Imaging was obtained in both backscatter (not presented in thesis) and secondary electrons (presented) from the same spot. Magnifications of 250x and 2000x were used. XRD was performed with MiniFlex 300/600 (Rigaku Corp, Tokyo, Japan) for B12.5 coarse specimen; untreated and sintered specimen, and for all fine particle size sintered specimen.

4.5 *In vitro* dissolution

Dissolution test was performed in SBF for time points ranging from 6 hours to two weeks (~336 hours) on all untreated glasses of investigations. SBF solution was prepared following the protocol presented first in Kokubo *et al.* 1990 (presented in Appendix A). Reagents used in the preparation were acquired from VWR Chemicals (NaCl, $NaHCO_3$, KCl, K_2HPO_4, MgCl, CaCl, Na_2SO_4) and MP Biomedicals (TRIS Ultra pure).

Glass samples of both coarse and fine particle size were introduced in 50 ml of SBF solution. Amount of immersed glass ranged from 75 mg to 80.3 mg (±0.5 mg) with constant surface area between the compared glass compositions, following method the standard method (Macon *et al.* 2015). The mass of sample was adjusted to maintain the surface area of glass in contact with the solution constant. The surface area was defined based on the measured density of the glasses. For this, assumption that of the average particles size was 375 µm for the coarse and 19 µm for the fine and particles are spherical was made. The glass powder were placed in glass containers and specimens were immersed and placed in a shaker (Multitron AJ 118 g, Infors, Bottmingen, Switzerland) at 37 °C and 100 RPM for approximate time points of 6, 24, 48, 72, 168 and 336 hours. All tests were performed in triplicates.

At each time points, the pH of the dissolution solution was measured, at 37 °C (±0.2 °C) with Mettler Toledo SevenMulti MP 225 pH-meter (Mettler-Toledo International Inc., Greifensee, Switzerland). From same solution, the ion concentration after glass immersion was analyzed with an inductively coupled plasma optical emission spectrometry (ICP-OES) (Agilent Technologies, USA). 5 ml of the dissolution SBF was diluted 10 times for ion concentration analysis. Analyzed elements were Si, B, Ca, P, Mg and Sr. The wavelength used for the measurement are listed in Table 4. Concentration of Na ions present in glass compositions were not analyzed as the SBF itself already contains large amount of Na, therefore leading to saturation of the detector and large inaccuracy.

Table 4. *Wavelengths of interest for each elements to be analyzed with ICP-OES.*

Element	Si	B	Ca	P	Sr	Mg
Wavelength (*nm*)	288.158	208.956	393.366	253.561	407.771	279.553

The immersed glass specimen were filtrated and rinsed with acetone to stop further hydrolysis reactions. The glasses were then analyzed with FTIR-ATR spectroscopy to analyze of evidence of any structural changes at the particle surfaces. Analysis was conducted on both fine and coarse particle size. The IR absorption spectra were recorded within the range 600-4000 cm^{-1}, corrected for Fresnel losses and normalized to the absorption band showing the maximum intensity.

5. RESULTS

5.1 Glass characterization

This section reports on the physical, structural and thermal properties of the glasses of investigation. Information gathered by glass characterization was used in planning of test conditions, an additionally in assessment of the obtained results.

5.1.1 Density and molar volume

Density and molar volume give an indication off the network compactness due to compositional change. Densities of the glasses were determined for melt-derived block with Archimedes' principle (utilizing equation 1), and grinded, coarse glass particles with helium pycnometer. Molar volume was calculated using equation 2, using the density obtained by pycnometry. The density as well as the calculated molar volume are reported in Table 5 and presented in Figure 7.

Table 5. *Measured densities ρ (g/cm^3) ± 0.02 with Archimedes' principle (for glass as blocks, in bulk form) and helium pycnometer ± 0.01, and calculated molar volume V_m (mol/cm^3) ± 0.2.*

Glass	**B12.5**	**-Mg5**	**-Mg10**	**-Sr5**	**-Sr10**	**-Mg5-Sr10**
Density						
Block	2.65	2.64	2.62	2.76	2.84	2.80
Coarse particles	2.66	2.65	2.62	2.75	2.84	2.82
Molar volume						
	23.2	23.0	22.9	23.3	23.4	23.3

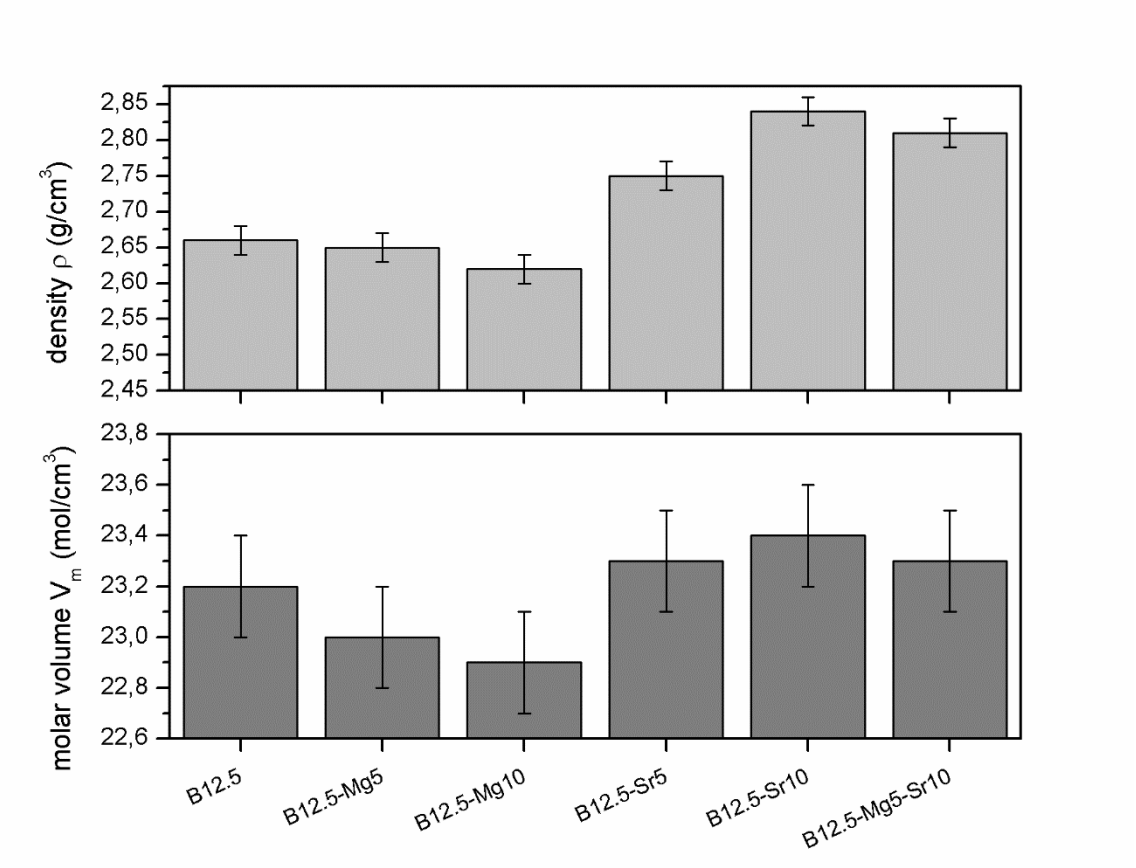

Figure 7. *Density (top) and molar volume (bottom) of the prepared glass compositions.*

The density and molar volume of the base glass B12.5 was found to be 2.66 ±0.01 g/cm^3 and 23.2 ±0.2 mol/cm^3, respectively. Partial substitution of Ca with Mg lead to a decrease in both the density and molar volume. Partial substitution of Ca with Sr while leading to a decrease in density does not seem to impact the molar volume, within the accuracy of the measurements.

5.1.2 Structural properties

Structural properties were analyzed by Raman and FTIR spectroscopy. The analyzed data was background corrected and normalized to the band with maximum intensity. Figures 8 and 9 present Raman and FTIR spectra of the glasses of investigation, respectively.

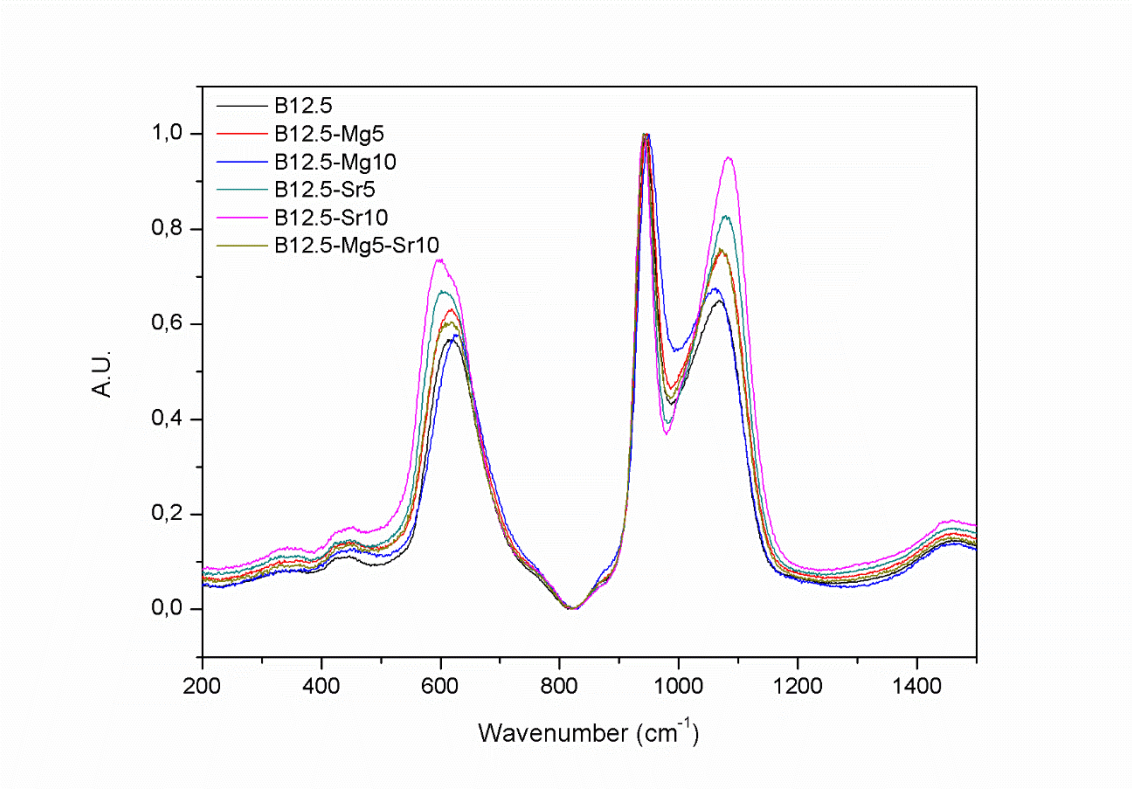

Figure 8. *Background corrected and normalized Raman spectra for all glass compositions.*

All of the investigated glass compositions exhibit similar Raman spectra (Fig. 8). From the figure, several peaks can be observed. Within the region 300-850 cm^{-1}, the small peaks between 300 and 500 cm^{-1} have been related to mixed stretching and bending modes of Si-O-Si bond. Additionally, peak around 500 cm^{-1} can be attributed to Si-O-Si bending. Peaks around 550-850 cm^{-1} have been found to indicate breathing ring modes of borate- and borosilicate ring units groups. Especially, high peak at 630 cm^{-1} attributes to breathing mode of borosilicate rings. (Bunker *et al.* 1990; Manara *et al.* 2009; Matson *et al.* 1983; Meera *et al.* 1990, 1993.)

On the region 850-1250 cm^{-1}, peaks around 900-920 cm^{-1}, 950-980 cm^{-1} and 1050-1100 cm^{-1} indicate respectively Si-O stretching with one, two and three non-bridging O atoms per silicon (i.e. Q^1, Q^2 and Q^3 structural units). High frequency band between 1120 and 1190 cm^{-1} indicates fully polymerized Si-O unit (Q^4). (Fukumi *et al.* 1990; Manara *et al.* 2009; Mysen & Frantz 1992; Neuville *et al.* 2006, 2008.)

Region of 1250-1500 cm^{-1} indicates B-O stretching with peak at around 1410 cm^{-1} demonstrating BO_3 units bonding BO_4, and around 1480 cm^{-1} BO_3 units bonding BO_3 units. (Akagi *et al.* 2001; Manara *et al.* 2009; Meera et al. 1990; Yano *et al.* 2003).

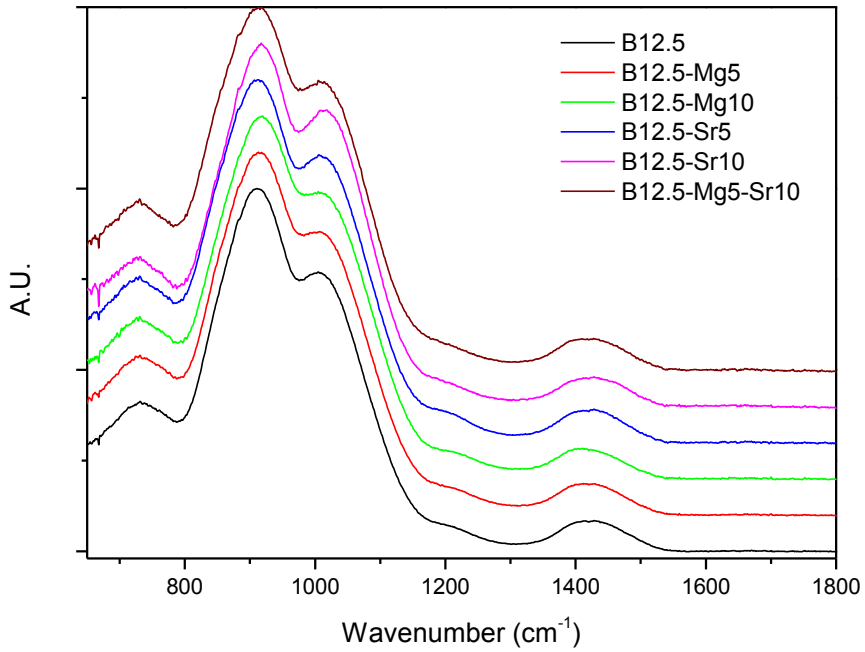

Figure 9. *Background corrected and normalized FTIR-ATR spectra of the untreated glass compositions.*

FTIR spectrum of the glass compositions are presented in Fig. 9. Spectra for all compositions is again highly similar. Peaks around 750 cm^{-1} may indicate Si-O bending, and absorption band at 950 cm^{-1} and around 1100-1150 cm^{-1} to $Si\text{-}O^-$ and $Si\text{-}O^-$ asymmetric stretching in SiO_4 units. Band located within the 1400-1515 cm^{-1} area can be attributed to carbonate within the structure. (Massera *et al.* 2012, 2014; Serra *et al.* 2003).

However, absorption around 850-1150 cm^{-1} range can also be attributed to B-O stretching vibration of BO_4 units, and band around 1400 cm^{-1} can be related to borate triangles formed by BO_3. Boron in form of BO_2O^- can additionally be indicated by a slight band at 1227 cm^{-1}. (Pascuta *et al.* 2008).

5.1.3 Particle size distribution

As the one of the aim of the study was to assess whether or not it is possible to sinter these glass compositions without inducing crystallization the thermal properties of the glasses should be studied. However, it is known that the sintering process as well as the crystallization kinetics is particle size dependent (Boccacini *et al.* 1996; Ray *et al.* 1991).

Determination of the particle size distribution for grinded glass specimen was analyzed with laser diffraction particle sizing. Results are presented as differential particle size

distributions as volume percent of the total analyzed particle amount in Figure 10. The D_{10}, D_{50} and D_{90} representing the range (10% and 90%) and midpoint (50%) of the cumulative particle sizes is presented in Table 6 and as column chart in Figure 11.

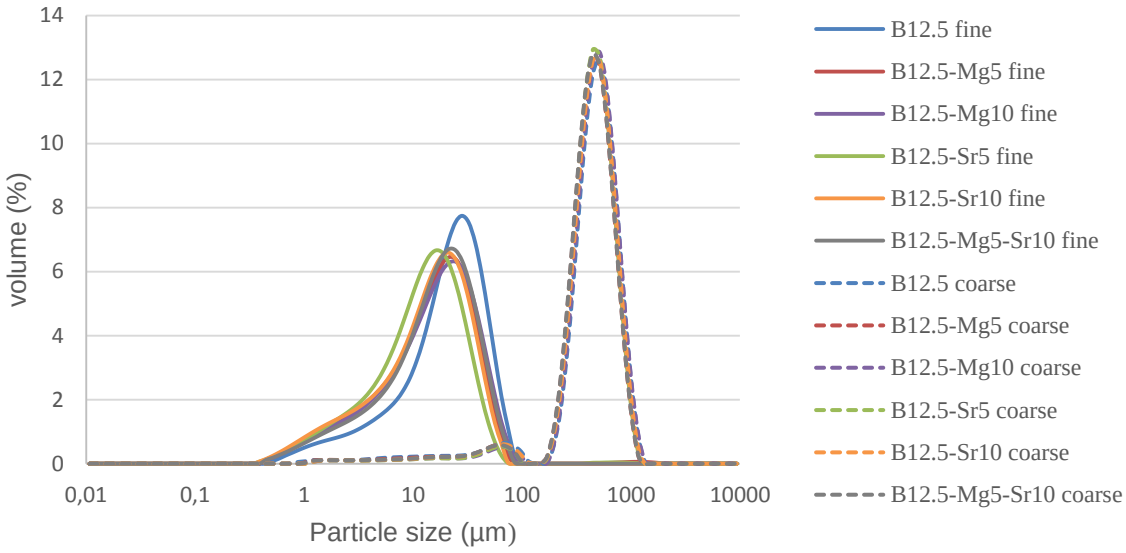

Figure 10. *Differential particle size distribution of the produced glass particles, showing the relative amount of each particle size. Graph is formed based on results for both fine and coarse particle size.*

Table 6. *Cumulative particle size diameter (in µm) distributions of 10%, 50% and 90% of the particles.*

	B12.5	**-Mg5**	**-Mg10**	**-Sr5**	**-Sr10**	**-Mg5Sr10**
fine particle size; sieved to < 38 µm						
D_{10}	4.1	2.5	2.7	2.5	2.3	2.9
D_{50}	21.7	15.2	16.1	12.6	14.5	16.4
D_{90}	47.7	38.9	41.7	32.7	36.2	40.4
coarse particle size; sieved to [250,500] µm						
D_{10}	223.3	225.2	255.2	243.4	232.8	229.9
D_{50}	473.4	441.9	476.4	451.1	455.5	441.6
D_{90}	790.5	733.7	792.4	746.0	758.0	733.2

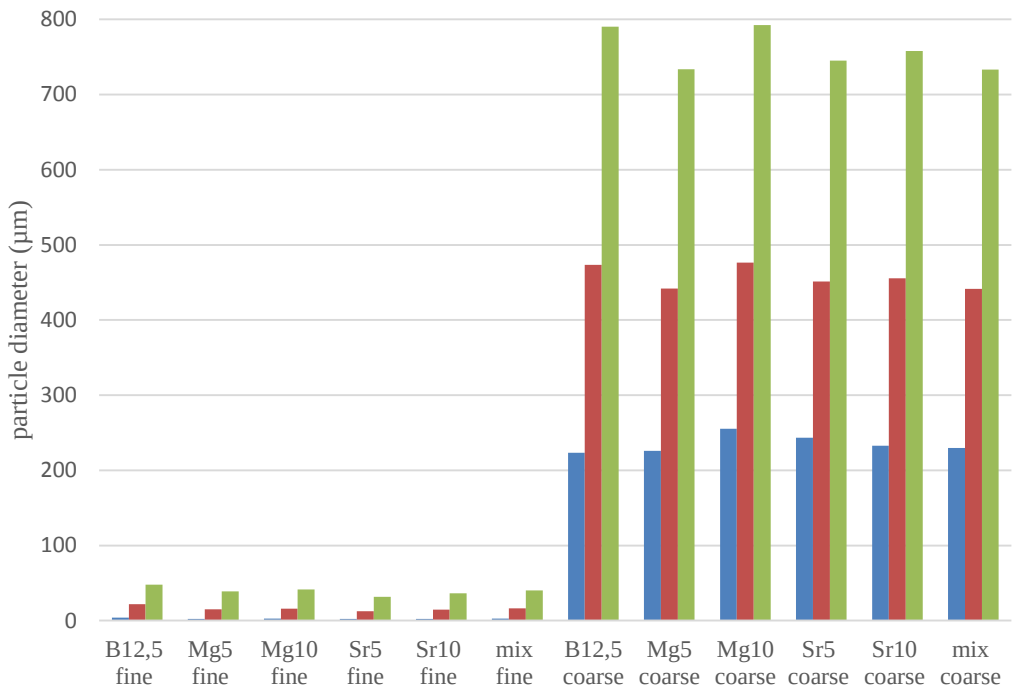

Figure 11. *Cumulative particle size distribution (in µm) showing D_{10}, D_{50} and D_{90} indicated in blue, red and green, respectively.*

Coarse particles were collected by sieving the particle with sieves having a grid diameter of 250-500 µm. Fine powder corresponds to particles collected after passing through a sieve with a grid size of 38 µm. From Fig. 10 it can be seen that all coarse glass samples exhibited particles with similar D_{10}, D_{50} and D_{90}. The particles size ranges from 223 to 792 µm with mass median diameter being 457 ±15 µm. For fine particles, the equivalent diameter sizes ranged from 2 to 48 with mass median diameter of 16 ±3 µm, glass composition B12.5 being slightly larger compared to the other compositions.

5.1.4 Differential thermal analysis

Differential thermal analysis was performed for glass compositions of both particle sizes with heating rate of 10 °C/min. The obtained DTA curves are plotted in Appendix B, and the determined T_g, T_x and T_p as well as the hot forming domain are presented in Tables 7 and 8. Determination was performed as presented in materials and methods; Fig. 6 in chapter 4.4.1. Determined temperatures are also illustrated in Figures 12 and 13.

Table 7. *Determination of glass transition temperature (T_g), onset of crystallization (T_x), crystallization peak (T_p) and hot forming domain, i.e. working range ΔT for coarse particles size.*

Glass composition	$\mathbf{T_g}$ (±2°C)	$\mathbf{T_x}$ (±2°C)	$\mathbf{T_p}$ (±2°C)	$\mathbf{\Delta T = T_g - T_x}$ (±4°C)
B12.5	529	691	772	162
B12.5-Mg5	513	678	781	165
B12.5-Mg10	500	687	795	187
B12.5-Sr5	512	659	780	147
B12.5-Sr10	502	675	772	173
B12.5-Mg5-Sr10	472/507	647	725	140

Table 8. *Determination of glass transition temperature (T_g), onset of crystallization (T_x), crystallization peak (T_p) and hot forming domain, i.e. working range ΔT for fine particles size.*

Glass composition	$\mathbf{T_g}$ (±2°C)	$\mathbf{T_x}$ (±2°C)	$\mathbf{T_p}$ (±2°C)	$\mathbf{\Delta T = T_g - T_x}$ (±4°C)
B12.5	531	638	676	107
B12.5-Mg5	511	652	683	141
B12.5-Mg10	502	660	701	158
B12.5-Sr5	514	622	667	108
B12.5-Sr10	506	628	675	122
B12.5-Mg5-Sr10	473/506	611	666	105

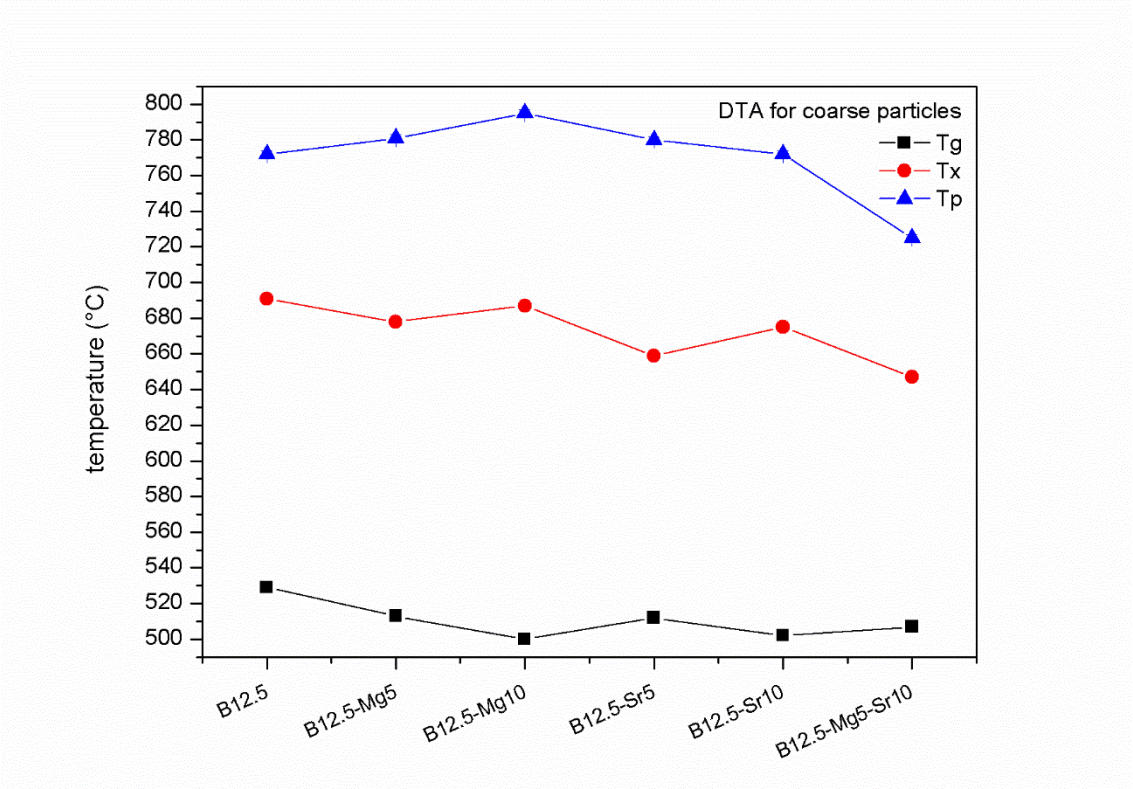

Figure 12. *T_g, T_x and T_p for coarse glass particles.*

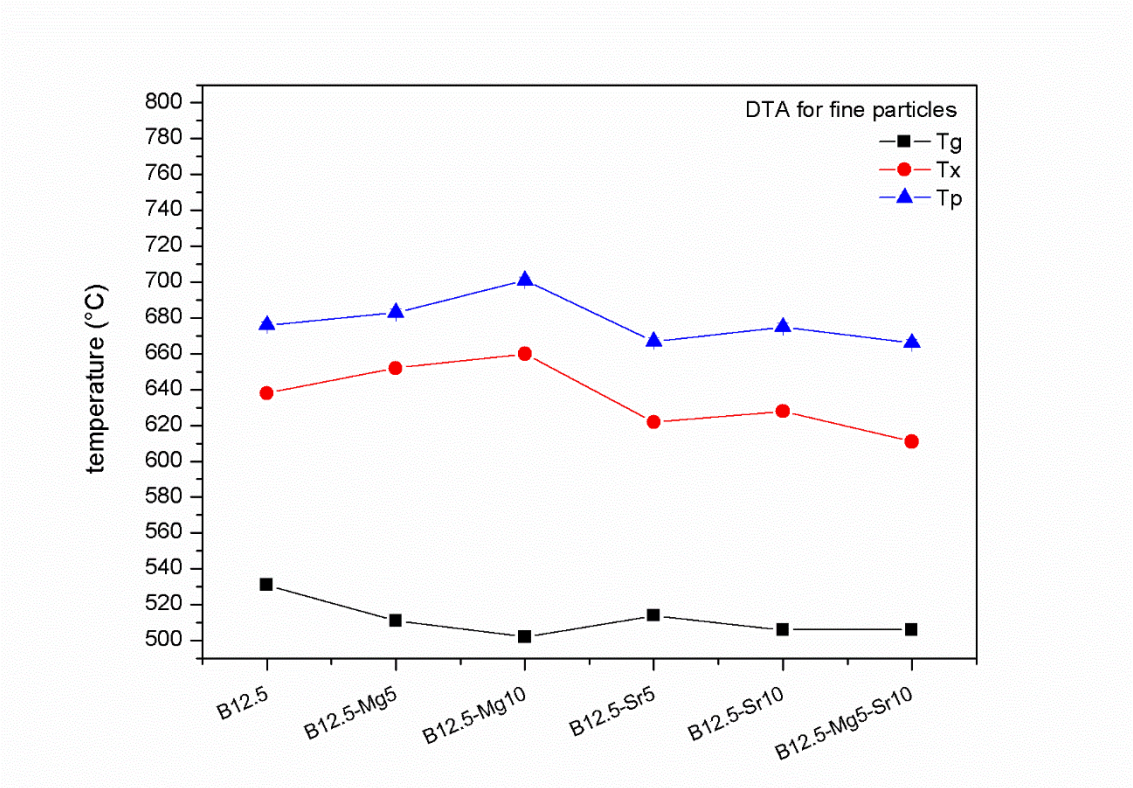

Figure 13. *T_g, T_x and T_p for fine glass particles.*

From the results, several observations can be made; *(i)* Within the range of accuracy, T_g's were same for both particle sizes, with all glass compositions. *(ii)* A decrease in particles size lead to a shift of the T_x and T_p to lower temperatures. *(iii)* Substitution of Mg for Ca leads to a decrease in T_g and an increase in T_x, T_p and ΔT. *(iv)* Substitution of Sr for Ca leads to a decrease in T_g. However, while a general decrease in T_x and T_p can be seen as well as an increase in ΔT for higher for 10 mol% substitution, no clear trend could be evidenced. *(v)* The SDTA curve for glass composition B12.5-Mg5-Sr10 containing both Mg and Sr exhibited two different T_g's. ΔT was calculated using the higher T_g. The mixture glass exhibits lower T_g, T_x, T_p and ΔT than the based glass B12.5.

5.2 Sintering and crystallization

Based on thermal properties, glass particles of both coarse and fine size were sintered in a metallic mold. The temperatures used for sintering where all within the $\Delta T=T_x-T_g$ domain. With the used sintering conditions, the coarse particle size did not sinter at all or sintered poorly. Therefore, the sintering study was focused on the small sized particles. The samples were heat treated at T_x-60, T_x-40 and T_x-20 °C. SEM imaging was performed only for specimen sintered at T_x-40 °C. The aim was to evidence neck growth and coarsening of the particles. XRD analysis was performed for B12.5 coarse particles sintered at several temperatures and for various conditions, and fine particles of all glass compositions, sintered at 60, 40 and 20 °C below their characteristic T_x. The aim was to assess the amorphousness or partial crystallinity of the produced sintered bodies.

5.2.1 SEM

SEM imaging with backscatter electrons was performed for fine particle size specimen with constant sintering time of 1h at T_x-40 °C. Specimen were imaged with magnifications of 250 and 2000 x. Results are presented in Figure 14 for B12.5 (A and B), B12.5-Mg5 (C and D) and B12.5-Mg10 (E and F), and in Figure 15 for B12.5-Sr5 (A and B), B12.5-Sr10 (C and D) and B12.5-Mg5-Sr10 (E and F).

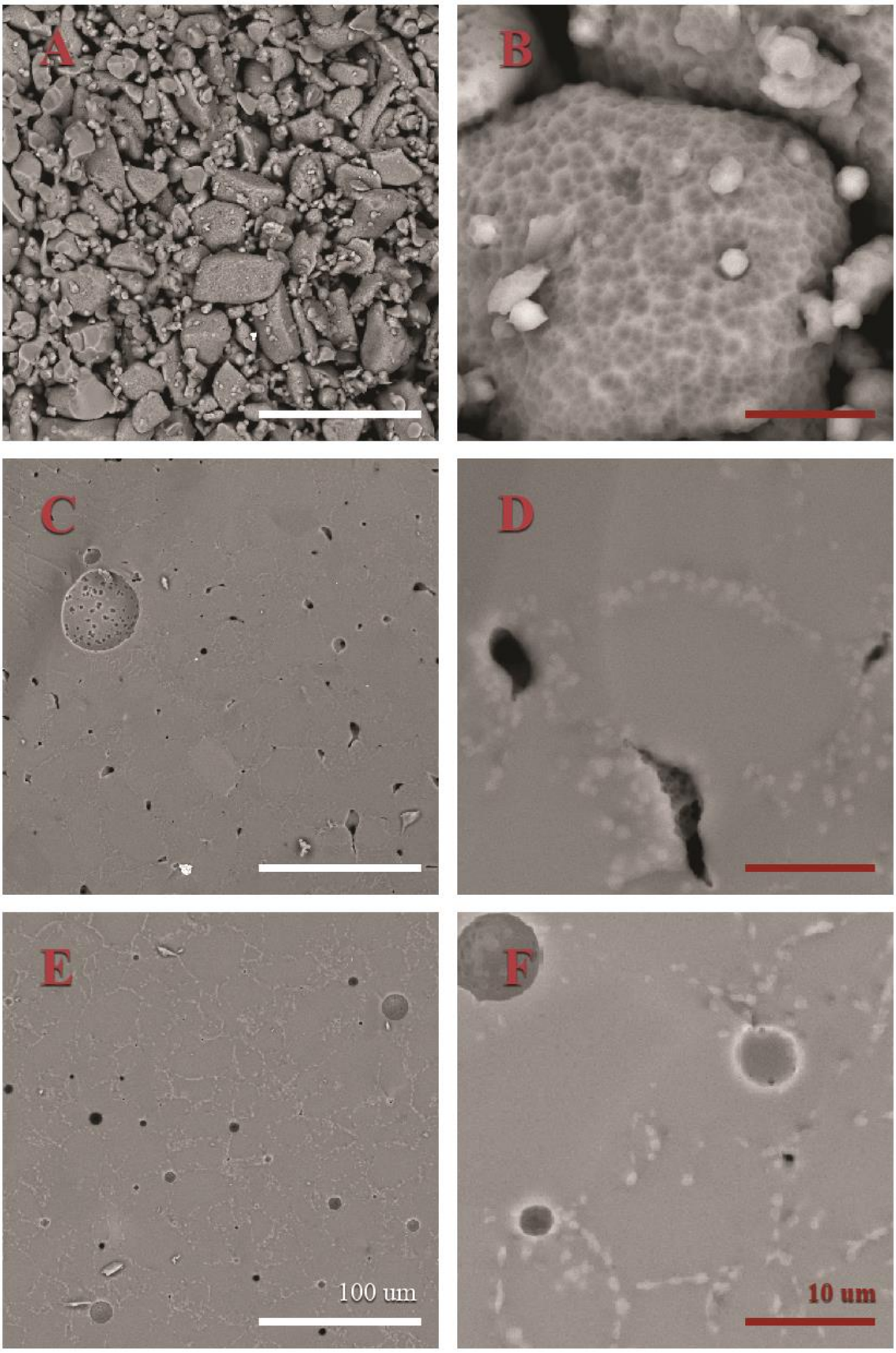

Figure 14. *SEM imaging of fine particles size of glasses* ***(A,B)*** *B12.5* ***(C,D)*** *B12.5-Mg5* ***(E,F)*** *B12.5-Mg10, sintered at their respective* T_x*-40 °C for 1h. Scale bars of 100 um (indicated as white) and 10 um (indicated as red).*

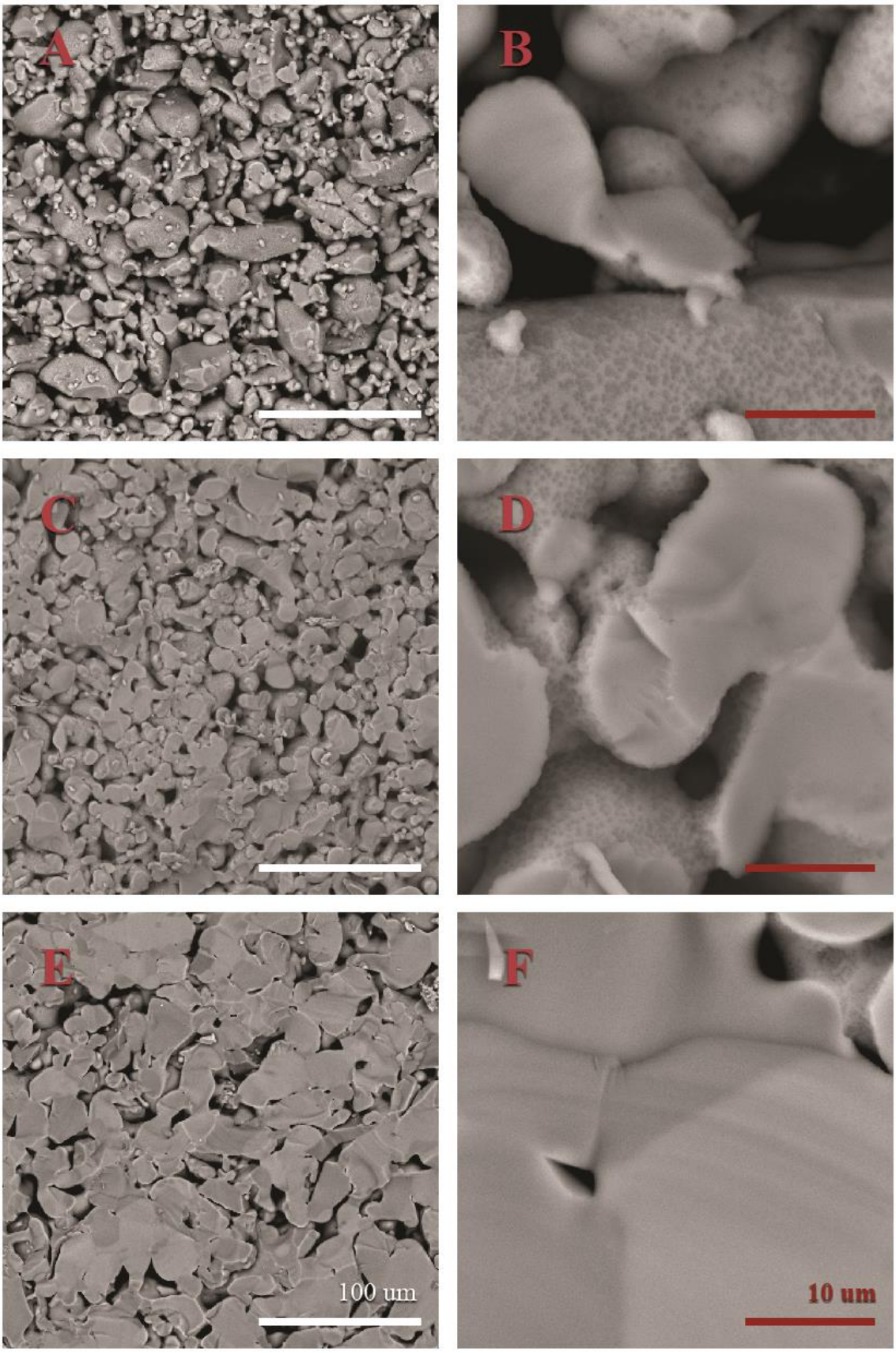

Figure 15. *SEM imaging of fine particles size of glasses* ***(A,B)*** *B12.5-Sr5* ***(C,D)*** *B12.5-Sr10* ***(E,F)*** *B12.5-Mg5-Sr10, sintered at their respective* T_x*-40 °C for 1h. Scale bars of 100 um (indicated as white) and 10 um (indicated as red).*

From Fig. 14A and 14B, it can be seen that in the fracture surface of B12.5 the particles had started to form a contact, neck growth, with the surrounding particles. At higher magnification (Fig. 14B), a pattern can be distinguished at the glass particle surfaces. Imaging using secondary electrons (not presented) indicated that the patterns were a result of topography, instead of differences in elemental composition.

Figures 14C-F illustrated smooth fracture surfaces of the Mg containing glass compositions. Glasses containing Mg (Fig. 14C and 14E) exhibited a pronounced neck growth and coarsening of the particles. Trapped gas bubbles can be seen as well as small pores. It seems that with increasing the Mg content the amount of remaining pores decreases. However, it can be noted that, at higher magnification (Fig. 14D and 14F), clear sign of glass crystallization are seen. The crystallization pattern seem to follow possible grain boundaries. This was observed to increase as the Mg content increased.

Sr containing glass specimen are presented in Fig. 15. The specimen of B12.5-Sr5 in Fig. 15A-B bored high resemblance to specimen B12.5 presented in Fig. 14A-B. Glass which contained more Sr, the B12.5-Sr10, demonstrated more advanced sintering of the particles than B12.5-Sr5. It should however be noted that in images of the higher Sr containing glass, some of the smooth looking surface is not result from fused particles, but from a fracture that proceeds through middle of a glass grain (best seen in Fig. 15D); outcome of cutting a solid particle in half while preparing the specimen.

Mixture glass where some of the Ca content was substituted with both Mg and Sr is presented in Fig. 15E-F. Sintering of the glass was fairly good, as some of the particles have clearly fused together. However, in the specimen there can be seen areas of clear difference in colour gradient. In SEM this indicates difference in materials density. Change in gradient does not in this case follow the grain boundaries (Fig. 15F). This phenomena was not observed with imaging with secondary electrons (not presented), therefore it is not likely cause by surface topography.

5.2.2 XRD

XRD analysis was performed for B12.5 coarse particles sintered at T_x -130 °C, T_x - 60 °C and T_x. At T_x - 60 °C, sintering time ranged from 1 h to 3h. Analysis was also performed for untreated glass specimen. The XRD diffractogram are presented in Figure 16.

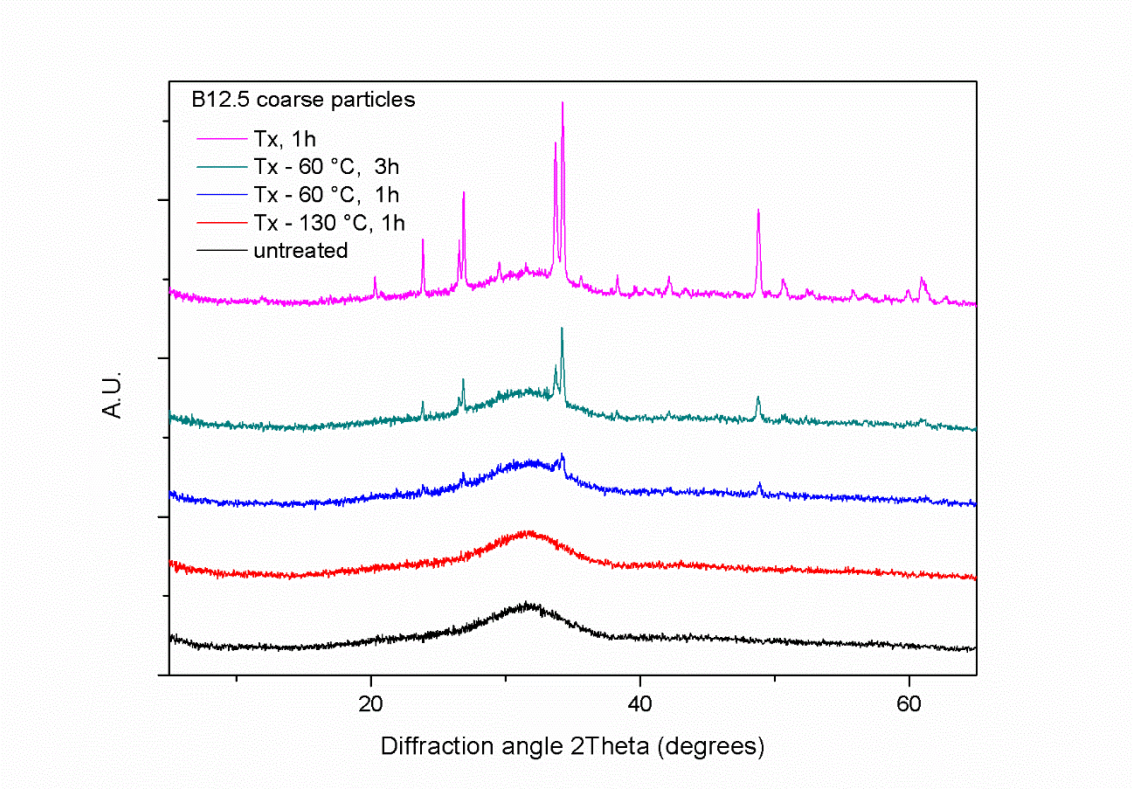

Figure 16. *XRD spectra of B12.5 coarse particle size sintered from T_x-130 ^oC to T_x for duration varying between 1 to 3h at T_x-60 ^oC.*

From Fig. 16, it can be seen that the coarse particles heat treated up to T_x-130 °C for 1h only exhibit a broad band. At increasing sintering temperature sharp peaks starts to form, which increases in intensity with increasing sintering temperatures. At T_x-60 °C an increase in sintering time also leads to an increase in the diffraction peaks intensity.

The diffractogram obtained for the sintered bodies obtained using fine particle size, constant sintering time of 1h and sintered at T_x - 60, 40 and 20 °C are presented in Figures 17-22.

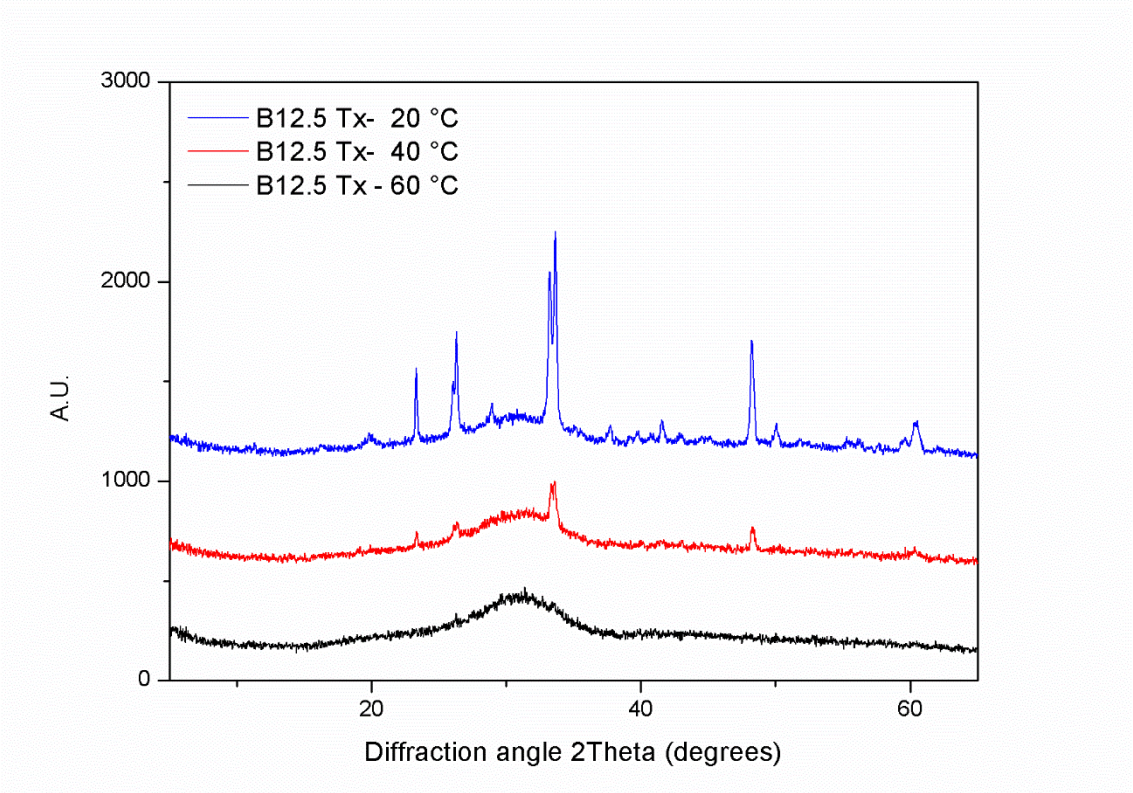

Figure 17. *XRD spectra of B12.5 fine particle sintered at T_x - 60, 40 and 20 °C.*

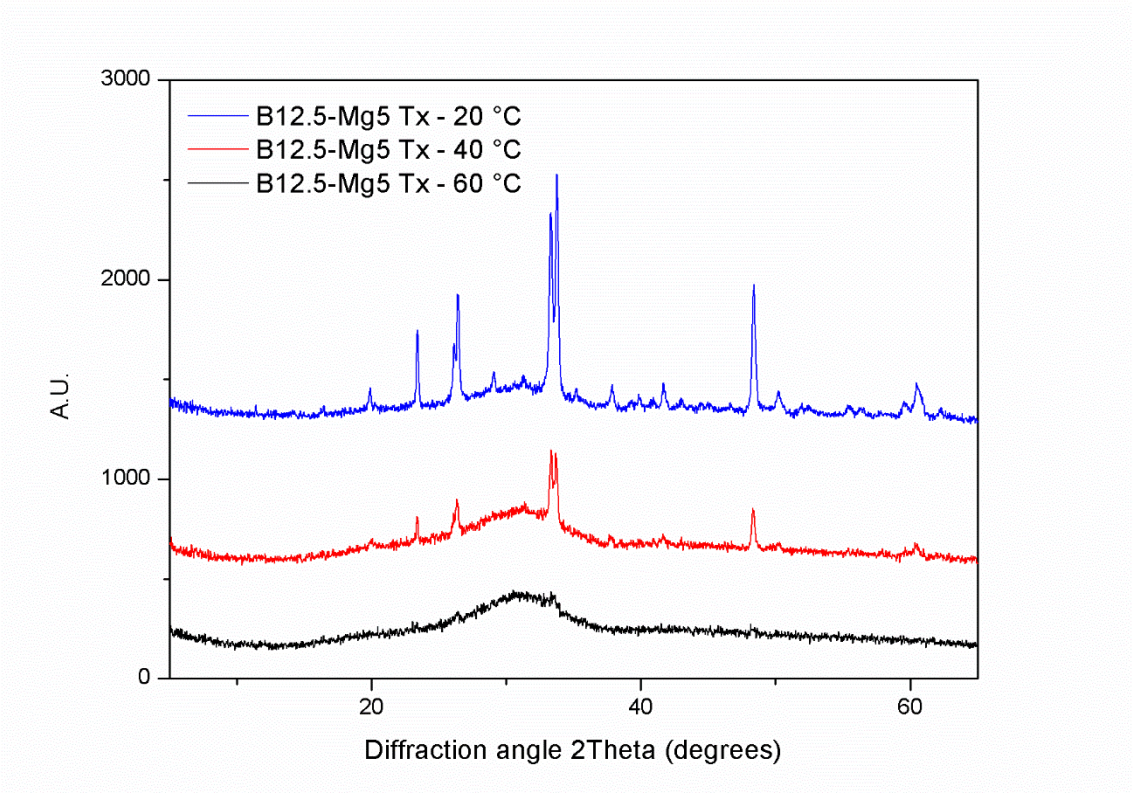

Figure 18. *XRD spectra of B12.5-Mg5 fine particle sintered at T_x - 60, 40 and 20 °C.*

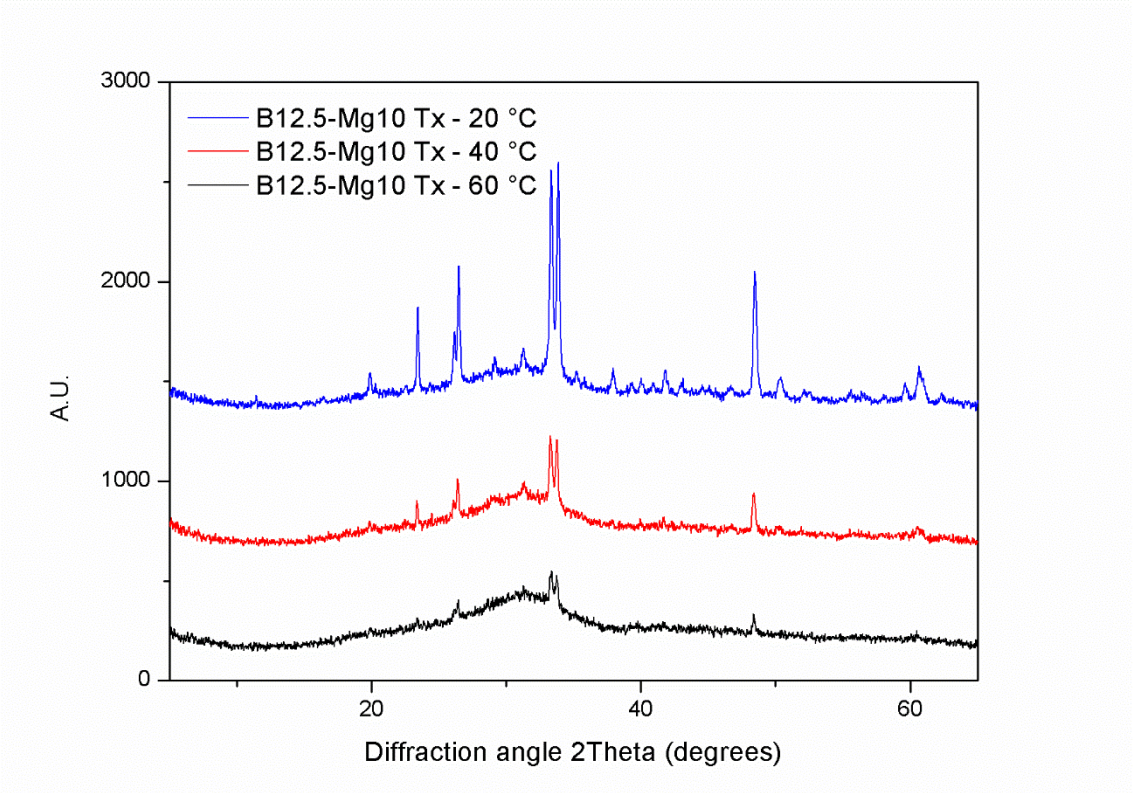

Figure 19. *XRD spectra of B12.5-Mg10 fine particle sintered at T_x - 60, 40 and 20 °C.*

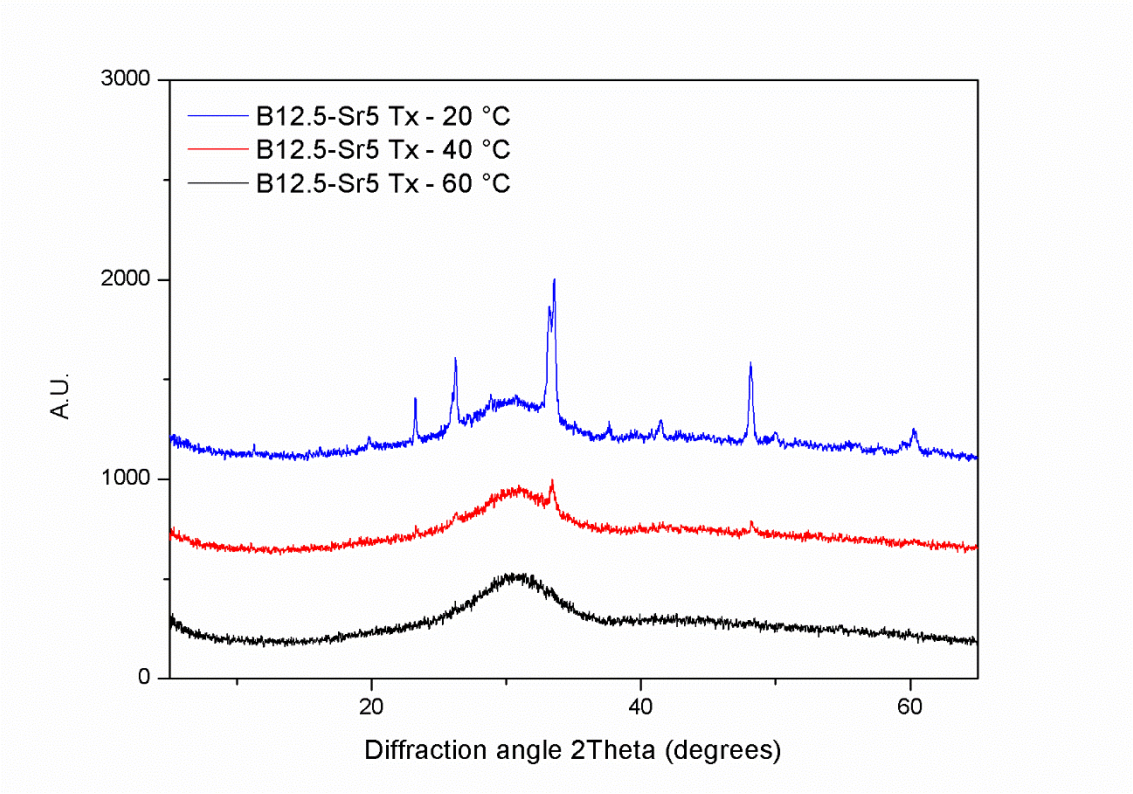

Figure 20. *XRD spectra of B12.5-Sr5 fine particle sintered at T_x - 60, 40 and 20 °C.*

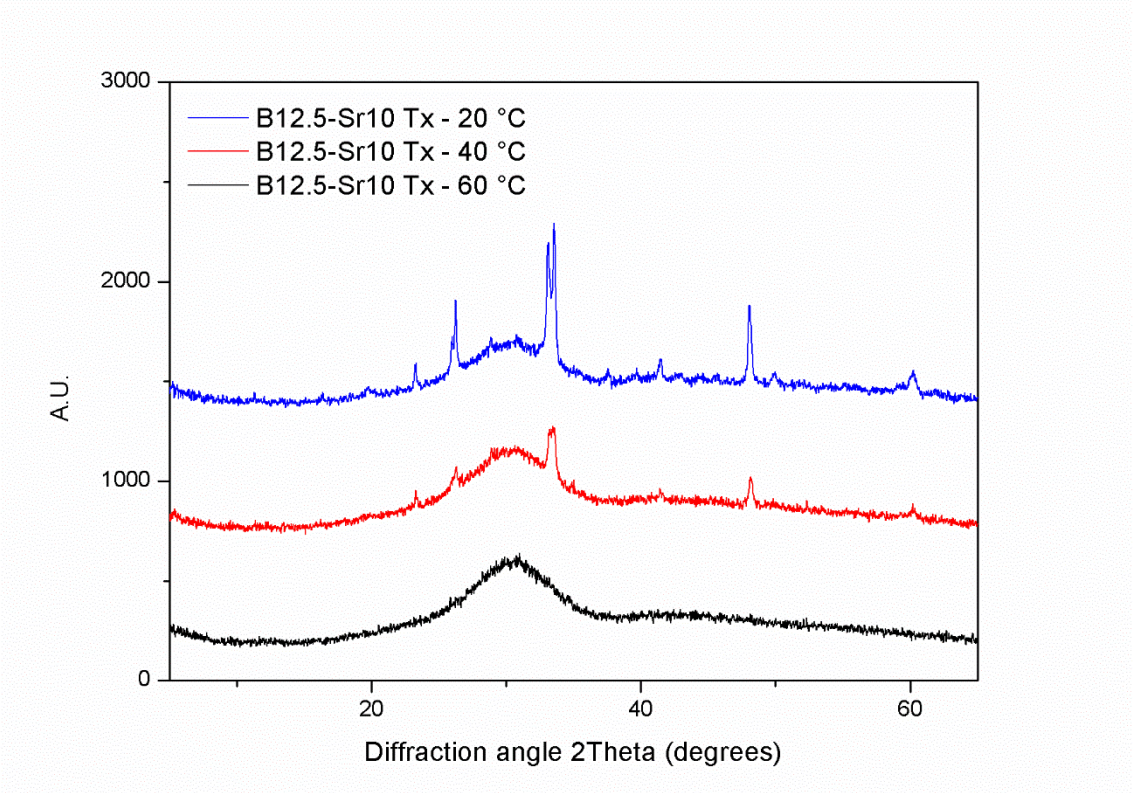

Figure 21. *XRD spectra of B12.5-Sr10 fine particle sintered at T_x - 60, 40 and 20 °C.*

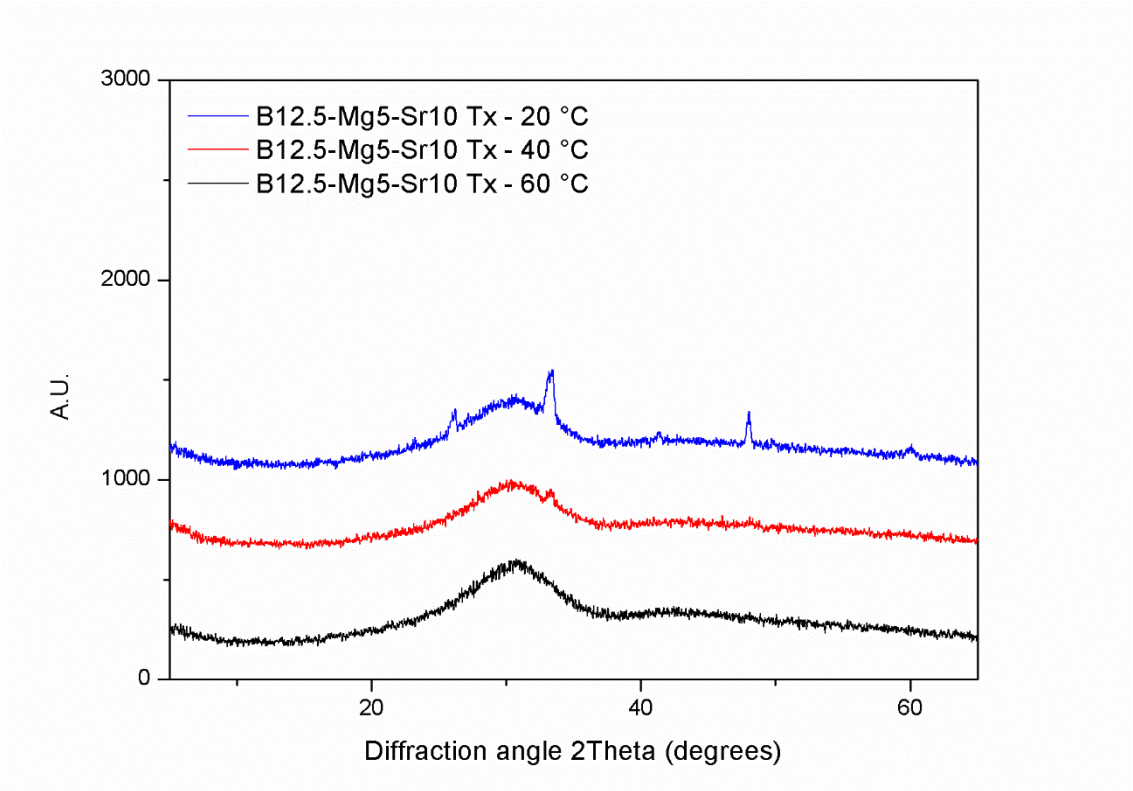

Figure 22. *XRD spectra of B12.5-Mg5-Sr10 fine particle sintered at T_x-60, 40 and 20 °C.*

As can be seen from Fig. 17-22, with all fine particle specimen, crystallization started to occur already at sintering temperature of T_x-40 °C for all glasses except for the glass Mg10 for which crystallization started at T_x-60°C. Sharp peaks indicating crystallization were most intense in glasses B12.5 and Mg containing variants. Glasses containing Sr had slightly less crystallization, and glass containing both Mg and Sr spectra indicated mainly an amorphous structure.

5.3 *In vitro* properties

All glasses of investigation were immersed in SBF from 6 h up to 2 weeks. Dissolution of the glasses was assessed by interpreting change in the pH and ion concentration in the SBF. FTIR spectra was recorded on all glass powders to better understand the change in glass structure upon dissolution and if a reactive layer deposit at the surface of the glasses particles

5.3.1 pH

Figure 23 presents pH of the SBF upon immersion of coarse glass particles for 24 h up to two weeks. Figure 24 presents, similarly, the pH of the SBF upon dissolution of the fine particles for 24 hours up to 1 week. All pH were measured at 37 ±0.2 °C.

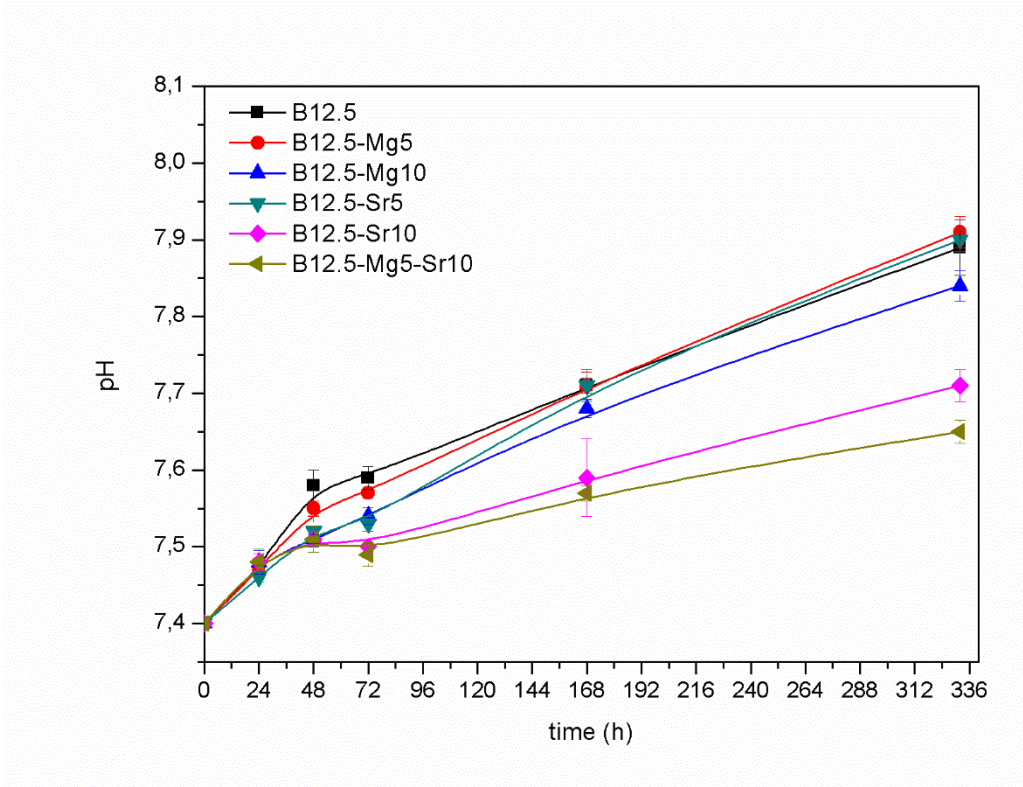

Figure 23. *pH of the SBF containing coarse glass particles as a function of immersion time. pH was measured after approximate time points of 24, 48, 72, 168 and 332h.*

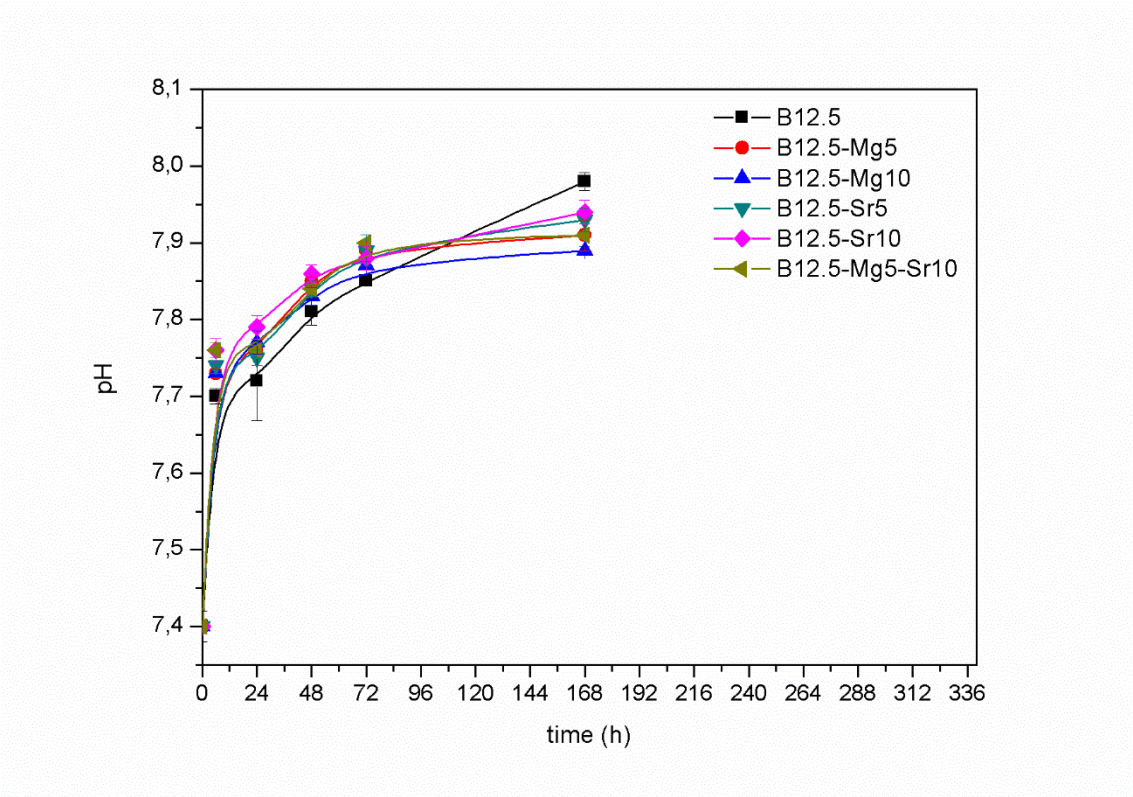

Figure 24. *pH of the SBF containing fine glass particles as a function of immersion time. pH was measured after approximate time points of 6, 24, 48, 72 and 168h.*

With both particle sizes, the pH was observed to increase with increasing the immersion time. From Fig. 23 can be observed that the pH seems to rise progressively with time, without saturation. Glasses containing 5 mol% of Sr or Mg expressed similar pH than the B12.5 glass. The glass containing 10 mol% of Mg show lower pH value compared to the base glass, while glass containing 10 mol% Sr and the mixture glass (B12.5-Mg5-Sr10) demonstrated even lower pH at the longest immersion times.

Results presented in Fig. 24 indicate, that the increase in pH occurs at faster rate than the one observed in coarse particles. The rise in the pH was found to be faster for glasses B12.5-Mg5, -Mg10, -Sr5, -Sr10 and –Mg5-Sr10 initially than of the glass B12.5. At immersion time longer than 72h, all of the investigated glasses demonstrate a saturation of the pH, except the base glass B12.5 which seemed to still induce pH increase at 1 week immersion.

5.3.2 ICP-OES

Si, B, P, Ca, Mg and Sr ion content concentration for the immersion solution were determined with ICP-OES. Results for all ions for all of the investigated glass composition, as a function of time for constant surface area to volume ratio, are presented in Appendix C.

In this chapter, the comparison of ion release of Si, B, Ca, P, Mg and Sr from dissolved coarse glass particles is presented in Figures 25-30, respectively. Zero-time point marks the SBF ion content before immersion of glass specimen.

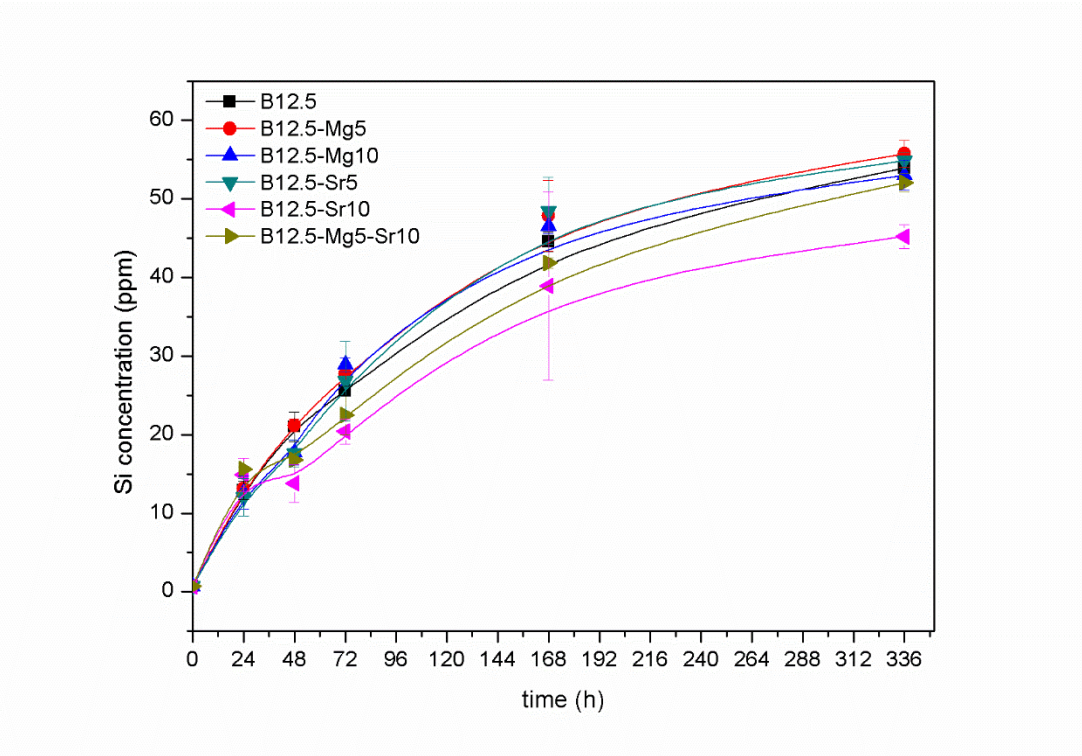

Figure 25. *Silicon ion concentration (ppm) presented as a function of immersion time. Graph presents ion release of coarse glass particles in SBF.*

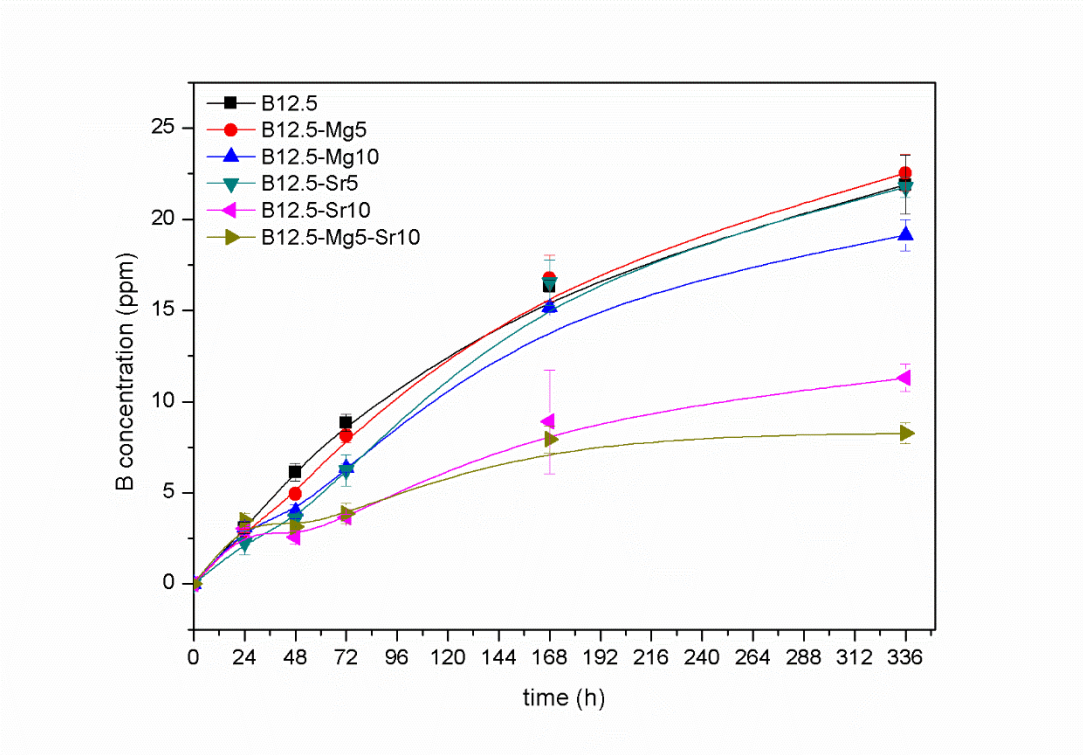

Figure 26. *Boron ion concentration (ppm) presented as a function of immersion time. Graph presents ion release of coarse glass particles in SBF.*

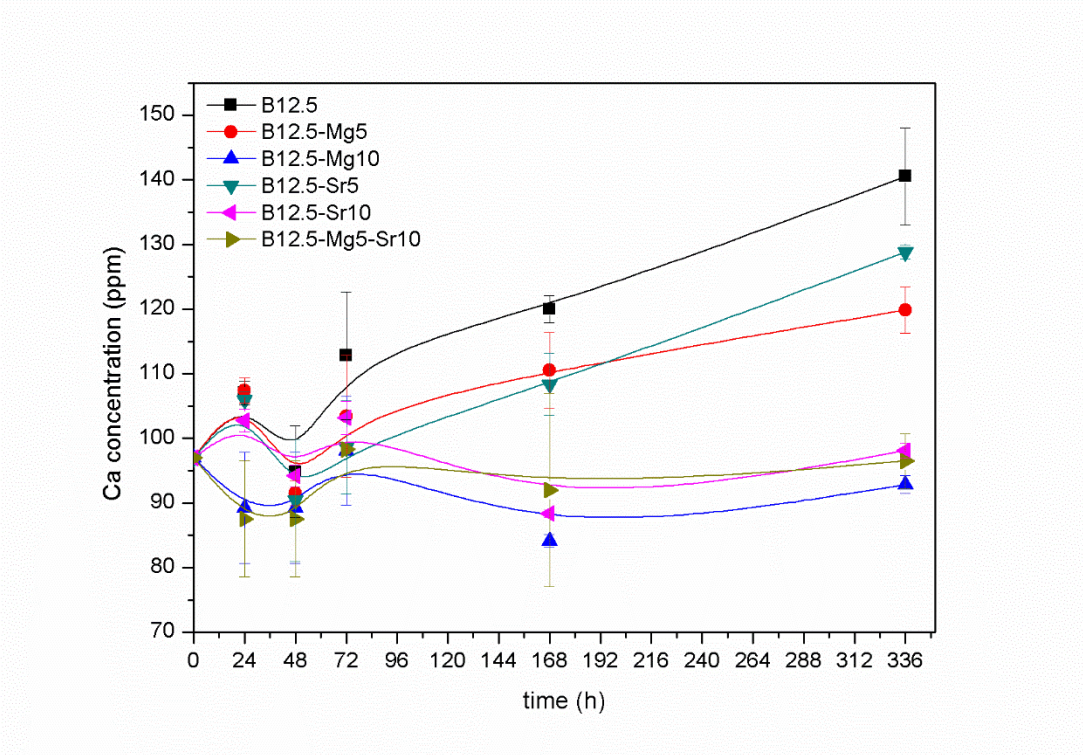

Figure 27. *Calcium ion concentration (ppm) presented as a function of immersion time. Graph presents ion release of coarse glass particles in SBF.*

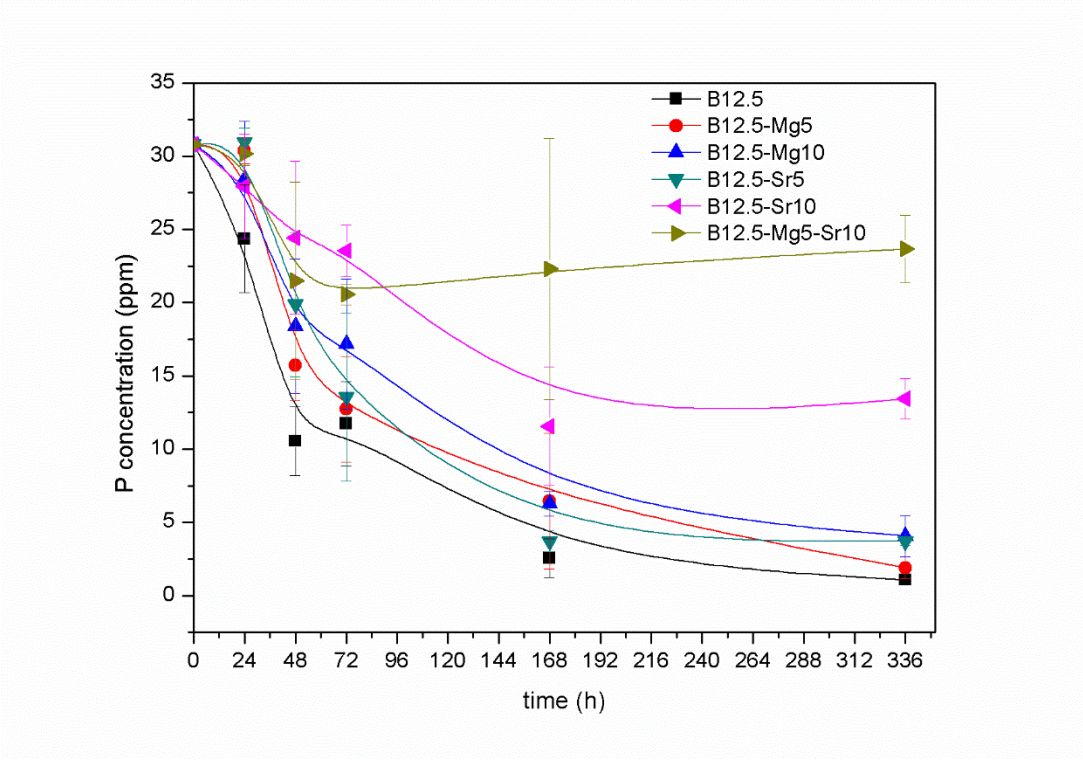

Figure 28. *Phosphorus ion concentration (ppm) presented as a function of immersion time. Graph presents ion release of coarse glass particles in SBF.*

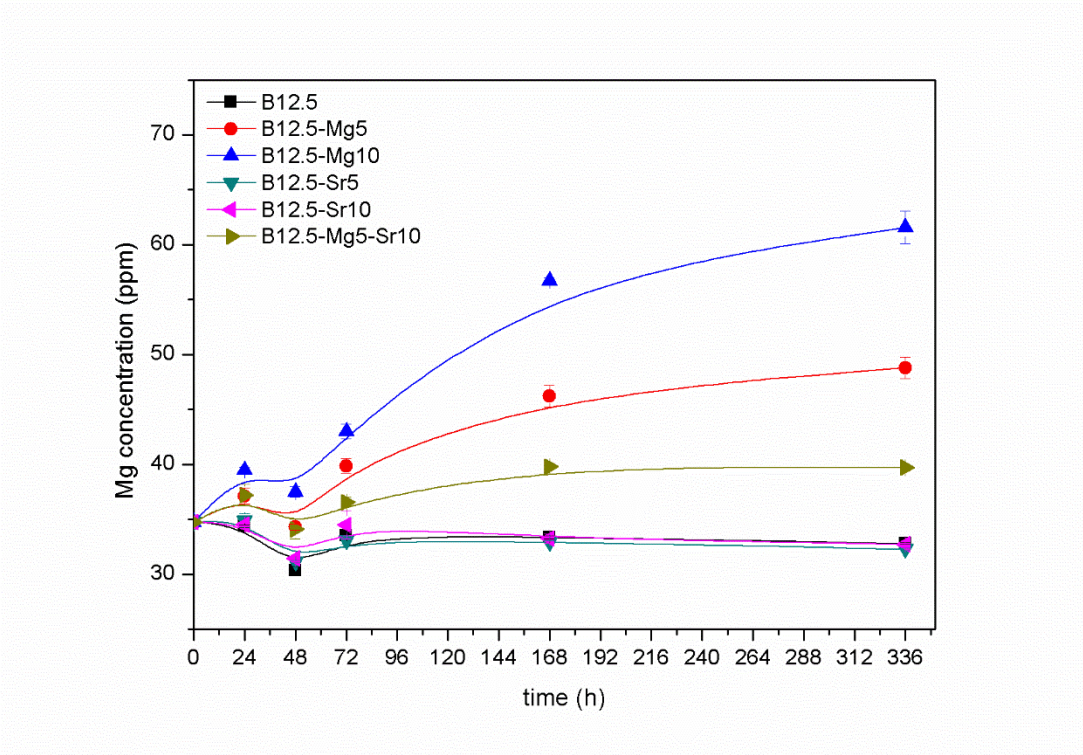

Figure 29. *Magnesium ion concentration (ppm) presented as a function of immersion time. Graph presents ion release of coarse glass particles in SBF.*

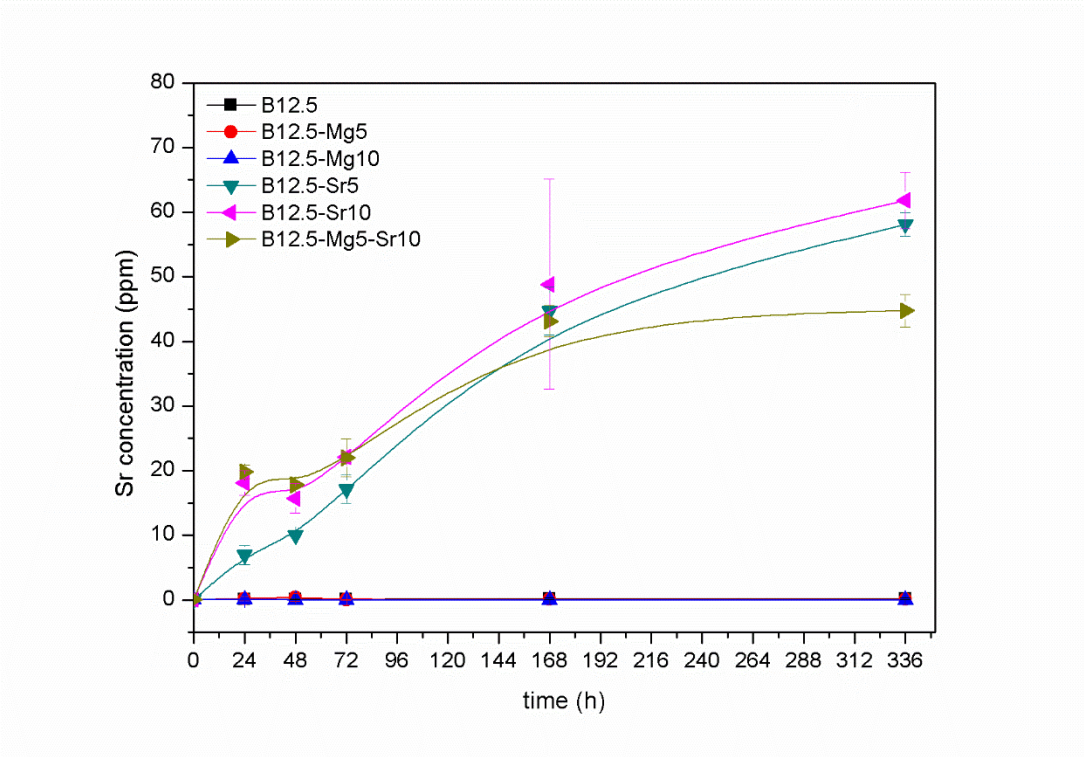

Figure 30. *Strontium ion concentration (ppm) presented as a function of immersion time. Graph presents ion release of coarse glass particles in SBF.*

From Fig. 25, it can be seen that the concentration of released silica from the coarse particles is initially similar in all glass compositions. Between time points of 24 – 48h, the Si concentration in B12.5-Sr10 starts to slightly decrease in comparison to other glass compositions. From Fig. 26, it can be seen that similar phenomena happens with boron ions. However, with boron more clear difference between glass compositions can be observed. Now, when increasing amount of the Ca had been substituted, the ion concentration of B in the dissolution solution decreased.

Fig. 27 present the calcium ion concentrations of the dissolution solutions. It can be seen that for glass where Ca content was substituted up to 5%, (i.e. compositions B12.5, -Mg5, -Sr5), the free Ca ion concentration in the solution increases, whereas with glasses B12.5-Mg10 and –Mg5-Sr10 Ca concentration remains fairly constant. Overall, the Ca concentration decreases with composition containing less Ca. Fig. 28 presents the P concentration. Amount of P in solution decreases as function of immersion time, and additionally with increasing Ca content in glass composition. An increase in Mg and Sr lead to lesser decrease in P ions, as compared to the B12.5 glass. The mixture glass with highest Ca substitution expresses the lowest decrease in P ions concentrations.

Fig. 29 and 30 present Mg and Sr ion concentration of coarse glass particle dissolution solutions. It can be observed that Mg release was initially slower in mixture composition containing both Mg and Sr. For Sr, release was of same rate in both B12.5-Sr5 and –Sr10,

and slightly slower in the mixture composition. However, results for fine glass particles (not presented), presents slightly different results. The results were indeed more in agreement with the glass composition, where B12.5-Mg5 released half of the Mg of B12.5-Mg10 and similarly B12.5-Sr5 released half the Sr ions than B12.5-Sr10. The mixed glass showed a Mg and Sr release similar to the glass B12.5-Mg5 and B12.5-Sr10. In general, it can be stated that release of all ions was observed to be faster in fine, than in coarse glass particles.

5.3.3 FTIR

Changes in the glass surface composition as a function of immersion time in SBF were assessed with FTIR. All spectra were background corrected and normalized to the band with maximum intensity. Figure 31 presents the FTIR spectra of coarse particle of glass B12.5, for various immersion times from 0 to 336 h (i.e. up to 2 weeks). Figure 32 presents similar spectra for fine glass particles immersed up to 168 h (i.e. 1 week).

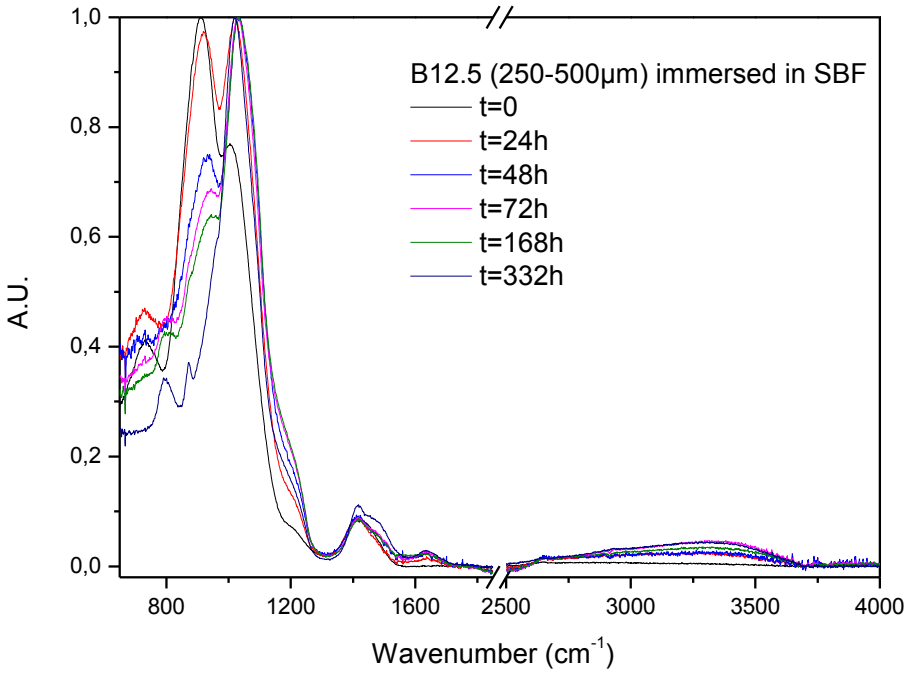

Figure 31. *FTIR-ATR spectra of the glass B12.5 coarse particles (250 -500 µm) immersed for up to 332h in SBF.*

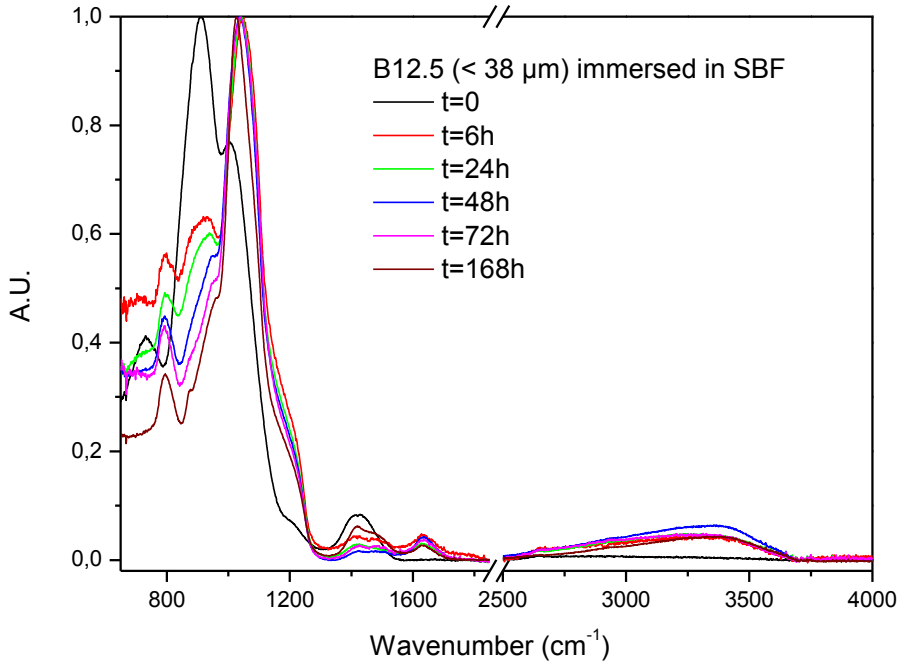

Figure 32. *FTIR-ATR spectra of the glass B12.5 fine particles (< 38 µm) immersed for up to 168h in SBF.*

Fig. 31 presents the FTIR spectra for glass B12.5 on coarse particles, immersed for up to 332 h and Fig. 32 for fine particles immersed for up to 168 h in SBF. With increasing immersion time, there can be observed that *(i)* the band located at ~950 cm^{-1} decreases in intensity, *(ii)* the band located at ~1100 cm^{-1} increases in intensity and shifts to ~1200 cm^{-1}, *(iii)* the shoulder at ~1200 cm^{-1} increases in intensity, and *(vi)* formation of peak in the 1600-1700 cm^{-1}, as well as a broad band in the 2500-3500 cm^{-1} region.

As mentioned earlier, the band at 950 cm^{-1} corresponds to Si-O-Si vibration whereas the band at 1100-1200 cm^{-1} to Si-O- (Massera *et al.* 2012b, 2014). The peak centered at 1020 cm^{-1} and 960 cm^{-1} for the longer immersion time are related to phosphate vibration and the shoulder at 1212 cm^{-1} can be related to presence of SiO_4 as Q^4 units, respectively. (Berzina-Cimdina & Borodajenko 2012; Massera & Hupa 2014; Raunaud *et al.* 2002). The peaks around 1630 cm^{-1} and the broad band on range 2600 - 3600 cm^{-1} are indications of H-O-H as absorbed water in the structure. (Ratner *et al.* 2004). Similar phenomenon was observed in other glasses of investigation. The change was faster with dissolution of finer particles.

Figure 33 present spectra of coarse particles of all investigated glass compositions, immersed for 168h, and Figure 34 presents spectra of fine particles, immersed for 168h, for glass compositions B12.5, -Mg5, -Sr10 and B12.5-Mg5-Sr10.

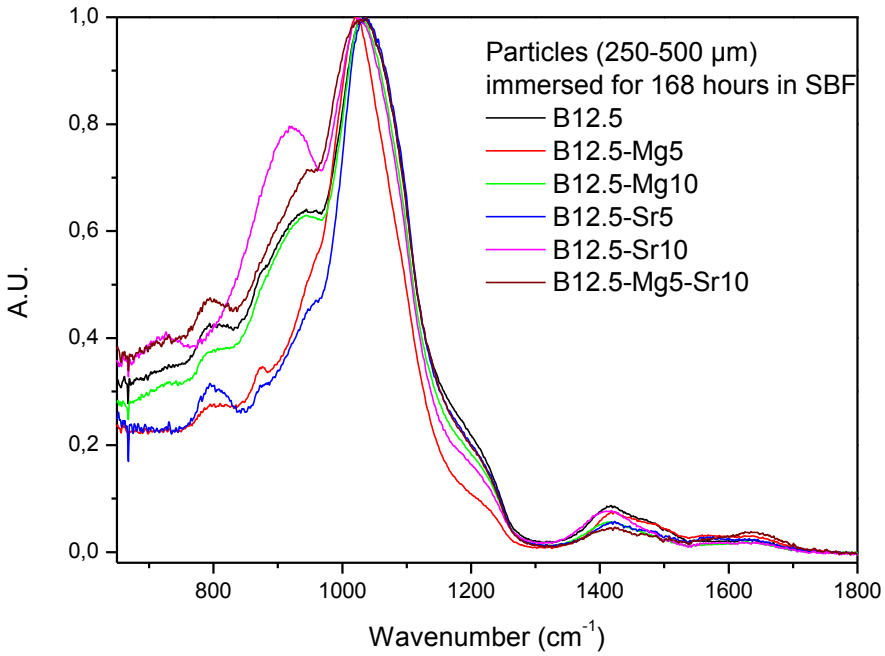

Figure 33. *FTIR spectra of all glasses (250-500 µm) immersed 168h (1 week) in SBF.*

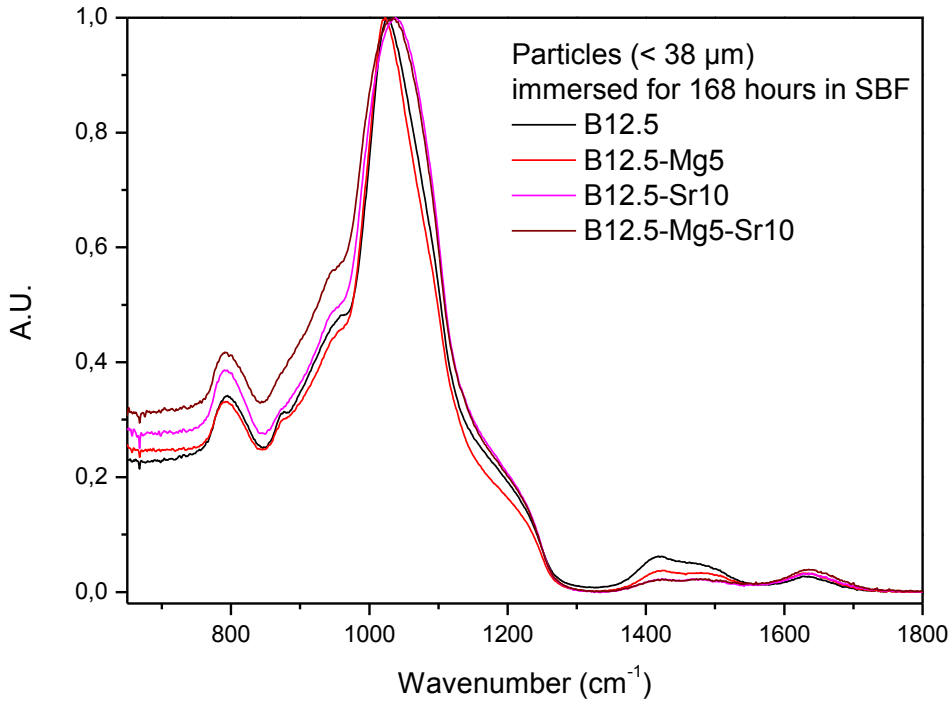

Figure 34. *FTIR spectra for fine particles of glasses B12.5, B12.5-Mg5, B12.5-Sr10 and B12.5-Mg5-Sr10 immersed 168h in SBF.*

In Fig. 33, the normalized spectra reveal changes around peaks of Si-O and/or B-O (850-950 cm^{-1}) at slightly different pace between investigated glass compositions. From after a bit longer immersion time, after 168h observed from Fig. 33, it seems that small addition (5% substitution of the Ca content) of Sr and Mg might speed up the disappearance, in comparison of other investigated glass compositions. In this time point, B12.5-Sr10 represents the highest peak at 850-950 cm^{-1} range.

Fig. 34 presents FTIR spectra for fine particles of glasses B12.5, B12.5-Mg5, B12.5-Sr10 and B12.5-Mg5-Sr10 immersed 168h in SBF. From this, we can observe that spectra for B12.5 and –Mg5 are highly similar. This was also the case with composition –Mg10 (not presented). B12.5 possesses slightly higher peak around 1460 cm^{-1}, attributable to CO_3 (Ratner *et al.* 2004), than other investigated glass compositions. Furthermore, addition of Sr seems to cause a slight shift in peak related on the range of the PO_4^{3-}, phosphate group as orthophosphate (1000-1100 cm^{-1}).

6. DISCUSSION

It is well known that the physical and thermal properties of glasses are strongly dependent on their structure and composition. (Massera *et al.* 2011). The aim of the study was to assess whether the introduction of Mg and Sr had positive impact on the thermal and dissolution properties of a borosilicate bioactive glass. Studied glass compositions were modifications of commercial BonAlive® S53P4, glass that is already utilized in clinical applications with good results (Lindfors *et al.* 2010). Similar glasses with modified boron content, and without substitution of alkali earth metals have been studied in thesis of Ojha, 2016. Study by Ojha showed that boron substitution for SiO_2 led to enhanced thermal properties as well as conversion of the glass to hydroxyapatite upon dissolution in SBF. For further enhancement of the glass properties, Sr and Mg have been introduced to tailor glass dissolution and thermal properties.

6.1 Characteristic properties of studied glasses

Sr and Mg substitution for Ca led to significant changes in the physical properties (table 5). When some of the Ca was substituted with Mg, a lighter element, the density and molar volume decreased. The decrease in density can be correlated to the lighter mass of Mg compared to Ca, while the decrease in V_m indicates a contraction of the glass network, most likely due to the smaller size of the Mg ion compare to Ca. Sr is heavier than Ca and therefore an increase in the density was expected. However, no change in V_m, within the error of the measurements could be evidence. In conclusion, these results are consistent with both the molecular mass and size of the elements. Molar volume refers to the volume occupied by one mole of substance. In this case, it is directly linked to the glass network; V_m indicates the physical size of the network one mole of this specific glass composition forms. When linked with density, these properties correlates to how dense or open the glass network is (Sharmin *et al.* 2013). In other studies, substitution of modifier cations that have same valence but difference size (as it is the case in Sr and Mg substitution for Ca), the network, depending on the size of the cations, has been shown to become more compact, or expand. (Brauer 2015; Fredholm *et al.* 2010; Morikawa *et al.* 2013; Xiang & Du 2011). From Fig. 7 can therefore be interpreted that Mg substitution leads to a less open network which might have lower dissolution rate, whereas Sr had no notable effect on the network compactness.

The structural properties of the investigated glasses were analyzed with both Raman and FTIR spectroscopy. The observed peaks, presented in Fig. 8 and 9, could be attributed mostly to bonds related to the boron and silicon network forming ions. Where FTIR gives good indication on the amount of bridging and non-bridging oxygen in the silica network,

as well as boron conformation (BO^3 vs BO^4 units, ring vs. linear structure) Raman spectroscopy gives more specific information on the amount of Q^n units, where n =0 to 4 and corresponds to the number of bridging oxygen. From Fig. 8 presenting the Raman spectra of all glasses of investigation, it appears that major changes occur in the 500-700 cm^{-1} region, where the band centered at 630 cm^{-1} increases in intensity with Ca substitution. The change is more pronounced for the Sr containing glasses. This band is related to breathing mode of borosilicate rings. (Bunker *et al.* 1990; Manara *et al.* 2009; Matson *et al.* 1983; Meera *et al.* 1990, 1993). This could indicate an increase in the boron structural units in the glass structure when Mg (10 mol%) and/or Sr are introduced instead of Ca in the glass structure. This is further confirmed by the changes the relative band intensity in the 800-1200 cm^{-1} region, as the band at 1090 cm^{-1} increases in intensity compare to the band with maximum intensity at 950 cm^{-1}. This could be attributed to an increase in the overall silica network connectivity, evidenced by an increase in Q^3 units at the expense of the Q^2 units. Furthermore, the band related to the breathing modes of borosilicate rings shifts to lower wavenumber whereas the bands attributed to the silica network shifts to higher wavenumber (Fig.8). This may be contributed to the borate network that is enriched in alkaline earth elements, leading to structural distortion. The silica network, pertaining to the shift seem to become more stable upon substitution of the Ca with Mg and/or Sr. (Hill & Brauer 2011).

The FTIR spectra presented in Fig. 9 tend to further confirm the speculations, as the ratio between the intensity of the peak at 950 and at ~1050 cm^{-1} (I_{950}/I_{1050}) decrease from 1.25 to 1.20 when Ca is replaced with Mg, and it decreases from 1.25 to 1.17 when Ca is replaced with Sr. For the mixture glass B12.5-Mg5.Sr10 the ratio is of 1.15. The decrease in this ratio indicates that the band at higher wavenumber increases in intensity, compared to the main band, indicating an increase in oxygen bridged to silica and a decrease in non-bridging oxygen in the silica network. This is in agreement with an increase in Q^3 units. (Fukumi *et al.* 1990; Manara *et al.* 2009; Mysen & Frantz 1994; Neuville *et al.* 2006, 2008.)

In order to study the glass crystallization tendency upon heat treatment, DTA must be performed. However, sintering and crystallization, two thermally activated process, are known to be glass particles size dependent (Boccacini *et al.* 1996; Chatzistavrou *et al.* 2006; Rabinovich 1985). Most of the test were conducted with glass particles of two different sizes. Particles were produced by crushing glass with mortar and pestle, then sieved to either < 38 µm sieve (fine particles) or with 250 and 500 µm sieves (coarse particles). The analysis of particle size distribution however revealed that for coarse particles, the diameter ranged between 223 and 792 µm, mass median being approximately 460 µm (table 6). This indicates that the average particle size was on the upper limit of expected size, and batches contained additionally much larger particles than expected. This can be attributed to the particles being produced by mechanically crushing, therefore leading to needle like shaped particles rather than spherical.

For fine glass particles, diameter ranged from 2 to 48 µm, with mass median of 16 µm. Additionally, from Fig. 7 can be seen that particles of glass composition B12.5 were slightly larger than with other compositions. This is likely cause by the production method, than anything related to glass composition. However, the small variation in mean particles size should not impair the comparison of the thermal and dissolution properties of the glasses of investigation. This is especially true as the cumulative size distribution shows that the differences between D_{10}, D_{50} and D_{90} is not significant.

6.2 Thermal properties and sintering

The current commercial melt-derived glasses have been shown to be challenging in hot forming processes because of their high tendency to crystallize, as a result of their composition. Crystallization in the other hand has been shown to lead to loss of glasses bioactive properties. (Hupa *et al.* 2016; Massera *et al.* 2012a). This is problematic when considering preparation of products based on bioactive glasses, e.g. porous implant materials for the needs of tissue engineering applications, by forming process such as heat sintering. Therefore, the utilized bioactive glasses would need to tolerate thermal treatments without crystallization. (Arstila *et al.* 2007, 2008). Because of this, glass composition of commercial BonAlive® S53P4 was adjusted, first of all, by addition of B_2O_3, but especially with introduction of MgO in some of the investigated glasses. In general, alkali earth metals have been found to increase the working range for hot forming applications. (Brink 1997).

DTA results for the fine glass particles are presented on Fig. 13. These results show the effect of increasing MgO content on both T_g and T_x values of the investigated glasses. As a result of decreased T_g, the working range ΔT was observed to increase from approximately 30 to 50 °C with 5 to 10 mol% substitution, respectively. The impact was not as self-explanatory with the coarse particles, however similar trend could be observed. Surprisingly, also glass composition with 10 mol% Sr introduction expressed relatively preferable properties. This results were in agreement with study of Massera & Hupa 2014, where it was found that when molar content of SrO in glass exceeding 5 mol%, the crystallization rate and peak intensity decreased, yet however during this study, this did not cause decrease in the working range (table 7 and 8). Results acquired with DTA indicated two different T_g´s for glass containing both Mg and Sr. This could be attributed to phase separation; an uneven distribution of forming ions within the structure. (Moynihan *et al.* 1971). As expected, DTA traces exhibit a shift towards higher crystallization temperatures for the coarse glass particles (Chatzistavrou *et al.* 2006; Massera *et al*. 2012a). This is typically expected as larger particles tend to exhibit a thermal lag compared to fine particles (Rabinovitch 1985).

During the sintering, it was found out that in tested conditions, the glasses of larger particle size did not sinter properly. With DTA, coarse glass of B12.5 was determined to have hot forming domain of approximately 160 °C. When sintered within this temperature

range, inspected glass B12.5 did not form to a solid specimen. Not only the sintering did not lead to a solid samples but crystallization started already in temperature 60 °C below T_x. Similar phenomenon was observed with other inspected compositions of the larger particle size. Therefore it appears that these glasses were not as promising for sintering when using large particles.

Sintering of finer glass particles was more successful, indicating that problems of the coarse glass particles could possibly be attributable to the non-uniformity and relatively large size distribution observed (Fig. 8). In general, uniformity in particle size is more favourable for sintering. (Rabinovich 1985). Additionally, result can be attributed to more rapid sintering of fine particles with annihilation of the significant part of the surface before the onset of crystallization. (Arstila *et al.* 2008; Chatzistavrou *et al.* 2006). Nevertheless, the glass B12.5 shows limited sinterability as seen in the SEM images (Fig. 14A). Especially the SEM images of the fine glass B12.5 shows low sinterability and initial crystallization at T_x-40 °C. Such behavior was expected from the study of Ojha (Ojha 2016). Addition of Mg seem to improve greatly the sinterability of the glass. Indeed, SEM images (Fig. 14C and 14E) shows almost fully sintered body with very limited residual porosity and air bubbles. Despite the XRD diffractogram showing initial crystallization at T_x-40 °C, the crystallinity of the material seems to be relatively low. Crystallite can be observed as bright spherical shapes in the SEM images. The small extent of crystallization along with the really high viscous flow of the glass particles could lead to assume, that sintering, prior to glass crystallization, could be achieved at lower temperature. A slightly lower sintering temperature could lead to a partially sintered body, with some porosity and without crystallite. This is even further supported by the low intensity of the crystallization peaks at the studied sintering temperature (Fig. 18-19).

Glass containing increasing amount (10 mol%) of Sr (Fig. 15C) also expressed better sinterability than the based glass B12.5. Sintering was however not as good as the ones observed in Mg containing glasses. Similarly to the other glasses, the XRD pattern suggest crystallization already at T_x-40 °C (Fig. 20 and 21). Based on the results, it appears that both Sr and Mg tend to shift the viscosity curve to lower temperatures as expected from (Massera & Hupa 2014) and (Massera *et al.* 2012b).

Mixture composition of B12.5-Mg5-Sr10 was perhaps the most interesting, as the composition seemed to sinter relatively well (Fig. 15E) while remaining amorphous (Fig. 22). In addition, there is a hypothesis that phase separation may be important for controlling or preventing crystallization. This depends likely from multiple factors, including the composition, network and its connectivity, phosphate content, modifiers and initial glass treatment. (Brauer 2015). Phase separation was suspected from the SDTA analysis and was confirmed with the contrast change within particles cross section seen in Fig. 15E, indicating two distinct glass composition.

Crystallization, in most cases, starts from the surface of the glass, and should be greater in the case of a higher surface area**.** Also, defects caused by crushing of glass can act as nucleation points where crystallization may occur. (Arstila *et al.* 2008.) The crystallization on the possible grain boundaries observed with SEM in Mg containing glasses could suggest that crystallization of these composition starts from the materials surface. This could be further studied analysing for example if intensity of the crystal peaks is affected by surface-to-volume ratio of the inspected glass specimen. (Massera *et al.* 2012a). Nevertheless, more detailed crystallization study is needed to confirm glass crystallization kinetics and dimensionality.

6.3 Dissolution and bioactivity

Dissolution of ions is one the most important characteristic when selecting bioactive glasses for different applications (Hupa *et al.* 2016). In this study, dissolution was analyzed by the means of pH measurements, ICP-OES for the dissolution solution SBF, and FTIR for the immersed glass specimen.

It is well known that the surface apatite layer of glass is formed by a chemical reaction of the material with the ions in the body fluid. SBF is a solution which has the ion concentration and pH almost equal to human blood plasma. However, when performing *in vitro* dissolution studies the conditions used and the simulated body fluid solution do not completely match those of a human body. (Brauer 2015; Macon *et al.* 2015). As a dissolution solution, SBF is highly supersaturated toward apatite formation; therefore, dissolution in this medium usually results in relatively quick precipitation of HA (Kokubo *et al.* 1990).

As seen in Fig. 23 and 24, the pH of all immersion solutions increased with increasing the immersion time. These changes are typical in *in vitro* dissolution of both silicate and borate bioactive glass compositions (George 2015; Varila *et al.* 2012). Increase in pH indicates more free ions in dissolution solution, which can be attributed to release of ions from the dissolving glass. Typically, an increase in pH is due to the release of large amount of alkali and alkaline earth ions. Change in pH was observed to be faster for finer particle size glasses than for the coarse ones (Fig. 23 and 24). This is due to the higher surface area of fine glass particles opposed to the coarse one. This, in turn, leads to more atoms in contact with the surrounding solution and likely to be leached out of the network into the solutions.

It is important to note that the surface area between the compared glass compositions was kept at relatively fixed ratio for the compared glass compositions, in order to maintain the amount of glass surface in contact with the solution. The surface area as an attribute is highly important, as maintaining it constant will allow to mimic a critical size defect filled with similar amount of glass. Only by maintaining the surface area constant, the changes in dissolution kinetics can be discussed as a function of composition. (Macon *et al.* 2015). This is also one aspect that has to be noted when designing scaffold structures; overall

surface area of the devices is affected by the porosity and how well the structure has been formed.

From Fig. 24, showing the pH of the SBF as a function of immersion time for all glasses of investigation with fine particles size, it can be noted that all glasses containing Mg and/or Sr ions seemed to initially dissolve faster, however at longer immersion times the pH saturates, indicating the dissolution reaction is slowing down. The base B12.5 glass of the study was found to still have a sustain pH increase even at 168h of immersion, indicating that reaction is still proceeding. Although these particles were noted to be slightly bigger than rest of the fine particles (Fig.10), however the fast reaction of fine particles in SBF is often difficult to fully interpret due to fast reaction. Fig. 23 shows similar figure obtained for immersion of coarse particles. As compared to pH obtained for fine particles, the increase in pH is more sustained over the two weeks of immersion. The glasses containing 5 mol% of Mg and Sr do not seem to exhibit significant differences compared to the B12.5 glass. However, glass with 10 mol% of Mg and even more so, for the glass with 10 mol% of Sr and the mixture glass B12.5-Mg5-Sr10, the pH increase is reduced compared to the base glass.

The pH of the solution should be related to the ion concentration in the solution, in this case the release of Si, B, Ca, P, Sr and Mg. The leaching of Si to the solution does not seem to be greatly affected by the glass composition. Only the glasses with 10 mol% SrO and the mixture glass seem to have slightly lower Si release. This is in agreement with Raman spectroscopy which indicated a larger number of Q^3 units in the silica glass structure, less prone to be hydrolyzed. (Hill & Brauer 2011). The boron release was found be decrease with 10 mol% MgO and decreased even further for the glass containing 10 mol% SrO and the mixture glass. This is interesting as it could be interpreted that the introduction of Mg and Sr in large amounts at the expense of Ca stabilizes the boron network in the glasses. This is in agreement with the structural properties discussed which indicated increased stability of the boron groups in the glass system.

The release of Ca ion is more challenging to interpret. Typically, in the case of bioactive glasses the Ca concentration in SBF first increases, and afterwards either remains constant or decreases. Such behavior is seen in parallel of a decrease of the P ion concentration with respect to time of immersion. This behavior can be related to precipitation of Ca-P on surface of the material. In case of bioactive glasses, this usually indicates formation of HA. (Massera & Hupa 2014). Here, the glass containing more Ca, as expected, release more Ca within the solution, whereas with glasses containing less Ca, namely B12.5-Mg10, B12.5-Sr10 and the mixture glass, the Ca ion concentration did not seem to increase during the immersion period (Fig. 27). Nonetheless, it can be noticed that the P concentration decreases in all of the solutions (Fig. 28). However, at 2 weeks of immersion, it is clearly seen that an increase in Mg and Sr in the glass composition lead to a decrease in P consumption. The mixture glass exhibited lowest P consumption from all

of the investigated glasses. As the decrease in the P content can be related to HA precipitation, it can be assumed that large (in this case, 10 mol%) substitution of Ca in the studied borosilicate glass composition slows down the precipitation of HA. This would be in line with the lower pH increase (Fig. 23) indicating a slower dissolution rate due to stabilization of the borate and silicate sub network.

As expected the Mg and Sr release (Fig. 29 and 30) shows release of these cations within the solution. With coarse particles, the initial dissolution rate of Sr seemed to be faster than one of Mg, and somewhat slower in the mixture composition, however results with fine particle size (not presented) indicated, that eventually the release saturates to be in consistency of the content of Mg and Sr in the glasses.

Changes in the FTIR spectra suggest disappearance of silicate and borate bonds (band at ~950 cm^{-1} range in Fig. 9), at the expanse of the band at ~1100 cm^{-1}, attributed to phosphate, which gets stronger. Overall, this indicates that the glass backbone is breaking down, and a reactive phosphate layer forms at the surface of the glasses as seen in previous studies (Massera & Hupa 2014; Massera *et al.* 2012b) (Fig. 31 & 32). At longer immersion times, it can be observed than small addition of Mg and Sr improve the assumed Ca-P formation (Fig. 33), whereas larger concentrations reduce the reaction rate. This has also been noted in studies by Massera *et al.* (Massera *et al.* 2012b; Massera & Hupa 2014). It is conceivable that Mg and Sr doped glasses could lead to Mg and Sr doped HA, which may have different precipitation rate and stability. This might be indicated by broader phosphate related peak in Sr containing compositions (Fig.34). In previous study (Massera & Hupa 2014), it was found that a minimum of 10 mol% of Sr was necessary to precipitate Sr substituted HA layer. Results suggested slower HA formation rate on the composition of mixture glass which contained both Mg and Sr. This could be due to either the phase separation, or precipitation of a Mg-Sr HA. Among other following analysis, this will be studied more in depth in the future.

In conclusion, the formation of HA at the surface of all glass compositions indicates that the studied materials should be bioactive. The presence of large amount of Sr (10 mol%) leads to a decrease in glass reactivity, in turns leading to slower B release. This is beneficial, as it was found in the other research performed in the group, that fast dissolving glasses are poor substrate to the cell adhesion and large B content within the media tend to decrease the cells activity (data not yet published). Furthermore, the release of Sr in the media as well as Sr in the HA layer was found to be beneficial to gingival fibroblasts cells viability and proliferation (Massera *et al.* 2015b). Therefore, the combination of Mg and Sr within the glass may reveal to be beneficial for bone applications.

7. CONCLUSIONS

In this study, six novel borosilicate glass composition based on commercial S53P4 glass were produced, and characterized for their physical and structural properties. The properties of the borosilicate glass were modified by introduction of Mg and Sr, hoping to manufacture glasses with enhanced thermal and dissolution properties.

In preliminary assessing of sintering behavior, notable differences in thermal properties and sinterability were observed between studied glass compositions. The particle size of the sintered glass had a notable effect, as sintering of coarse glass particles sieved to size of 250-500 µm did not work in the tested conditions. Good results were obtained, in the other hand, with fine particles with diameter smaller than 38 µm. Overall, introduction of Mg and Sr did seem to improve the properties. However, further analysis of sintered specimen revealed crystallization in all of the glass compositions. Mg did seem to widen hot forming domain and sinterability, but as crystallization was observed, sintering in lower temperatures could be investigated in more detail. This is made possible as Mg seem to lower the viscosity of the glass. Sr seemed to have decreasing impact to the crystallization of the investigated compositions. While the mixture composition possessed quite narrow hot forming domain and phase separation within the structure, it proved to be perhaps the most interesting composition due to relatively good sinterability and low crystallization. Both sinterability and crystallization of the bioactive glass could relate directly to mechanical properties of sintered scaffold structures prepared from the material. Although in general crystallization is not desired, it should be noted that glasses showing higher tendency to crystallize have been shown to have higher *in vitro* bioactivity. (Arstila *et al.* 2008).

The possible bioactivity was assessed by dissolution of the glasses in SBF. Rapid HA formation was seen with all investigated specimen, indicating bioactivity of all studied glass compositions. Additionally, it was suspected that the introduced alkali earth metals resulted in Mg and Sr doped HA. Interestingly, it appears from structural investigation and deep analysis of *in vitro* dissolution test that substitution of large amount of Sr and Mg for Ca stabilize the borate network. Such stabilizing effect could be of tremendous interest to control the release of boron and maintain it at a level where it has a beneficial effect on bone formation. However, further testing is needed with *in vitro* cell tests to gain more insight about the effects of the glasses on cell proliferation and differentiation.

Based on the results, the investigated borosilicate glass compositions seem promising for tissue engineering applications. Further testing in terms of both bioactivity and sintering and crystallization behavior is needed to assess if these bioactive glasses would be suitable for example production of porous scaffold structures. Hence, the studies with the investigated glasses continue.

REFERENCES

Akagi, R., Ohtori, N. & Umesaki, N. (2001). Raman spectra of K2O-B2O3 glasses and melts, Journal of Non-Crystalline Solids, Vol. 293-295(1), pp. 471-476.

Alberts, B., Johnson,A.,Lewis,J.,Raff,M., Roberts, K. & Walter, P. (2008). Molecular Biology of the Cell, 5th ed., Garland Science, New York, USA, 1392 p.

Amini, A.R., Laurencin, C.T. & Nukavarapu, S.P. (2012). Bone tissue engineering: Recent advances and challenges, Critical Reviews in Biomedical Engineering, Vol. 40(5), pp. 363-408.

Arstila, H., Vedel, E., Hupa, L. & Hupa, M. (2007). Factors affecting crystallization of bioactive glasses, Journal of the European Ceramic Society, Vol. 27(2-3), pp. 1543-1546.

Arstila, H., Hupa, L., Karlsson, K.H. & Hupa, M. (2008). Influence of heat treatment on crystallization of bioactive glasses, Journal of Non-Crystalline Solids, Vol. 354(2-9), pp. 722-728.

Baino, F. & Vitale-Brovarone, C. (2011). Three-dimensional glass-derived scaffolds for bone tissue engineering: Current trends and forecasts for the future, Journal of Biomedical Materials Research - Part A, Vol. 97 A(4), pp. 514-535.

Baino, F., Novarja, G. & Vitale-Brovarone, C. (2015). Bioceramics and Scaffolds: A Winning Combination for Tissue Engineering. Frontier is Bioengineering and Biotechnology, Vol. 3pp. 1-17.

Bankoff, A.D.P. (2012). Biomechanical Characteristics of the Bone, in: Goswami, T. (ed.), Human Musculoskeletal Biomechanics, pp. 61-84.

Bellucci, D., Cannillo, V. & Sola, A. (2010). An overview of the effects of thermal processing on bioactive glasses, Science of Sintering, Vol. 42(3), pp. 307-320.

Berzina-Cimdina, L. & Borodajenko, N. (2012). Research of Calcium Phosphates Using Fourier Transform Infrared Spectroscopy, in: Theophile, T. (ed.), Infrared Spectroscopy - Materials Science, Engineering and Technology, InTech, Available (accessed 10/2/2016): http://www.intechopen.com/books/infrared-spectroscopy-materials-science-engineering-and-technology/research-of-calcium-phosphates-using-fourier-transformation-infrared-spectroscopy.

Boccaccini, A.R., Stumpfe, W., Taplin, D.M.R. & Ponton, C.B. (1996). Densification and crystallization of glass powder compacts during constant heating rate sintering, Materials Science and Engineering A, Vol. 219(1-2), pp. 26-31.

Bohner, M. & Lemaitre, J. (2009). Can bioactivity be tested in vitro with SBF solution? Biomaterials, Vol. 30(12), pp. 2175-2179.

BonAlive® product line- the new era of bone regeneration, BonAlive Biomaterials Ltd., web page. Available (accessed 10/12/2016): http://www.bonalive.com/products/.

Bonnelye, E., Chabadel, A., Saltel, F. & Jurdic, P. (2008). Dual effect of strontium ranelate: Stimulation of osteoblast differentiation and inhibition of osteoclast formation and resorption in vitro, Bone, Vol. 42(1), pp. 129-138.

Brauer, D.S., Rüssel, C., Li, W. & Habelitz, S. (2006). Effect of degradation rates of resorbable phosphate invert glasses on in vitro osteoblast proliferation, Journal of Biomedical Materials Research - Part A, Vol. 77(2), pp. 213-219.

Brauer, D.S. (2015). Bioactive glasses - Structure and properties, Angewandte Chemie - International Edition, Vol. 54(14), pp. 4160-4181.

Brink, M. (1997). The influence of alkali and alkaline earths on the working range for bioactive glasses, Journal of Biomedical Materials Research, Vol. 36(1), pp. 109-117.

Brown, R.F., Day, D.E., Day, T.E., Jung, S., Rahaman, M.N. & Fu, Q. (2008). Growth and differentiation of osteoblastic cells on 13–93 bioactive glass fibers and scaffolds, Acta Biomaterialia, Vol. 4, pp. 387-396.

Bunker, B.C., Tallant, D.R., Kirkpatrick, R.J. & Turner, G.L. (1990). Multinuclear nuclear magnetic resonance and Raman investigation of sodium borosilicate glass structures, Physics and Chemistry of Glasses, Vol. 31(1), pp. 30-41.

Chatzistavrou, X., Zorba, T., Chrissafis, K., Kaimakamis, G., Kontonasaki, E., Koidis, P. & Paraskevopoulos, K.M. (2006). Influence of particle size on the crystallization process and the bioactive behavior of a bioactive glass system, Journal of Thermal Analysis and Calorimetry, Vol. 85(2), pp. 253-259.

Chen, Q.Z., Thompson, I.D. & Boccaccini, A.R. (2006). 45S5 Bioglass®-derived glass-ceramic scaffolds for bone tissue engineering, Biomaterials, Vol. 27(11), pp. 2414-2425.

De Jonghe, L.C. & Rahaman, M.N. (2003). Sintering of Ceramics, in: Sominua, S. (ed.), Handbook of Advanced Ceramics, Elsevier Inc., pp. 187-264.

Dimitriou, R., Jones, E., McGonagle, D. & Giannoudis, P.V. (2011). Bone regeneration: Current concepts and future directions, BMC Medicine, Vol. 9, pp.1-10.

Fagerlund, S., Massera, J., Moritz, N., Hupa, L. & Hupa, M. (2012). Phase composition and in vitro bioactivity of porous implants made of bioactive glass S53P4, Acta Biomaterialia, Vol. 8(6), pp. 2331-2339.

Figure:Grain growth during the sintering process, Keramverband.de, web page. Available (accessed 10/2/2016): http://www.keramverband.de/pic/ebild59.gif.

Fredholm, Y.C., Karpukhina, N., Law, R.V. & Hill, R.G. (2010). Strontium containing bioactive glasses: Glass structure and physical properties, Journal of Non-Crystalline Solids, Vol. 356(44-49), pp. 2546-2551.

Fredholm, Y.C., Karpukhina, N., Brauer, D.S., Jones, J.R., Law, R.V. & Hill, R.G. (2012). Influence of strontium for calcium substitution in bioactive glasses on degradation, ion release and apatite formation, Journal of the Royal Society Interface, Vol. 9(70), pp. 880-889.

Fu, H., Fu, Q., Zhou, N., Huang, W., Rahaman, M.N., Wang, D. & Liu, X. (2009). In vitro evaluation of borate-based bioactive glass scaffolds prepared by a polymer foam replication method, Materials Science and Engineering C, Vol. 29(7), pp. 2275-2281.

Fu, Q., Rahaman, M.N., Bal, B.S., Bonewald, L.F., Kuroki, K. & Brown, R.F. (2010). Silicate, borosilicate, and borate bioactive glass scaffolds with controllable degradation rate for bone tissue engineering applications. II. In vitro and in vivo biological evaluation, Journal of Biomedical Materials Research - Part A, Vol. 95(1), pp. 172-179.

Fu, Q., Saiz, E., Rahaman, M.N. & Tomsia, A.P. (2011a). Bioactive glass scaffolds for bone tissue engineering: State of the art and future perspectives, Materials Science and Engineering C, Vol. 31(7), pp. 1245-1256.

Fu, Q., Saiz, E. & Tomsia, A.P. (2011b). Bioinspired strong and highly porous glass scaffolds, Advanced Functional Materials, Vol. 21(6), pp. 1058-1063.

Fukumi, K., Hayakawa, J. & Komiyama, T. (1990). Intensity of Raman band in silicate glasses, Journal of Non-Crystalline Solids, Vol. 119(3), pp. 297-302.

Gentleman, E., Fredholm, Y.C., Jell, G., Lotfibakhshaiesh, N., O'Donnell, M.D., Hill, R.G. & Stevens, M.M. (2010). The effects of strontium-substituted bioactive glasses on osteoblasts and osteoclasts in vitro, Biomaterials, Vol. 31(14), pp. 3949-3956.

George, J.L. (2015). Dissolution of borate glasses and precipitation of phosphate compounds. Doctoral Dissertations, Missouri University of Science and Technology, USA, Paper 2382.

Gimble, J.M., Katz, A.J. & Bunnell, B.A. (2007). Adipose-derived stem cells for regenerative medicine, Circulation research, Vol. 100(9), pp. 1249-1260.

Goel, A., Rajagopal, R.R. & Ferreira, J.M.F. (2011). Influence of strontium on structure, sintering and biodegradation behaviour of CaO-MgO-SrO-SiO 2-P 2O 5-CaF 2 glasses, Acta Biomaterialia, Vol. 7(11), pp. 4071-4080.

Groh, D., Döhler, F. & Brauer, D.S. (2014). Bioactive glasses with improved processing. Part 1. Thermal properties, ion release and apatite formation, Acta Biomaterialia, Vol. 10(10), pp. 4465-4473.

Haro Durand, L.A., Vargas, G.E., Romero, N.M., Vera-Mesones, R., Porto-López, J.M., Boccaccini, A.R., Zago, M.P., Baldi, A. & Gorustovich, A. (2015). Angiogenic effects of ionic dissolution products released from a boron-doped 45S5 bioactive glass, Journal of Materials Chemistry B, Vol. 3(6), pp. 1142-1148.

Hench, L.L. (1991). Bioceramics: From Concept to Clinic, Journal of the American Ceramic Society, Vol. 74(7), pp. 1487-1510.

Hench, L.L. (2006). The story of Bioglass®, Journal of Materials Science: Materials in Medicine, Vol. 17(11), pp. 967-978.

Hench, L.L. & Wilson, J. (2013). An Introduction to Bioceramics. 2nd edition. World Scientific, Singapore, 620 p.

Hench, L.L. & Jones, J.R. (2015). Bioactive Glasses: Frontiers and Challenges. Review, Frontiers in Bioengineering and Biotechnology, Vol. 3(194), pp. 1-12.

Hill, R.G. & Brauer, D.S. (2011). Predicting the bioactivity of glasses using the network connectivity or split network models, Journal of Non-Crystalline Solids, Vol. 357(24), pp. 3884-3887.

Huang, W., Day, D.E., Kittiratanapiboon, K. & Rahaman, M.N. (2006). Kinetics and mechanisms of the conversion of silicate (45S5), borate, and borosilicate glasses to hydroxyapatite in dilute phosphate solutions, Journal of Materials Science: Materials in Medicine, Vol. 17(7), pp. 583-596.

Hupa, L., Fagerlund, S., Massera, J. & Björkvik, L. (2016). Dissolution behavior of the bioactive glass S53P4 when sodium is replaced by potassium, and calcium with magnesium or strontium, Journal of Non-Crystalline Solids, Vol. 432pp. 41-46.

Hutmacher, D.W. (2000). Scaffolds in tissue engineering bone and cartilage, Biomaterials, Vol. 21(24), pp. 2529-2543.

Isaac, J., Nohra, J., Lao, J., Jallot, E., Nedelec, J.-., Berdal, A. & Sautier, J.-. (2011). Effects of strontium-doped bioactive glass on the differentiation of cultured osteogenic cells, European Cells and Materials, Vol. 21pp. 130-143.

ISO Standard 23317:2014 - Implants for surgery -- In vitro evaluation for apatite-forming ability of implant materials.

Jones, J.R., Ehrenfried, L.M. & Hench, L.L. (2006). Optimising bioactive glass scaffolds for bone tissue engineering, Biomaterials, Vol. 27(7), pp. 964-973.

Jones, J.R. (2013). Review of bioactive glass: From Hench to hybrids, Acta Biomaterialia, Vol. 9(1), pp. 4457-4486.

Karageorgiou, V. & Kaplan, D. (2005). Porosity of 3D biomaterial scaffolds and osteogenesis, Biomaterials, Vol. 26(27), pp. 5474-5491.

Kokai, L.E., Marra, K. & Rubin, J.P. (2014). Adipose stem cells: Biology and clinical applications for tissue repair and regeneration, Translational Research, Vol. 163(4), pp. 399-408.

Kokubo, T., Kushitani, H., Sakka, S., Kitsugi, T. & Yamamuro, T. (1990). Solutions able to reproduce in vivo surface-structure changes in bioactive glass-ceramic A-W3, Journal of Biomedical Materials Research, Vol. 24(6), pp. 721-734.

Kolios, G. & Moodley, Y. (2013). Introduction to stem cells and regenerative medicine, Respiration, Vol. 85(1), pp. 3-10.

Langer, R. & Vacanti, J.P. (1993). Tissue engineering, Science, Vol. 260(5110), pp. 920-926.

Liang, W., Rahaman, M.N., Day, D.E., Marion, N.W., Riley, G.C. & Mao, J.J. (2008). Bioactive borate glass scaffold for bone tissue engineering, Journal of Non-Crystalline Solids, Vol. 354(15-16), pp. 1690-1696.

Lindfors, N.C., Koski, I., Heikkilä, J.T., Mattila, K. & Aho, A.J. (2010). A prospective randomized 14-year follow-up study of bioactive glass and autogenous bone as bone graft substitutes in benign bone tumors, Journal of Biomedical Materials Research - Part B Applied Biomaterials, Vol. 94(1), pp. 157-164.

Lindroos, B., Suuronen, R. & Miettinen, S. (2011). The Potential of Adipose Stem Cells in Regenerative Medicine, Stem Cell Reviews and Reports, Vol. 7(2), pp. 269-291.

Liu, X., Rahaman, M.N., Hilmas, G.E. & Bal, B.S. (2013). Mechanical properties of bioactive glass (13-93) scaffolds fabricated by robotic deposition for structural bone repair, Acta Biomaterialia, Vol. 9(6), pp. 7025-7034.

Ma, J., Chen, C.Z., Wang, D.G., Meng, X.G. & Shi, J.Z. (2010). In vitro degradability and bioactivity of mesoporous CaO-MgO-P_2O_5-SiO_2 glasses synthesized by sol-gel method, Journal of Sol-Gel Science and Technology, Vol. 54(1), pp. 69-76.

Maçon, A.L.B., Kim, T.B., Valliant, E.M., Goetschius, K., Brow, R.K., Day, D.E., Hoppe, A., Boccaccini, A.R., Kim, I.Y., Ohtsuki, C., Kokubo, T., Osaka, A., Vallet-Regí, M., Arcos, D., Fraile, L., Salinas, A.J., Teixeira, A.V., Vueva, Y., Almeida, R.M., Miola, M., Vitale-Brovarone, C., Verné, E., Höland, W. & Jones, J.R. (2015). A unified in vitro evaluation for apatite-forming ability of bioactive glasses and their variants, Journal of Materials Science: Materials in Medicine, Vol. 26(2), pp. 1-10.

Manara, D., Grandjean, A. & Neuville, D.R. (2009). Advances in understanding the structure of borosilicate glasses: A raman spectroscopy study, American Mineralogist, Vol. 94(5-6), pp. 777-784.

Marion, N.W., Liang, W., Reilly, G.C., Day, D.E., Rahaman, M.N. & Mao, J.J. (2005). Borate glass supports the in vitro osteogenic differentiation of human mesenchymal stem cells, Mechanics of Advanced Materials and Structures, Vol. 12(3), pp. 239-246.

Massera, J., Claireaux, C., Lehtonen, T., Tuominen, J., Hupa, L. & Hupa, M. (2011). Control of the thermal properties of slow bioresorbable glasses by boron addition, Journal of Non-Crystalline Solids, Vol. 357(21), pp. 3623-3630.

Massera, J., Fagerlund, S., Hupa, L. & Hupa, M. (2012a). Crystallization mechanism of the bioactive glasses, 45S5 and S53P4, Journal of the American Ceramic Society, Vol. 95(2), pp. 607-613.

Massera, J., Hupa, L. & Hupa, M. (2012b). Influence of the partial substitution of CaO with MgO on the thermal properties and in vitro reactivity of the bioactive glass S53P4, Journal of Non-Crystalline Solids, Vol. 358(18-19), pp. 2701-2707.

Massera, J. & Hupa, L. (2014). Influence of SrO substitution for CaO on the properties of bioactive glass S53P4, Journal of Materials Science: Materials in Medicine, Vol. 25(3), pp. 657-668.

Massera, J., Mayran, M., Rocherullé, J. & Hupa, L. (2015a). Crystallization behavior of phosphate glasses and its impact on the glasses' bioactivity, Journal of Materials Science, Vol. 50(8), pp. 3091-3102.

Massera, J., Kokkari, A., Närhi, T. & Hupa, L. (2015b). The influence of SrO and CaO in silicate and phosphate bioactive glasses on human gingival fibroblasts, Journal of Materials Science: Materials in Medicine, Vol. 26(6), pp. 196.

Matson, D.W., Sharma, S.K. & Philpotts, J.A. (1983). The structure of high-silica alkali-silicate glasses. A Raman spectroscopic investigation, Journal of Non-Crystalline Solids, Vol. 58(2-3), pp. 323-352.

Meera, B.N., Sood, A.K., Chandrabhas, N. & Ramakrishna, J. (1990). Raman study of lead borate glasses, Journal of Non-Crystalline Solids, Vol. 126(3), pp. 224-230.

Meera, B.N. & Ramakrishna, J. (1993). Raman spectral studies of borate glasses, Journal of Non-Crystalline Solids, Vol. 159(1-2), pp. 1-21.

Meyer, U., Wiesmann, H.P., Handschel, J. & Kübler, N.R. (2009). Bone tissue engineering, in: Fundamentals of Tissue Engineering and Regenerative Medicine, ed. Meyer U, Meyer T, Handscheld J, Wiesmann H.P. pp. 211-232.

Morikawa, H., Lee, S., Kasuga, T. & Brauer, D.S. (2013). Effects of magnesium for calcium substitution in P2O 5-CaO-TiO2 glasses, Journal of Non-Crystalline Solids, Vol. 380pp. 53-59.

Moynihan, C.T., Macedo, P.B., Aggarwal, I.D. & Schnaus, U.E. (1971). Direct observation of the double glass transition in a phase-separated glass, Journal of Non-Crystalline Solids, Vol. 6(4), pp. 322-328.

Mysen, B.O. & Frantz, J.D. (1992). Raman spectroscopy of silicate melts at magmatic temperatures: Na2O1bSiO2, K2O1bSiO2 and Li2O1bSiO2 binary compositions in the temperature range 25-1475°C, Chemical Geology, Vol. 96(3-4), pp. 321-332.

Neuville, D.R. (2006). Viscosity, structure and mixing in (Ca, Na) silicate melts, Chemical Geology, Vol. 229(1-3), pp. 28-41.

Neuville, D.R., Cormier, L., Montouillout, V., Florian, P., Millot, F., Rifflet, J.-. & Massiot, D. (2008). Structure of Mg- and Mg/Ca aluminosilicate glasses: 27Al NMR and Raman spectroscopy investigations, American Mineralogist, Vol. 93(11-12), pp. 1721-1731.

Nguyen, L.H., Annabi, N., Nikkhah, M., Bae, H., Binan, L., Park, S., Kang, Y., Yang, Y. & Khademhosseini, A. (2012). Vascularized bone tissue engineering: Approaches for potential improvement, Tissue Engineering - Part B: Reviews, Vol. 18(5), pp. 363-382.

Ojha, N. (2016). Borosilicate glass with enhanced got forming properties and conversion to hydroxyapatite, Master of Science thesis, Tampere University of Technology, Finland.

Oonishi, H., Hench, L.L., Wilson, J., Sugihara, F., Tsuji, E., Matsuura, M., Kin, S., Yamamoto, T. & Mizokawa, S. (2000). Quantitative comparison of bone growth behavior in granules of Bioglass®, A-W glass-ceramic, and hydroxyapatite, Journal of Biomedical Materials Research, Vol. 51(1), pp. 37-46.

Pascuta, P., Bosca, M., Rada, S., Culea, M., Bratu, I. & Culea, E. (2008). FTIR spectroscopic study of Gd_2O_3-Bi_2O_3-B_2O_3 glasses, Journal of optoelectronics and advanced materials, Vol. 10(9), pp. 2416-2419.

Rabinovich, E.M. (1985). Preparation of glass by sintering. Review. Journal of Materials Science, Vol. 20pp. 4259-4297.

Rahaman, M.N., Day, D.E., Sonny Bal, B., Fu, Q., Jung, S.B., Bonewald, L.F. & Tomsia, A.P. (2011). Bioactive glass in tissue engineering, Acta Biomaterialia, Vol. 7(6), pp. 2355-2373.

Ratner, B., Hoffman, A., Schoen, F. & Lemons, J.E. (2014). Biomaterials Science. An Introduction to Materials in Medicine, 2nd ed., Academic Press, London, UK, 864 p.

Ray, C.S., Huang, W. & Day, D.E. (1991). Crystallization Kinetics of a Lithia–Silica Glass: Effect of Sample Characteristics and Thermal Analysis Measurement Techniques, Journal of the American Ceramic Society, Vol. 74(1), pp. 60-66.

Raynaud, S., Champion, E. & Bernache-Assollant, D. (2002). Calcium phosphate apatite with variable Ca/P atomic ratio I. Synthesis, characterisation and thermal stability of powders. Biomaterials, Vol. 23pp. 1065-1072.

Romagnoli, C. & Brandi, M.L. (2014). Adipose mesenchymal stem cells in the field of bone tissue engineering, World Journal of Stem Cells, Vol. 6(2), pp. 144-152.

Ross, M.H. & Pawlina, W. (2011). Histology - A Text and Atlas with Correlated Cell and Molecular Biology, 6th ed., Lippincott Williams & Wilkins.

Salgado, A.J., Coutinho, O.P. & Reis, R.L. (2004). Bone tissue engineering: State of the art and future trends, Macromolecular Bioscience, Vol. 4(8), pp. 743-765.

Schroeder, J.E. & Mosheiff, R. (2011). Tissue engineering approaches for bone repair: Concepts and evidence, Injury, Vol. 42(6), pp. 609-613.

Sharmin, N., Hasan, M.S., Parsons, A.J., Furniss, D., Scotchford,C.A.,Ahmed,I. & Rudd, C.D. (2013). Effect of Boron Addition on the Thermal, Degradation, and Cytocompatibility Properties of Phosphate-Based Glasses, BioMed Research International, pp. 1-12.

Serra, J., González, P., Liste, S., Serra, C., Chiussi, S., León, B., Pérez-Amor, M., Ylänen, H.O. & Hupa, M. (2003). FTIR and XPS studies of bioactive silica based glasses, Journal of Non-Crystalline Solids, Vol. 332(1-3), pp. 20-27.

Sikavitsas, V.I., Temenoff, J.S. & Mikos, A.G. (2001). Biomaterials and bone mechanotransduction, Biomaterials, Vol. 22(19), pp. 2581-2593.

Takahashi, K., Tanabe, K., Ohnuki, M., Narita, M., Ichisaka, T., Tomoda, K. & Yamanaka, S. (2007). Induction of Pluripotent Stem Cells from Adult Human Fibroblasts by Defined Factors, Cell, Vol. 131(5), pp. 861-872.

Tsuji, W., Rubin, J.P. & Marra, K.G. (2014). Adipose-derived stem cells: Implications in tissue regeneration, World Journal of Stem Cells, Vol. 6(3), pp. 312-321.

van Blitterswijk, C., de Boer, J., Thomsen, P.R. & Williams, D. (ed.). 2008. Tissue Engineering. 1st ed. Academic press. 760 p.

Varila, L., Fagerlund, S., Lehtonen, T., Tuominen, J. & Hupa, L. (2012). Surface reactions of bioactive glasses in buffered solutions, Journal of the European Ceramic Society, Vol. 32(11), pp. 2757-2763.

Vedel, E., Arstila, H., Zhang, D., Hupa, L. & Hupa, M. (2007). Control of the forming properties of bioactive glasses, Glass Technology: European Journal of Glass Science and Technology Part A, Vol. 48(4), pp. 191-195.

Vitale-Brovarone, C., Miola, M., Balagna, C. & Verné, E. (2008). 3D-glass-ceramic scaffolds with antibacterial properties for bone grafting, Chemical Engineering Journal, Vol. 137(1), pp. 129-136.

Xiang, Y. & Du, J. (2011). Effect of strontium substitution on the structure of 45S5 bioglasses, Chemistry of Materials, Vol. 23(11), pp. 2703-2717.

Xynos, I.D., Edgar, A.J., Buttery, L.D.K., Hench, L.L. & Polak, J.M. (2001). Gene-expression profiling of human osteoblasts following treatment with the ionic products of Bioglass® 45S5 dissolution, Journal of Biomedical Materials Research, Vol. 55(2), pp. 151-157.

Yano, T., Kunimine, N., Shibata, S. & Yamane, M. (2003). Structural investigation of sodium borate glasses and melts by Raman spectroscopy. I. Quantitative evaluation of structural units, Journal of Non-Crystalline Solids, Vol. 321(3), pp. 137-146.

Zhang, X., Jia, W., Gu, Y., Xiao, W., Liu, X., Wang, D., Zhang, C., Huang, W., Rahaman, M.N., Day, D.E. & Zhou, N. (2010). Teicoplanin-loaded borate bioactive glass implants for treating chronic bone infection in a rabbit tibia osteomyelitis model, Biomaterials, Vol. 31(22), pp. 5865-5874.

APPENDIX A: SIMULATED BODY FLUID

1 liter of SBF solution was prepared by adding reagents to solution in the following order;

Order	*Reagent*	*mass (g) / volume*
1.	NaCl	7.996
2.	$NaHCO_3$	0.350
3.	KCl	0.224
4.	$K_2HPO_4 \cdot 3H_2O$	0.228
5.	$MgCl2 \cdot 6H_2O$	0.305
6.	1M HCl *(aq)*	~ 40 ml
7.	$CaCl_2 \cdot 2H_2O$	0.368
8.	Na_2SO_4	0.071
9.	2-Amino-2-(hydroxymethyl)-1,3-propane-diol *	6.057

* Tris base

pH of the prepared solution was measured at +37 ±0.2°C and adjusted to pH 7.38-7.42 with HCl. Solution was stored in +4 °C.

APPENDIX B: DTA CURVES

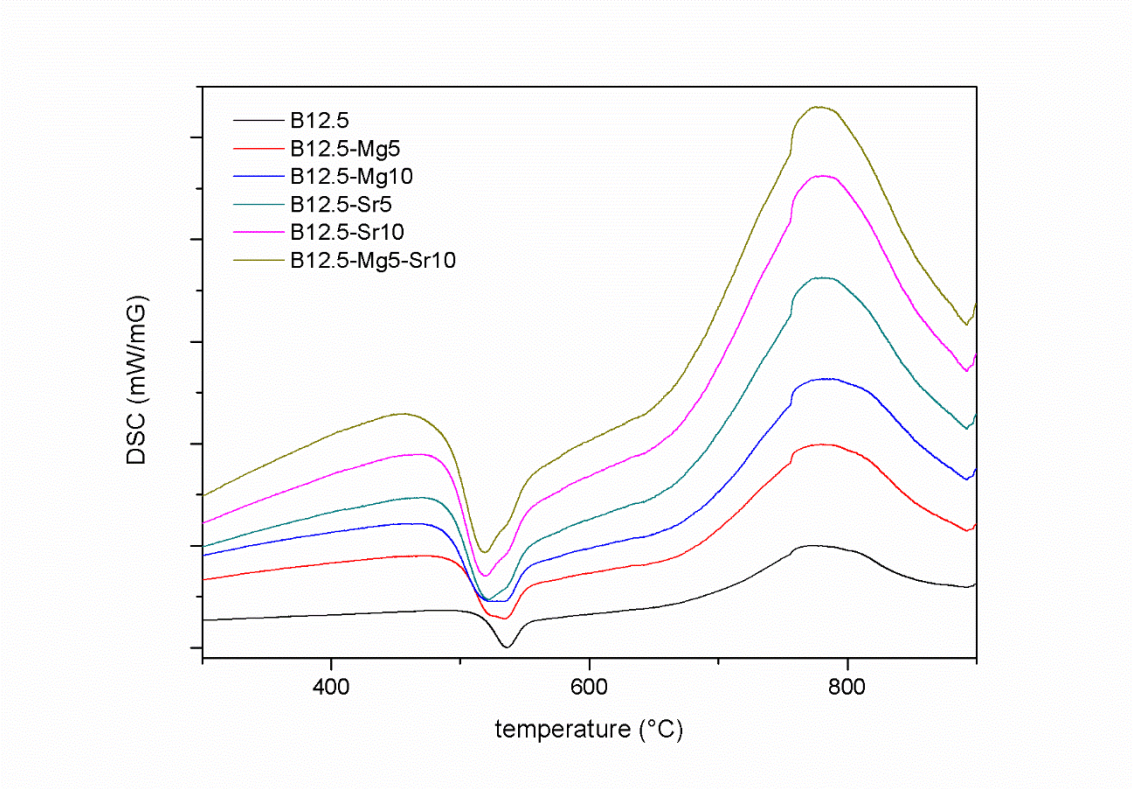

Figure A. *Plotted SDTA curves for coarse glass particles*

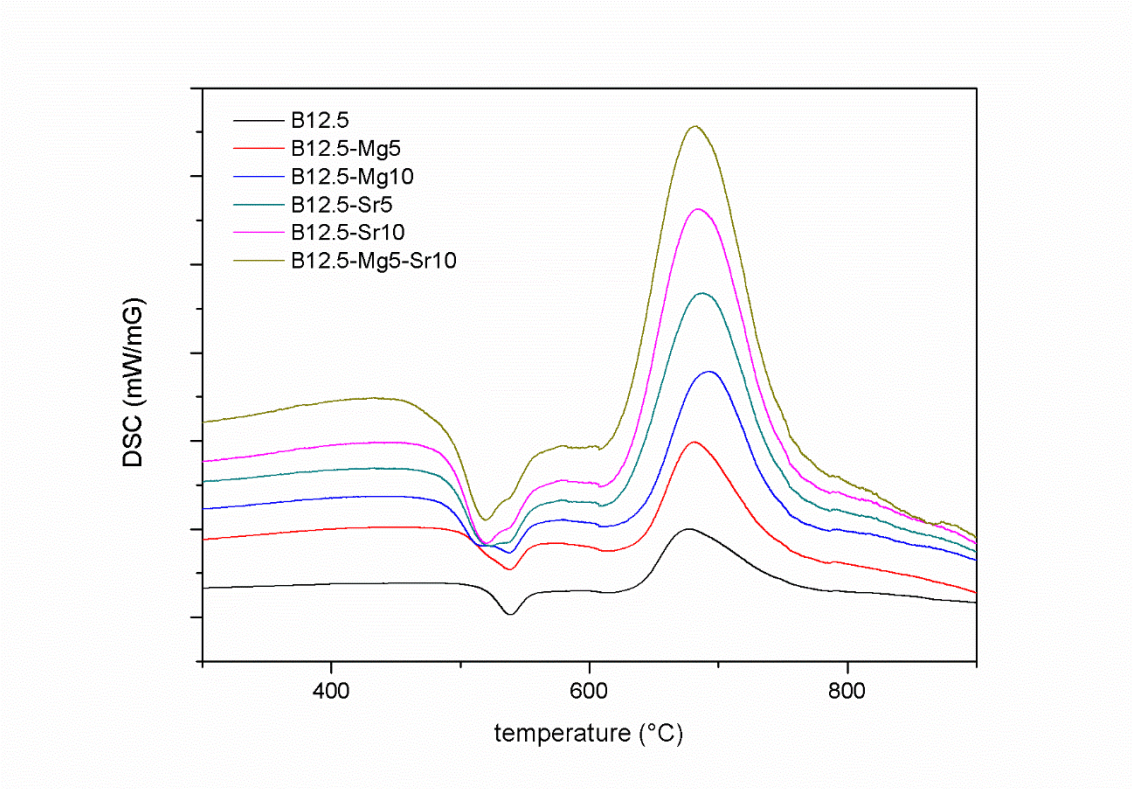

Figure B. *Plotted DTA curves for fine glass particles*

APPENDIX C: ICP-OES RESULTS

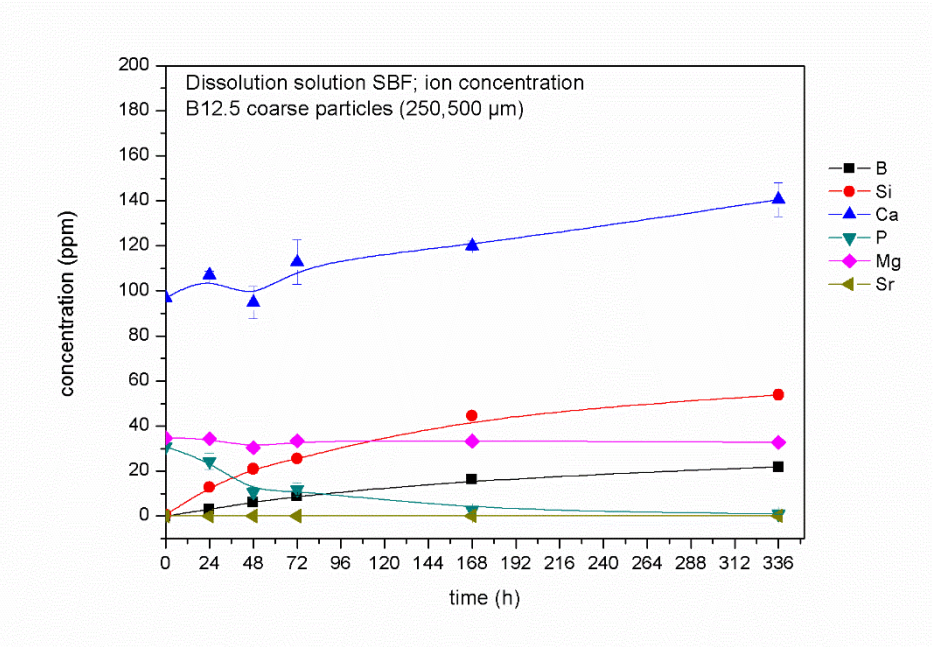

1) B12.5 coarse particle size

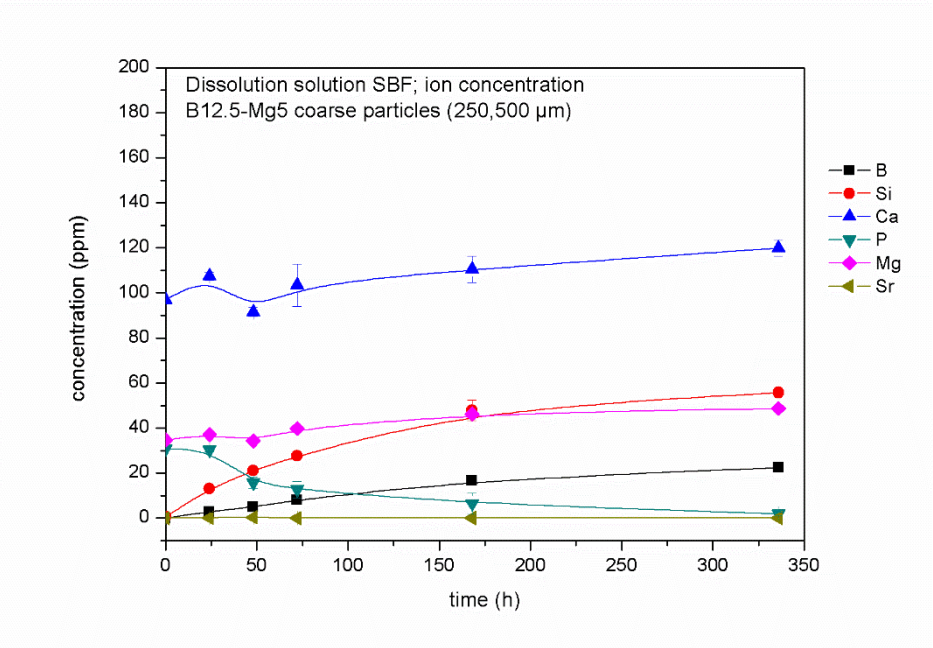

2) B12.5-Mg5 coarse particle size

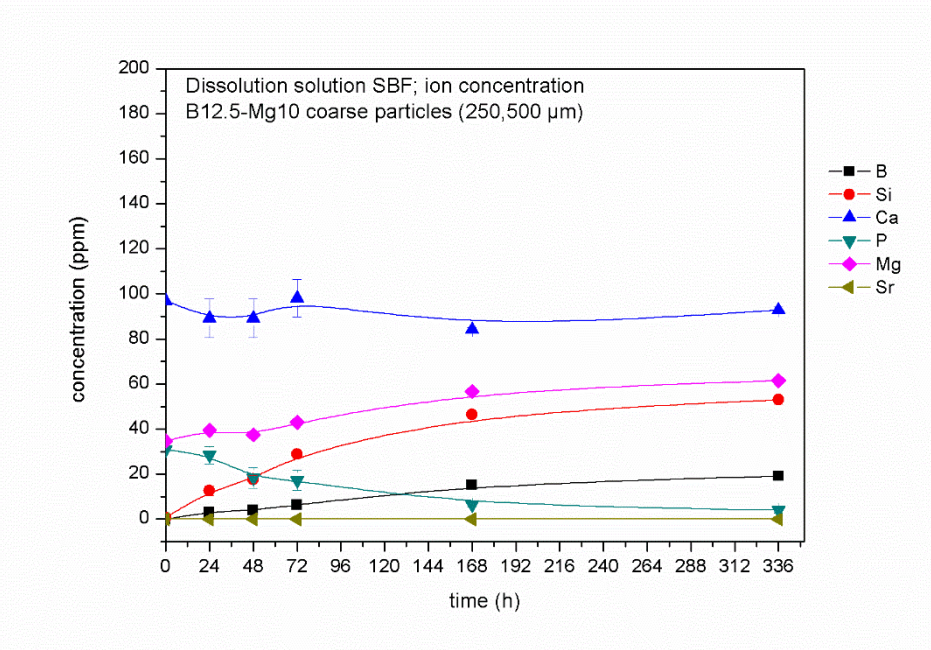

3) B12.5-Mg10 coarse particle size

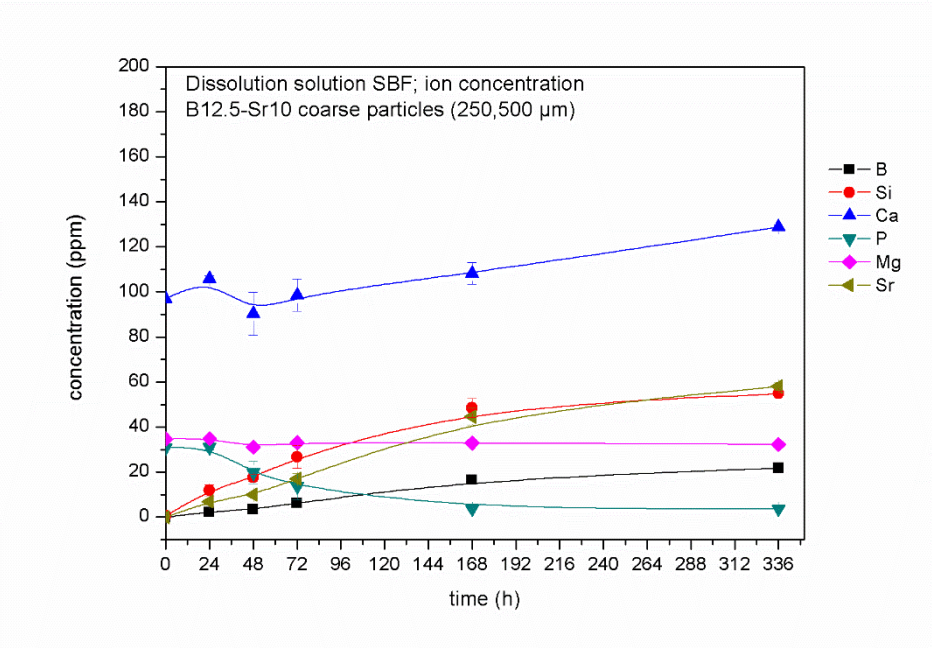

4) B12.5-Sr5 coarse particle size

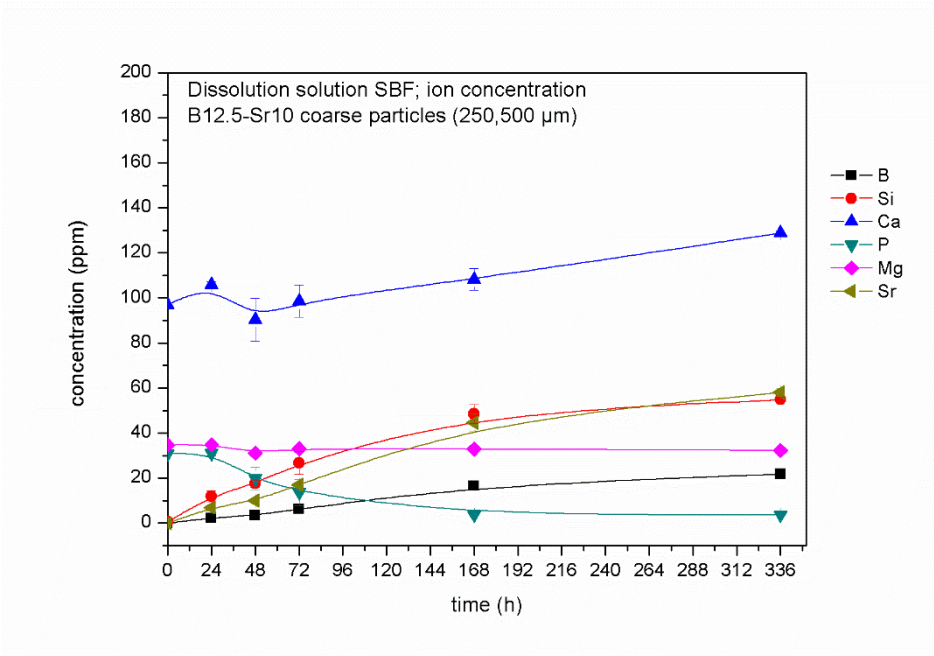

5) B12.5-Sr10 coarse particle size

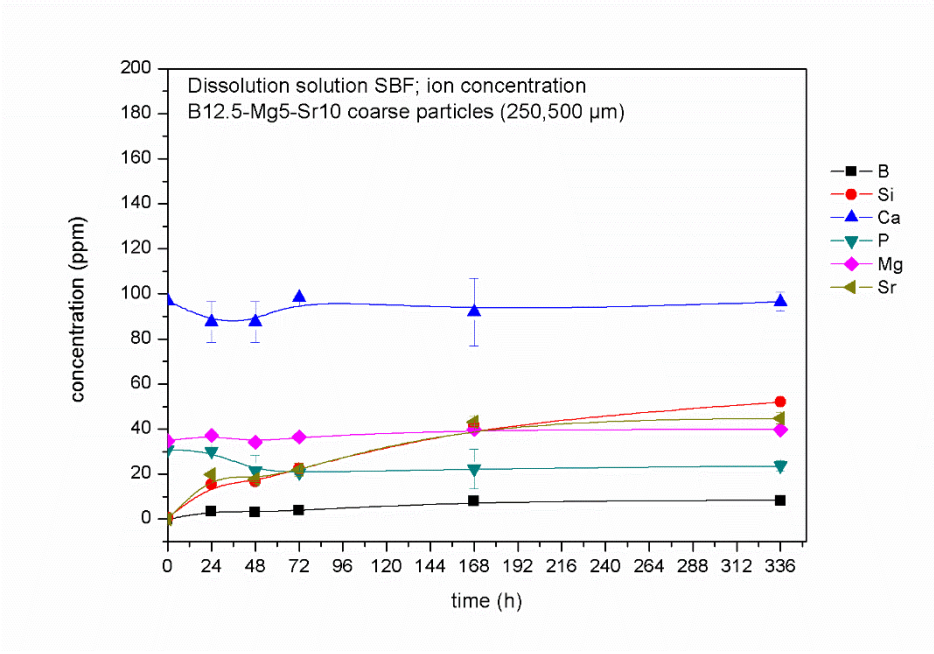

6) B12.5-Mg5-Sr10 coarse particle size

Figure C. *Ion release concentration (ppm) for elements B, Si, Ca, P, Mg, Sr as a function of immersion time. Elements determined for coarse glass particles of all studied glass compositions (1-6), for immersion in SBF up to 2 weeks.*

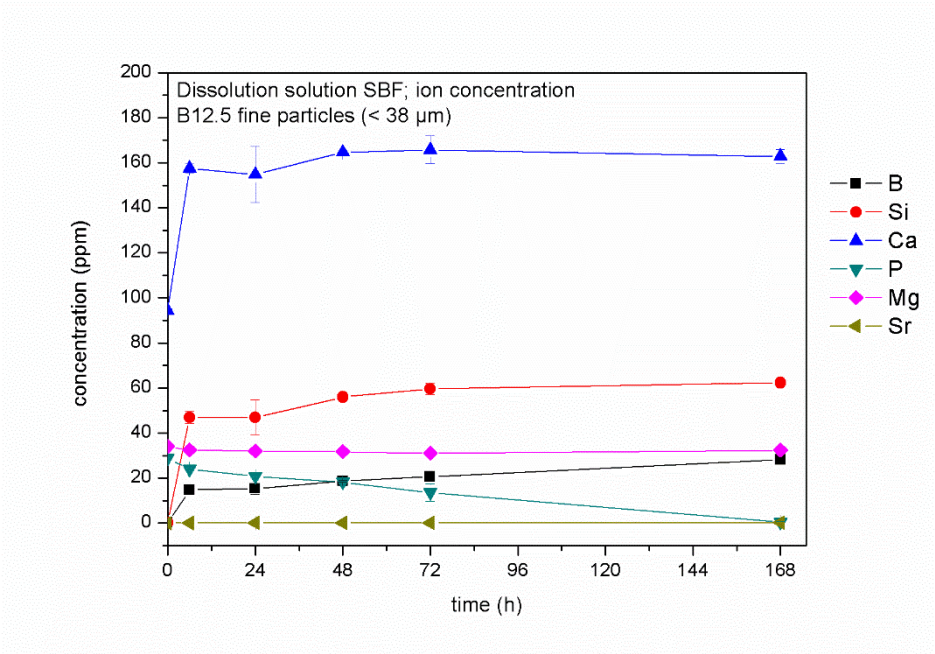

1) B12.5 fine particle size

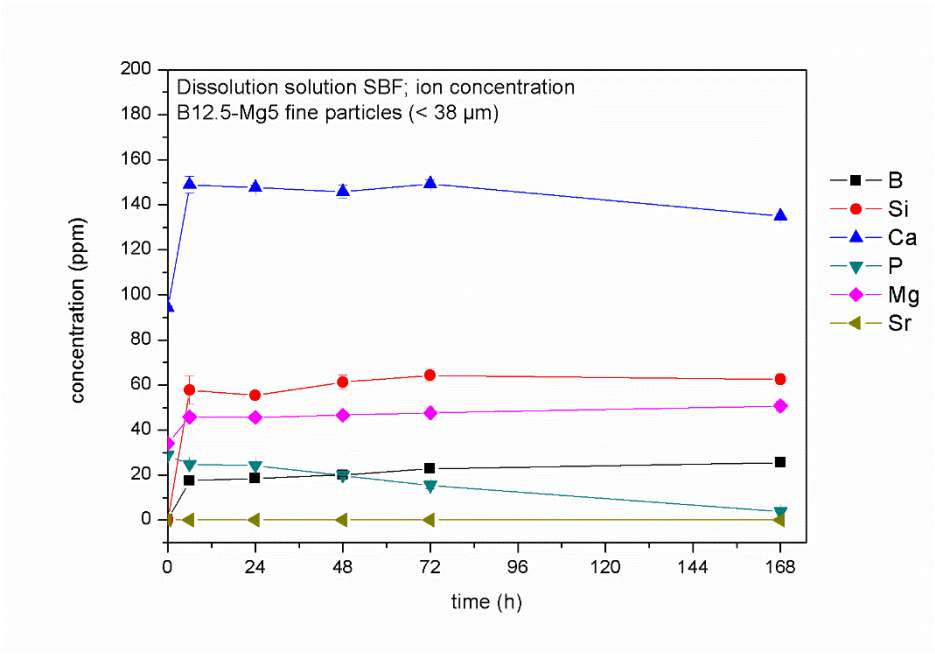

2) B12.5-Mg5 fine particle size

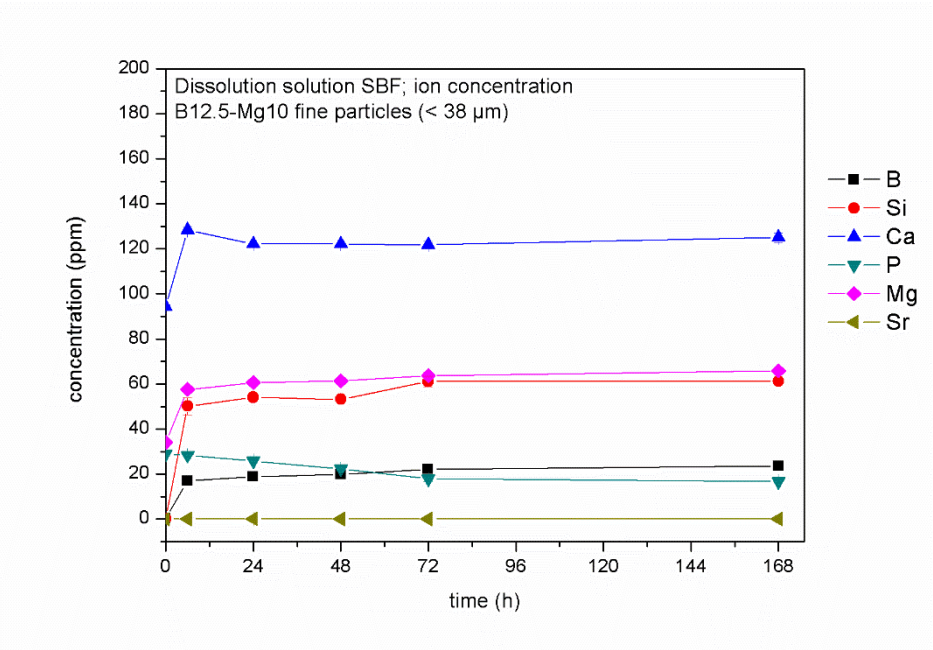

3) B12.5-Mg10 fine particle size

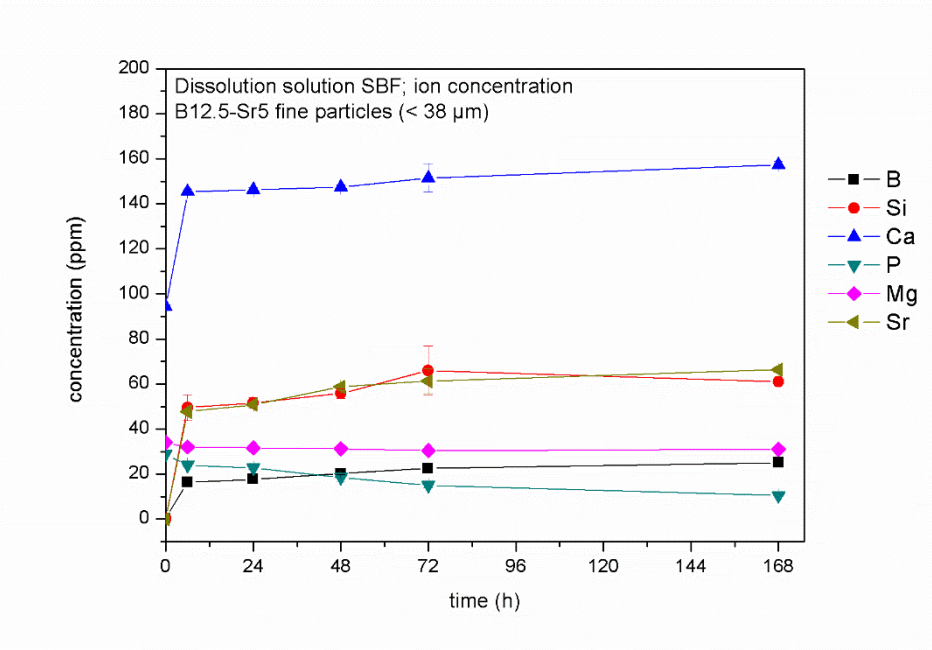

4) B12.5-Sr5 fine particle size

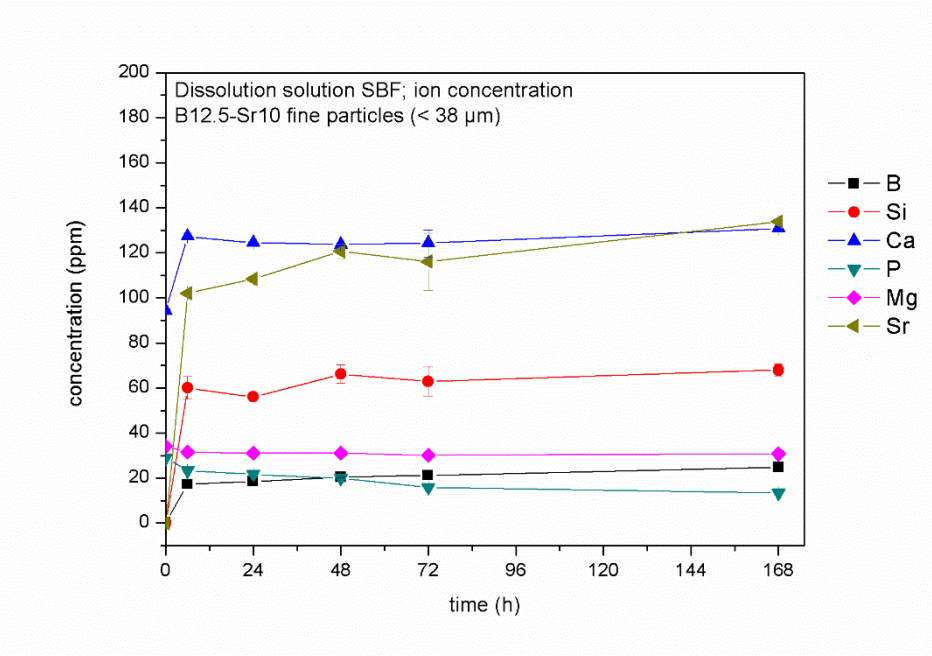

5) B12.5-Sr10 fine particle size

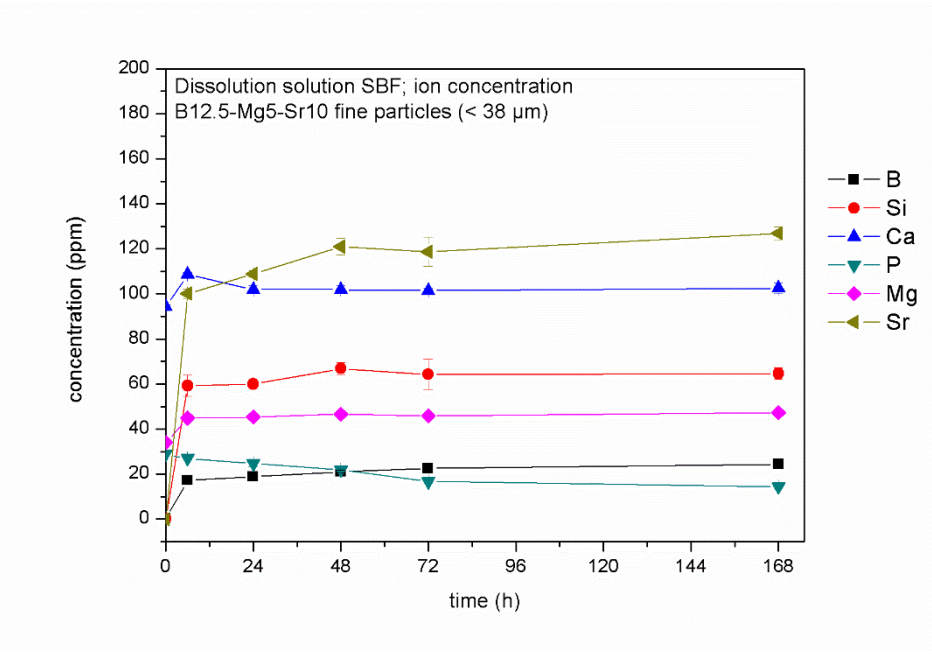

6) B12.5-Mg5-Sr10 fine particle size

Figure D. *Ion release concentration (ppm) for elements B, Si, Ca, P, Mg, Sr as a function of immersion time. Elements determined for fine glass particles of all studied glass compositions (1-6), for immersion in SBF up to 1 week.*